A Moment Approach

to

Mixed Quantum-Classical Dynamics

A Thesis Submitted

By

STEVEN MATHEW PARRY MChem

To the University of Wales in candidature for the degree of

Philosophiae Doctor

School of Chemistry

Bangor University

October 2009

Acknowledgements

Abstract

This thesis is primarily concerned with the description and development of the Quantum Classical Moment (QCM) approach introduced by Burghardt and Parlant. This scheme combines the quantum hydrodynamic and classical Liouvillian representations by generating partial hydrodynamic moments. The time evolution of the partial moments are governed by a hierarchy of coupled equations. For pure quantum states, the hierarchy terminates at the first order. The application of the QCM approach for pure states subject to anharmonic potentials (double well and Eckart barrier) coupled to a classical harmonic mode is demonstrated in Chapter 4. However, in the hydrodynamic formulation of mixed quantum states, no simple closure to the hierarchy exists.

Chapter 5 develops a closure scheme that uses information embedded in the known lower order moments to expand the underlying Wigner phase space distribution function in a Gauss-Hermite orthonormal basis. The application of the closure scheme is demonstrated for both dissipative and nondissipative dynamics of various potentials.

The thesis concludes with a presentation of the extended molecular hydrodynamic approach to describe non-adiabatic solvation phenomena. A mixed quantum-classical description of the system is derived where a classical solvent interacts with a quantum two level solute. A comparison of the dynamics of the hydrodynamic fields obtained from the extended molecular hydrodynamic approach is made with the phase space approach. The differences observed are

attributable to the moment hierarchy approximation made in the molecular hydrodynamic scheme.

Contents

Chapter 1

Introduction

Quantum dynamics is recognised as a key area of science that is indispensable in developing our understanding of a wide range of processes and phenomena. In chemistry, it has been applied to diverse areas such as reactive collisions, photochemistry, and simulations of gas surface encounters and has generally resulted in our development of a deeper understanding of matter and physical phenomena. It has been widely used to rationalise experimental results from ultrafast spectroscopy [1, 2]. Predictions of quantum mechanics have been verified experimentally to a very high degree of accuracy. Indeed, there are no known instances where the predictions given by quantum mechanics are in conflict with experimental data.

The dynamics of such processes can be understood by solving the time-dependent Schrödinger equation (for wavefunctions) or the Liouville-von Neumann equation (for density operators). Molecular systems which are of particular interest to chemists, may compose of many atoms, clusters, polymers etc. These systems are rarely isolated from the surrounding environment, an interaction with the environment is

always present. As a result, these systems have an enormous number of degrees of freedom. Although a fully quantum dynamical treatment is essential to capture non-classical effect such as quantisation, it is unfeasible due to the large number of degrees of freedom involved. While an exact quantum dynamical description is currently computationally prohibitive for such systems, there are a variety of innovative approximate schemes that have been proposed which show considerable promise in their applicability.

The usual approach is to try to partition the global system to a relevant part that can be treated by quantum mechanics and an irrelevant part that can either be treated approximately or, as is often done, ignored. This is limited to situations where the quantum subsystem interacts weakly with the remaining degrees of freedom. In most cases the interaction with the remaining degrees of freedom cannot be ignored. Typical examples include electron transfer in solvated molecules and intramolecular proton transfer. A number of approaches exist for the treatment of such complicated molecular systems. Among these are multiconfigurational methods [3], semi-classical approaches [4, 5], reduced density matrix approaches and mixed quantum-classical approaches [6, 7]. The latter mixed quantum-classical description is particularly appropriate if the system can be described in terms of light "quantum" particles that couple to external heavy particles. The dynamics of the heavy degrees of freedom may then justifiably be treated explicitly in a classical mechanics framework. Theoretical and computational advances in mixed quantum-classical methods are growing at a rapid pace. The subject is an intense area of research [8], providing insights into a

wide range of systems [9, 10, 11] - from molecular electronics [12] to understanding the structure and dynamics of proteins [13].

The aim of mixed quantum-classical dynamics is to treat only a few degrees of freedom quantum mechanically and the remaining degrees of freedom are treated classically, usually in a trajectory approach. The key strength of a mixed quantum-classical approach is its applicability to a wide range of very large systems that are far beyond the capabilities of pure quantum dynamical or even semi-classical methods. The idea of treating a large number of degrees of freedom classically in a molecular dynamics type approach is an attractive one; however, it is not straightforward as to how a mixture of classical and quantum subsystems can be combined in a single scheme. The two approaches are fundamentally different. Quantum mechanics is statistical/probabilistic and non-local in nature, and is deterministic only insofar that the wavefunction, ψ, or the density operator, $\hat{\rho}$, can be determined for all time, provided the initial conditions and the Hamiltonian are known. Classical mechanics on the other hand, is a local approach and, provided the initial conditions and the forces acting on the system are known, is completely deterministic. Several approaches have been developed to address this self-consistency issue; mainly, the Ehrenfest mean field approach [14], surface hopping methods developed by Tully *et al.* [15, 16], and more recently, mixed quantum-classical Liouville methods [17, 18] and the mixed quantum-classical Bohmian (MQCB) method [19, 20].

The central focus of this thesis is the approach that was recently introduced by Burghardt and Parlant [21, 22, 23]. In this scheme,
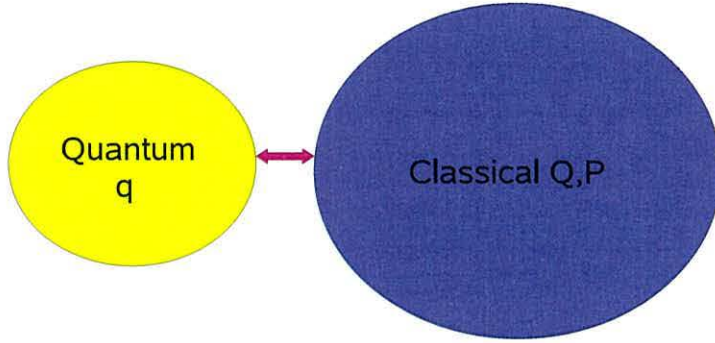
Figure 1.1: Quantum subsystem coupled to a classical subsystem.

which is referred to as the quantum-classical moment (QCM) approach, the quantum sub-system is treated hydrodynamically and the classical sub-system is described in a Liouville phase-space setting (see Fig. (1.1)). This allows the simulation of larger systems with many degrees of freedom. The QCM approach is ideally suited to develop a mixed quantum-classical analogy of the immensely successful classical MD approach. The key concept of the methodology is the combination of quantum hydrodynamic trajectories with classical Liouvillian trajectories. The approach fully accounts for correlations between the quantum and classical subsystems as they couple the same type of objects i.e. trajectories. The definition of quantum trajectories comes from Bohmian (or hydrodynamic) representation of quantum mechanics [24]. In this interpretation, the wavefunction takes on the role of guiding the motion of particles. The evolution of quantum trajectories are governed by a *quantum* force as well as

the classical force seen for Hamiltonian, classical trajectories.

The combination of the two distinct pictures (i.e. quantum hydrodynamic and classical Liouvillian) is achieved by constructing *partial* moments, $\langle \mathcal{P}^n \rho \rangle_q$. These are obtained by integrating the Wigner function ρ_W over only one of the phase space momentum variables p. This yields an infinite hierarchy of moments, $\langle \mathcal{P}^n \rho \rangle_q$. For pure states, only the first two partial moments are required to fully characterise the system. In the case of Gaussian mixed density, the first three moments are required [22, 23]. For a ge eral mixed state quantum density, the infinite hierarchy is required to describe the system. For the QCM approach to be applicable in mixed quantum states, a method of terminating the hierarchy must be developed. This is a major drawback of the QCM approach. Different methods, based on the maximum entropy method, are investigated in this thesis [25, 26, 27, 28], in order to terminate the moment hierarchy.

There are many physical situations where the QCM description is appropriate. In chemistry many isomerisations are governed by double well potentials, where each potential well corresponds to a stable conformation of the molecule. A typical example is intramolecular proton transfer. Proton transfer plays a fundamental role in many molecular processes and is crucial for understanding the properties of many liquids such as water and alcohols. Furthermore, it plays an integral role in the structure of proteins and DNA. The transfer of a proton between the heavy atoms such as nitrogen and oxygen is a process that involves tunnelling and so a quantum mechanical description of the process is essential. However, the proton transfer

9
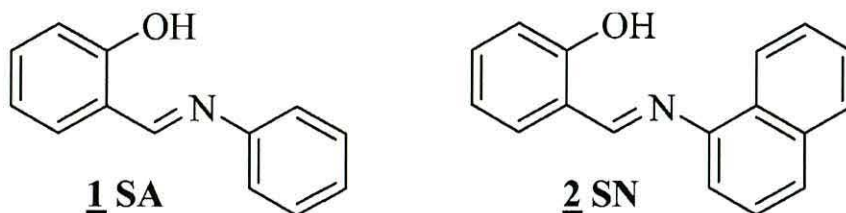
Figure 1.2: Structure of salicylideneaniline and salicylidene-1-naphthylamine of Ref. [29].

is influenced by the motion of the other atoms in the molecule, particularly the vibrational motion of the heavy atoms. This provides a natural setting for a QCM description. A pertinent example of this is seen in Schiff bases, where an ultra fast proton transfer occurs when the molecule is excited to a higher electronic state [29]. Examples of Schiff bases studied in the literature are illustrated in Fig. (1.2). There is much interest in pursuing dynamical modelling of proton transfers [30] as it has many potential interesting applications [31] in laser dyes, molecular storage devices and optical switches.

In nanotechnology, the fact that certain molecules have the ability to isomerise from one characteristic form to another suggest that they are capable of acting as molecular switches. The two different physical forms of the compound acts as 'on' and 'off' states of the switch. It is apparent that azo compounds fit the above criteria [32, 33]. This class of compounds are of the form R-N=N-R (see Fig. (1.3)) and can isomerise with the two R groups *cis* or *trans* to each other. The mechanism of this photoisomerisation has been extensively studied in the literature in recent years to discover whether the torsion or the inversion process is favoured. In most of these studies, the R groups are large and cannot be described purely quantum me-
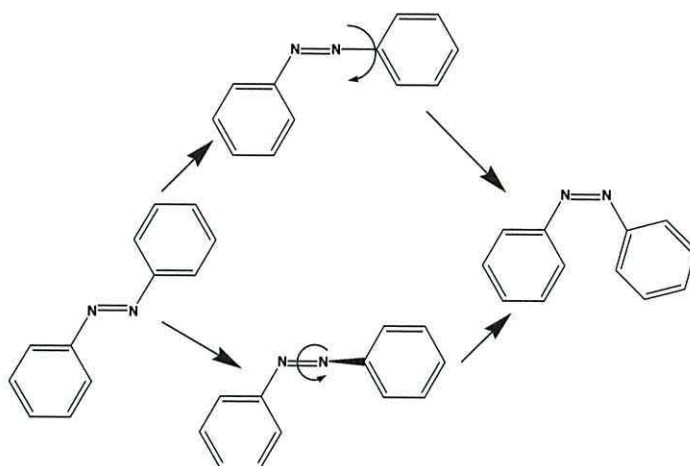
Figure 1.3: Mechanisms of the inversion (top) and torsion (bottom) of the photoisomerisation of azobenzene.

chanically. The mixed quantum-classical moments approach may be feasible here, describing the isomerisation mode quantum mechanically and the remaining modes of the molecule classically.

A further example in nanotechnology is the conduction of an electron along a molecular wire. The conduction is dependent on electron-phonon coupling and the QCM description is ideally suited for such processes.

It is clear that there is huge potential for the application of the QCM approach. It is crucial that a robust method is developed to terminate the moment hierarchy. This would allow the QCM approach to be further developed for even larger systems, beyond what is achievable with other mixed quantum-classical methods.

Structure of Thesis

Chapter 2 presents the general background theory that underpins the concepts developed in the thesis. In particular pure and mixed quantum states are defined. Furthermore, the Bohmian (or hydrodynamic) interpretation of pure state quantum mechanics is developed with the intention of introducing *quantum* trajectories. In Chapter 3 the hydrodynamic picture for mixed states derived by Burghardt *et al.* is presented. The connection between pure (Bohmian) and mixed state hydrodynamics is also shown. Emphasis is placed upon classical limit considerations in hydrodynamic phase space. This along with a comparison of the hydrodynamic space versus Liouville space motivates the construction of a hybrid quantum-classical scheme fundamentally based on the hydrodynamic picture. Chapter 3 finishes by presenting the time evolution of key concepts presented in the thesis i.e. Wigner function, hydrodynamic moments and quantum trajectories subject to differing potential functions.

In Chapter 4, the mixed quantum-classical dynamical scheme of Burghardt and Parlant is described that couples quantum hydrodynamic trajectories with classical Hamiltonian trajectories. This is achieved by generating partial moments i.e. taking a hydrodynamic projection for selected degrees of freedom. This quantum-classical moment (QCM) approach has the potential of simulating large dynamical systems containing many degrees of freedom. The application of the QCM is shown for a double well coupled to a harmonic mode and an Eckart barrier coupled to a harmonic mode. The hydrodynamic quantities for these examples were extracted from the un-

derlying wavefunction, ψ (i.e. pure states). The extension to mixed states would require the propagation of an infinite hierarchy of moment equations. To this end, Chapter 5 investigates methodologies to close the hydrodynamic hierarchy which is the major drawback of the QCM approach. Very simple schemes such as the dampening of the effect of higher order moments offer very little or no improvement over a cold cut-off. Numerical methods based on maximum entropy estimates are presented including the Grad Hermite approach and results are shown for the Hermite closure scheme. Application to both dissipative and non-dissipative systems are presented.

Finally, Chapter 6 describes solvation phenomena, i.e. the response of a solvent environment to a change in the charge distribution of a solute. The extended molecular hydrodynamic approach is presented for a two state quantum solute. Preliminary results of the solvent response to a change in the charge distribution of a solute is presented.

Bibliography

[1] M. Kimble and W. Castleman Jr., Eds., *Femtochemistry: Fundamental Ultrafast Processes in Chemistry, Physics, and Biology: Pt. 7*, Elsevier, 2006.

[2] S. Mukamel, *Principles of Nonlinear Optical Spectroscopy*, Oxford University Press Inc, 1999.

[3] M. H. Beck, A. Jäckle, G. A. Worth, and H.-D. Meyer, Phys. Rep. **324**, 1 (2000).

[4] D. J. Tannor and S. Garashchuk, Ann. Rev. Phys. Chem. **51**, 553 (2000).

[5] K. G. Kay, Ann. Rev. Phys. Chem. **56**, 255 (2005).

[6] R. Kapral, Ann. Rev. Phys. Chem. **57**, 129 (2006).

[7] G. Ciccotti, D. Coker, and R. Kapral, Quantum statistical dynamics with trajectories, in *Quantum Dynamics of Complex Molecular Systems*, edited by D. A. Micha and I. Burghardt, Springer, 2006.

[8] Q. Zhang and B. Wu, Phys. Rev. Lett. **97**, 190401 (2006).

[9] O. Asvany, P. Kumar, B. Redlich, I. Hegemann, S. Schlemmer and D. Marx, Science **309**, 1219 (2005).

[10] L. Vocadlo, D. Alfe, M. J. Gillan, I. G. Wood, J. P. Brodholt and G. D. Price, Nature **424**, 536 (2003).

[11] T. László, S. Wen-Shyan and P. J. Rossky, Science **309**, 914 (2005).

[12] C. Verdozzi, G. Stefanucci, and C. O. Almbladh, Phys. Rev. Lett. **97**, 046603 (2006).

[13] O. Weingart, J. Am. Chem. Soc. **129**, 10618 (2007).

[14] G. D. Billing, Int. Rev. Phys. Chem. **183**, 335 (1994).

[15] J. C. Tully, J. Chem. Phys. **93**, 1061 (1990).

[16] J. C. Tully, Faraday Discuss. Chem. Soc. **110**, 407 (1998).

[17] O. V. Prezhdo and V. V. Kisil, Phys. Rev. A **56**, 162 (1997).

[18] I. V. Aleksandrov, Z. Naturforsch. **36**, 902 (1981).

[19] E. Gindensperger, C. Meier, and J. A. Beswick, J. Chem. Phys. **113**, 9369 (2000).

[20] E. Gindensperger, C. Meier, and J. A. Beswick, J. Chem. Phys. **116**, 8 (2002).

[21] I. Burghardt and G. Parlant, J. Chem. Phys. **120**, 3055 (2004).

[22] I. Burghardt, J. Chem. Phys. **122**, 094103 (2005).

[23] I. Burghardt, K. B. Møller, and K. H. Hughes, Quantum hydrodynamics and a moment approach to quantum-classical theory, in *Quantum Dynamics of Complex Molecular Systems*, edited by D. A. Micha and I. Burghardt, Springer, 2006.

[24] P. R. Holland, *The Quantum Theory of Motion*, Cambridge University Press, New York, 1993.

[25] K. H. Hughes, S. M. Parry and I. Burghardt, J. Chem. Phys. **130**, 054115 (2009)

[26] C. D. Levermore, J. Stat. Phys. **83**, 1021 (1996).

[27] P. Degond and C. Ringhofer, J. Stat. Phys. **112**, 587 (2003).

[28] M. Trovato and P. Falsaperla, Phys. Rev. B **57**, 4456 (1998).

[29] W. Rodriquez-Córdoba, J. S. Zugazagoitia, E. Collado-Fregoso and J. Peon, J. Phys. Chem. A **111**, 6241 (2007).

[30] O. Kwon and A. Zewail, Proc. Natl. Acad. Sci. USA **104**, 8703 (2007).

[31] K. Kuldova, A. Corval, H. P. Trommsdorff and J. M. Lehn, J. Phys. Chem. A **101**, 151 (1997).

[32] H. Satzger, S. Spörlein, C. Root, J. Wachteveitl, W. Zinth and P. Gilch, Chem. Phys. Lett, **372**, 216 (2002).

[33] C. Chang, Y. Lu, T. Wang and E.W. Diau, J. Am. Chem. Soc, **126**, 10109 (2004).

Chapter 2

Background Theory

2.1 Schrödinger equation

In quantum mechanics, the time-dependent Schrödinger Equation describes how the states of a physical system varies with time,

$$i\hbar\frac{\partial}{\partial t}\psi(r,t) = H\psi(r,t) \qquad (2.1)$$

where $i = \sqrt{-1}$, H is the Hamiltonian operator, $\psi(r,t)$ is the time dependent wavefunction and $\hbar$ is the reduced Planck's constant. This wavefunction is inherently statistical and has the probabilities of the outcomes of all possible measurements that can be made on the system [1]. Assuming normalisation,

$$\int_{-\infty}^{\infty} |\psi(r,t)|^2 dr = 1 \qquad (2.2)$$

the conventional interpretation of quantum mechanics defines $|\psi(r,t)|^2$ as the time dependent probability density of finding the particle at position r. Given the initial wavefunction $\psi(r,0)$ is known, the wavefunction is determined for all time. This yields a complete description of the state of an individual system.

The Hamiltonian is an operator given by the sum of the kinetic and potential energy such that,

$$H = T + V = -\frac{\hbar^2}{2m}\nabla^2 + V(r) \tag{2.3}$$

With a time independent Hamiltonian, the wavefunction can be expanded in the eigen basis, $\{\phi_n(r)\}$, of H,

$$\psi(t) = \sum_{n=0}^{\infty} c_n\phi_n(r)e^{-\frac{i}{\hbar}E_n t} \tag{2.4}$$

where E_n are the eigenvalues of the system. The complex valued coefficients c_n,

$$c_n = \int \phi_n(r)\psi(r,t_0)dr \tag{2.5}$$

are such that $|c_n|^2$ represent the probability that measurement of the energy of the system yields E_n. The time dependent probability density is then given by,

$$|\psi(r,t)|^2 = \sum_{n=0}^{\infty}\sum_{m=0}^{\infty} c_n^* c_m e^{-\omega(m-n)t}\phi_n^*\phi_m \tag{2.6}$$

where $\omega(m-n) = (E_m - E_n)/\hbar$.

Average or expectation values of any experimental observable can be obtained by taking each possible outcome weighted by the probability of obtaining that outcome. For a normalised wavefunction, the average value of an observable is given by [2],

$$\langle A \rangle = \int_{-\infty}^{\infty} \psi^*(r,t)\hat{A}\psi(r,t)dr = \langle \psi(t)|\hat{A}|\psi(t)\rangle \tag{2.7}$$

Furthermore, the expectation value of the total energy of the wavefunction is given by,

$$\langle E \rangle = \langle \psi(t)|\hat{H}|\psi(t)\rangle \tag{2.8}$$

The Dirac Bra-Ket notation [3] has been introduced in Eq. (2.7). The wavefunction is represented by the ket vector $|\psi\rangle$ and its complex conjugate is denoted $\langle\psi|$. Combining the Bra and Ket gives $\langle\psi|\psi\rangle = \int \psi^*\psi d\tau$.

The solution of the Schrödinger equation and its probabilistic interpretation has been the cornerstone of quantum dynamics. However, an alternative formulation of the equation leads to different interpretations of the wavefunction and indeed yields different methods to solve quantum dynamical problems.

2.2 Bohmian Mechanics

The Bohmian (or hydrodynamic) approach is an alternative interpretation of quantum mechanics and in particular of the measurement process. In the early days of quantum mechanics, de Broglie [4, 5, 6, 7, 8] suggested that the wavefunction does not only predict the likely outcome of every experiment, but also guides the motion of an ensemble of identical particles according to $|\psi(r,t)|^2$. This concept was developed by Bohm in 1952 [9, 10]. This is known as the de Broglie-Bohm *pilot wave* theory or the *causal* interpretation of quantum mechanics. Within this formalism, the wave-particle duality of conventional quantum mechanics is divorced so the system has both waves and particles. These particles are understood to have precise trajectories. This trajectory picture directly emerges from a reinterpretation of the quantum state, ψ. The key difference between quantum trajectories and their classical versions is the presence of the quantum potential $Q(r,t)$ in the quantum formulation.

The quantum potential is a dynamical quantity which depends on the curvature of the wavefunction. A brief derivation of the equations of Bohmian mechanics is presented here.

The one dimensional r wavefunction may be written in the polar form of Madelung [11],

$$\psi(r,t) = R(r,t)e^{\frac{i}{\hbar}S(r,t)} \tag{2.9}$$

where $R(r,t)$ is the amplitude of the wavefunction and $S(r,t)$ is the action, both of which are real-valued. The action function is related to the wavefunction by

$$\frac{S}{\hbar} = \frac{1}{2i}\ln\left(\frac{\psi}{\psi^*}\right) \tag{2.10}$$

Inserting the polar form of the wavefunction Eq. (2.9) into the Schrödinger equation,

$$i\hbar\frac{\partial\psi}{\partial t} = -\frac{\hbar^2}{2m}\frac{\partial^2}{\partial r^2}\psi + V(r,t)\psi \tag{2.11}$$

and separating the real and imaginary parts (see Appendix A), two real coupled equations are obtained,

$$\frac{\partial R^2}{\partial t} = -\frac{1}{m}\frac{\partial}{\partial r}\left(R^2\frac{\partial S}{\partial r}\right) \tag{2.12}$$

which is derived from the imaginary part, and,

$$-\frac{\partial S}{\partial t} = \frac{1}{2m}\left(\frac{\partial S}{\partial r}\right)^2 + Q(r,t) + V(r,t) \tag{2.13}$$

derived from the real part.

Eq. (2.13) is the quantum Hamilton-Jacobi equation, and differs from its classical form by the presence of the quantum potential

20

$Q(r, t)$. This quantum potential is dependent on the quantum state via the curvature of the amplitude $R(r, t)$,

$$Q(r, t) = -\frac{\hbar^2}{2mR} \frac{\partial^2 R}{\partial r^2} \qquad (2.14)$$

Taking the gradient of the quantum Hamilton-Jacobi equation Eq. (2.13) yields (see Appendix B),

$$m\frac{dv}{dt} = -\left[\frac{\partial V}{\partial r} + \frac{\partial Q}{\partial r}\right] \qquad (2.15)$$

which has the form of Newton's second law of motion. Because of the presence of the quantum potential term $Q(r, t)$, the classical trajectory becomes a quantum trajectory.

Recognising that $\rho(r, t) = R(r, t)^2 = |\psi(r, t)|^2$, Eq. (2.12) can be written,

$$\frac{\partial \rho}{\partial t} = -\frac{1}{m}\frac{\partial}{\partial r}\left(\rho\frac{\partial S}{\partial r}\right) \qquad (2.16)$$

The velocity field [1], v, is defined as,

$$v = \frac{1}{m}\frac{\partial S}{\partial r} \qquad (2.17)$$

Eq. (2.16) may then be written as

$$\frac{\partial}{\partial t}\rho + \frac{\partial}{\partial r}(\rho v) = 0 \qquad (2.18)$$

This is the continuity equation for the quantum density which is now treated as a fluid. The total time derivative of the continuity equation Eq. (2.18) results in the second equation of motion,

$$\frac{d\rho}{dt} = -\rho\frac{\partial v}{\partial r} \qquad (2.19)$$

This shows that the evolution of the quantum fluid probability density is determined by the gradient of the velocity field,

$$\frac{d\ln\hat{\rho}}{dt} = -\frac{\partial v}{\partial r} \qquad (2.20)$$

2.3   Density Operator

The discussion so far has focussed on wavefunctions or state vectors. These are used for systems where a complete description is available. This is only possible if a set of observables exists from which all physical quantities can be measured simultaneously [3]. Such a system is known as a pure state. An example of a pure state is one with a perfectly known preparation history such as the polarisation state of photons that have passed through a polariser.

In many cases the state of a system cannot be perfectly known. This could be if the system has too many degrees of freedom. A pertinent example is an atom undergoing spontaneous emission when it is coupled to an environment. A state vector description is impossible, a more general methodology is required. The system must now be described by a statistical mixture of possible state vectors for the system - this is described as a *mixed* state. Instead of treating a statistical mixture of wavefunctions, it is more convenient to use the density operator $\rho(t)$ [12, 13]. This formalism maximises the partial information we have of the system in question.

In the general case, the density operator is given by,

$$\rho(t) = \sum_{\alpha} \omega_{\alpha} |\psi(t)\rangle \langle \psi(t)| \tag{2.21}$$

where ω_{α} is are weights of each pure state, i.e. the probability that a particular state is incorporated to the complete mixture of states. Given that the states $|\psi(t)\rangle$ are normalised, the weights ω_{α} must satisfy $\sum_{\alpha} \omega_{\alpha} = 1$. The density operator $\rho(t)$ can be used to describe both pure and mixed states. For a pure state, as there is only one

state present, the weight for that state equals unity such that,

$$\rho(t) = |\psi(t)\rangle\langle\psi(t)| \tag{2.22}$$

A measure of the purity of the system can be determined by taking the trace of the square of the density matrix, where $\text{Tr}(\rho^2) = 1$ for pure states and $\text{Tr}(\rho^2) < 1$ for mixed states [2]. As the wavefunction $|\psi(t)\rangle$ in the basis $|\phi(t)\rangle$ can be written,

$$|\psi(t)\rangle = \sum_i c_i(t)|\phi(t)\rangle \tag{2.23}$$

the matrix elements of the density operator $\rho(t)$ is given by,

$$
\begin{aligned}
\rho_{mm}(t) &= \langle\phi_m|\rho(t)|\phi_m\rangle = \sum_\alpha \langle\phi_m|\omega_\alpha|\psi_\alpha\rangle\langle\psi_\alpha|\phi_m\rangle \\
&= \sum_\alpha \omega_\alpha |\langle\phi_m|\psi_\alpha\rangle|^2 \\
&= \sum_\alpha \omega_\alpha |c_m(t)|^2
\end{aligned} \tag{2.24}
$$

for the diagonal elements and

$$
\begin{aligned}
\rho_{mn}(t) &= \langle\phi_m|\rho(t)|\phi_n\rangle = \sum_\alpha \langle\phi_m|\omega_\alpha|\psi_\alpha\rangle\langle\psi_\alpha|\phi_n\rangle \\
&= \sum_\alpha \omega_\alpha \langle\phi_m|\psi_\alpha\rangle\langle\psi_\alpha|\phi_n\rangle \\
&= \sum_\alpha \omega_\alpha c_m(t)c_n^*(t)
\end{aligned} \tag{2.25}
$$

for off-diagonal elements. The diagonal elements correspond to the probability that the outcome of measurement places the system in a particular state of the defined basis. They are often called populations. The off-diagonal elements of the density matrix however are the so-called coherences. These elements are associated with the interference effects of the states.

Just as the Schrödinger equation describes how pure states evolve in

time, the quantum Liouville equation describes how a density matrix evolves in time. As the time dependence of the density operator depends on the evolution of the individual state vectors, the quantum Liouville equation can in fact be derived from the Schödinger equation [12],

$$\begin{aligned}
\frac{\partial \rho}{\partial t} &= -\frac{i}{\hbar} \sum_\alpha w_\alpha \left[\hat{H} |\psi_\alpha\rangle\langle\psi_\alpha| - |\psi_\alpha\rangle\langle\psi_\alpha| \hat{H} \right] \\
&= -\frac{i}{\hbar} [\hat{H}, \rho] = -\frac{i}{\hbar} \mathcal{L} \rho
\end{aligned} \tag{2.26}$$

where $[H, \rho]$ denotes the commutator and $\mathcal{L}$ is the Liouvillian superoperator.

2.4 Phase Space and the Wigner Function

It can be concluded from previous discussions that a system of interest can be described quantum mechanically by a wavefunction ψ for pure states and by a density operator ρ for mixed states. The state of a classical system can be defined by a point in phase space that defines the coordinate, $Q(t)$, and momentum, $P(t)$ simultaneously. In a dynamical scheme, this point in phase space evolves along a trajectory. Instead of launching a range of trajectories from different initial points in phase space, it is more convenient to propagate a continuous time dependent probability density. This density ρ_{cl} has the probability of finding trajectories in a small phase space *cell* [14]. This density is nonnegative, $\rho_{cl} \geq 0$, and satisfies the normalisation condition,

$$\int \int \rho_{cl}(q, p, t) dq dp = 1 \tag{2.27}$$

This stage forms an essential part of classical statistical mechanics, as one can easily obtain average values of observables from the phase space probability density. The problem with extending this representation to quantum mechanics is that the uncertainty principle imposes a constraint on the correlation between q and p. However, if the product of the root-mean-square half widths of the marginal distributions [15],

$$\begin{aligned}
\rho(q,t) &= = \int_{\infty}^{\infty} \rho(q,p,t)dp \\
\rho(p,t) &= = \int_{\infty}^{\infty} \rho(q,p,t)dq
\end{aligned} \tag{2.28}$$

are not less than $\frac{\hbar}{2}$ then the uncertainty principle is satisfied.

There are several quantum phase space distribution functions available that satisfy the above conditions [16]. The choice of which function is used depends entirely on the physical system in question. For example, due to its smooth, coarse grained structure, the positive definite Husimi distribution function is popular for the quantum dynamical study of classically chaotic systems [17, 18]. In quantum optics, the Glauber-Sudarshan distribution function is widely used due to its suitability for evaluating expectation values of normally ordered operators.

For application in a mixed quantum-classical molecular dynamics scheme, the distribution function of choice is the Wigner function. This was developed by Wigner to study quantum corrections for thermodynamic equilibrium [19]. It is formulated in terms of the Fourier transform of an overlap function,

$$O(q,r) = \psi(q - r/2, t)\psi^*(q + r/2, t) \tag{2.29}$$

25

where r is the separation. The Fourier transform of the overlap function yields an expression for the Wigner function for pure states,

$$\rho_W = \frac{1}{2\pi\hbar} \int e^{ipr/\hbar} \psi(q - r/2, t)\psi^*(q + r/2, t)dr \qquad (2.30)$$

The Wigner density function can also be defined by its relation to the positional-dependent density operator where $\psi(x) = \langle x|\psi\rangle$

$$\begin{aligned}
\rho_W &= \frac{1}{2\pi\hbar} \int e^{\frac{ipr}{\hbar}} \Big\langle q - \frac{r}{2}\Big|\psi\Big\rangle\Big\langle\psi\Big|q + \frac{r}{2}\Big\rangle dr \\
&= \frac{1}{2\pi\hbar} \int e^{\frac{ipr}{\hbar}} \Big\langle q - \frac{r}{2}\Big|\rho\Big|q + \frac{r}{2}\Big\rangle dr \qquad (2.31)
\end{aligned}$$

Unfortunately, the Wigner function is not without its drawbacks. The function can take both positive and negative values and therefore, strictly it is not a true probability function. Instead, the Wigner distribution should be considered a quasi-probability distribution function. The origin of these negative *basins* is known to be diffraction fringes that occur when interference effects are dominant, for example during barrier scattering. A clear advantage of the Wigner function is that it provides an useful tool to compare classical and quantum dynamics in phase space. Furthermore, the equation of motion for the Wigner function has a simpler form than that of other distribution functions.

Dynamics of the Wigner Function

The equation of motion for ρ_W is obtained by taking the Wigner transform (prescription in Eq. (2.30)) of the quantum Liouville equation Eq. (2.26) (see Appendix C). The resulting Wigner Moyal equation is given by,

$$\frac{\partial \rho_W}{\partial t} = \{H, \rho_W\}_{qp} + \sum_{\substack{k=3 \\ \text{odd}}}^{n} \frac{1}{k!}\Big(\frac{\hbar}{2i}\Big)^{k-1} \frac{\partial^k V}{\partial q^k} \frac{\partial^k \rho_W}{\partial p^k}$$

26

$$= -\frac{p}{m}\frac{\partial \rho_W}{\partial q} + \frac{\partial V}{\partial q}\frac{\partial \rho_W}{\partial p} - \frac{\hbar^2}{24}\frac{\partial^3 V}{\partial q^3}\frac{\partial^3 \rho_W}{\partial p^3} + O(\hbar^4), \quad (2.32)$$

where the first term arises from the kinetic part of the Hamiltonian and the remaining terms accounts from the potential part. In particular, $\{,\}$ represents the Poisson bracket, $\{H, \rho_W\}_{qp} = 1/2(H\Lambda_{qp}\rho_W - \rho_W\Lambda_{qp}H)$, with

$$\Lambda_{qp} = \frac{\overleftarrow{\partial}}{\partial q} \cdot \frac{\overrightarrow{\partial}}{\partial p} - \frac{\overleftarrow{\partial}}{\partial p} \cdot \frac{\overrightarrow{\partial}}{\partial q} \quad (2.33)$$

If the quantum terms i.e. terms that contain $\hbar$ are set to zero, the *classical* Liouville equation of motion is recovered,

$$\frac{\partial \rho_{cl}}{\partial t} = -\frac{p}{m}\frac{\partial \rho_{cl}}{\partial q} + \frac{\partial V}{\partial q}\frac{\partial \rho_{cl}}{\partial p} \quad (2.34)$$

Bibliography

[1] P. R. Holland, *The Quantum Theory of Motion*, Cambridge University Press, New York, 1993.

[2] D. J. Tannor, *Introduction to Quantum Mechanics, A Time-Dependent Perspective*, University Science Books, 2007.

[3] P. A. M. Dirac. *The Principles of Quantum Mechanics*, Oxford University Press, London, 1958.

[4] L. de Broglie, Compt. Rend. **183**, 447 (1926).

[5] L. de Broglie, Nature **118**, 441 (1926).

[6] L. de Broglie, Compt. Rend. **184**, 273 (1926).

[7] L. de Broglie, Compt. Rend. **185**, 380 (1927).

[8] L. de Broglie, J. de Phys. **8**, 225 (1927).

[9] D. Bohm, Phys. Rev. **85**, 166 (1952).

[10] D. Bohm, Phys. Rev. **85**, 180 (1952).

[11] E. Madelung, Z. Phys. **40**, 332 (1926).

[12] J. von Neumann, *Mathematical Foundations of Quantum Mechanics*, Princeton University Press, 1983.

[13] L. D. Landau, Z. Phys. **45**, 430 (1927).

[14] R. E. Wyatt, *Quantum Dynamics with Trajectories: Introduction to Quantum Hydrodynamics*, Springer, Heidelberg, 2005.

[15] W. P. Schleich, *Quantum Optics in Phase Space*, Wiley-VCH, Berlin, 2001.

[16] H. W. Lee, Phys. Rep. **259**, 147 (1995).

[17] W. A. Lin and L. E. Ballentine, Phys. Rev. Lett. **65**, 2927 (1990).

[18] J. Y. Shin and H. W. Lee, Phys. Rev. E **50**, 902 (1994).

[19] E.Wigner, Physica (Utrecht) **7**, 749 (1940).

Chapter 3

Quantum Hydrodynamics for Mixed States

3.1 Introduction

The Schrödinger equation can be solved directly using many methods such as basis set expansions or grid based approaches and these have been widely investigated and documented in the literature [1]. In principle, it is also possible to solve the Schrödinger equation by propagating *quantum* trajectories. It has been recognised that there is a close analogy between the Schrödinger equation and the equations of motion for fluid dynamics. Hence the dynamical theory that governs quantum trajectories is known as the hydrodynamic formulation of quantum mechanics. This representation was developed initially by Madelung [2] and de Broglie [3], following a development into a theory by Bohm [4] and de-Broglie [5] again in later work.

Methodologies that use quantum trajectories can be split into two distinct categories depending on how they are calculated. In the first

type, the de Broglie analytical approach [4, 5, 6, 7], the time dependent Schrdinger equation is first solved (using traditional approaches such as basis set expansions). The 'particles' are then propagated along trajectories, guided by the wavefunction, such that

$$\frac{dr}{dt} = \left(\frac{\hbar}{\pi}\right) \text{Im}[\nabla \ln \psi] \tag{3.1}$$

Subsequent quantum trajectory analysis of the wavefunction involves the spatial evolution of the discrete particles. The intention of the analytical approach is to provide further insight and an alternative interpretation of quantum mechanics.

The second type of quantum trajectory method is the synthetic approach [8, 9, 10]. Here rather than compute quantum trajectories from the wavefunction, the trajectories become the computational tool for solving the quantum hydrodynamic equations of motion. This type of methodology is more than an interpretation, it is a novel computational technique for solving quantum dynamical problems. The quantum trajectory synthetic approach offers many advantages over conventional wavefunction propagation, including [11]

i) a relatively small number of grid point is required

ii) the equations of motion have intuitive dynamical quantities such as forces

iii) potential of new insight as trajectories shows how process evolves

iv) computational effort varies linearly with number of trajectories

v) potential mitigation of exponential scaling of computational effort with degrees of freedom

vi) no large basis sets or large fixed grids required.

The number of trajectories required for a quantum trajectory simulation depends strongly on the system in question. For example, for a scattering type problem that invokes an unbound potential, a large number of grid points is required to fully characterise the dynamics of the density. It is also important to emphasise that a quantum trajectory approach is formally equivalent and will give the same empirical predictions as conventional quantum dynamics (i.e. direct solution of the Schrödinger equation). Although a trajectory picture is normally associated within the classical framework, it is shown in this Chapter that a quantum mechanical equivalent may be derived.

A great deal of research has focussed on the hydrodynamic formulation for pure states [2, 4, 6, 7, 12]. This Chapter will show that mixed quantum states (defined by the density operator) can also be represented in the hydrodynamic framework. This dates back to the work done by Moyal [13], Zwanzig [14], Takabayasi [12] and Frölich [15]. The following sections derives the hydrodynamic moments from the density operator (or equivalent Wigner function). This lead to obtaining quantum trajectory equation by evaluating the *quantum* force from the hierarchy of hydrodynamic moments.

3.2 Hydrodynamic moments and their dynamical equations

The hydrodynamic equations that are solved to obtain trajectories are reduced, local descriptions which are obtained from the time evolution of the nonlocal density governed by the Liouville-von Neumann equation [16]. The derivation here focuses on a single degree

of freedom but can be readily extended to any number of degrees of freedom. The Liouville-von Neumann equation in the coordinate representation, with Hamiltonian $H = T + V$ is given by

$$i\hbar \frac{\partial}{\partial t} \rho(x, x^{'}) = - \frac{\hbar^2}{2m} \left[\frac{\partial^2}{\partial x^2} - \frac{\partial^2}{\partial x^{'2}} \right] \rho(x, x^{'})$$
$$+ [V(x) - V(x^{'})] \rho(x, x^{'}) \qquad (3.2)$$

Eq. (3.2) is now decomposed into coupled equations for a hierarchy of local fields which are coordinate dependent quantities such as local probability density $P(x)$, current density (flux) $j(x)$, kinetic energy density $T(x)$ etc. These fields are closely related to moments defined from the coordinate representation of the nonlocal density as

$$\langle \mathcal{P}^n \rho \rangle(q) = \int_{-\infty}^{\infty} dr \, [\mathcal{P}^n \rho(q + r/2, q - r/2)]_{r=0} \qquad (3.3)$$

where $\mathcal{P}$ is defined as a superoperator acting on the density

$$\mathcal{P} = \frac{\hbar}{i} \frac{\partial}{\partial r} = \frac{\hbar}{2i} \left[\frac{\partial}{\partial x} - \frac{\partial}{\partial x^{'}} \right] \qquad (3.4)$$

The coordinate density $\rho(x, x^{'})$ is redefined in terms of sum $q = 1/2(x + x^{'})$ and difference $r = x - x^{'}$ coordinates. These hydrodynamic moments correspond to the Taylor expansion of coordinate space density with respect to coordinate r, such that,

$$\rho(q, r) = \sum_n \frac{1}{n!} \langle \mathcal{P}^n \rho \rangle_q \left(\frac{ir}{\hbar} \right)^n \qquad (3.5)$$

The 0th moment corresponds to the probability density, $P(x) = \langle \rho \rangle_q$, the 1st moment is related to the current density, $j(x) = \langle \mathcal{P} \rho \rangle_q / m$ and the 2nd moment is related to the kinetic energy density, $T(x) = \langle \mathcal{P}^2 \rho \rangle_q / 2m$.

The moments can be equivalently obtained from the Wigner function [17, 18, 19], which is related to the coordinate density $\rho(x, x^{'})$

33

by Wigner transform,

$$\rho_W(q,p) = \frac{1}{2\pi\hbar} \int_{-\infty}^{\infty} dr\ \rho(q - r/2, q + r/2)e^{(ipr/\hbar)} \qquad (3.6)$$

The moments from this definition can be expressed as [16, 20, 21, 22],

$$\langle \mathcal{P}^n \rho \rangle_q = \int_{-\infty}^{\infty} dp\ p^n \rho_W(q,p) \qquad (3.7)$$

This integration over phase space momentum only was described by Takabayasi as *projection...onto coordinate space* [12].

By applying the procedure of Eq. (3.3) to the Liouville-von Neumann equation Eq. (3.2), a series of coupled equation is obtained [16] (see Appendix D),

$$\begin{aligned}
\frac{\partial}{\partial t}\langle \rho \rangle_q &= -\frac{1}{m}\frac{\partial}{\partial q}\langle \mathcal{P}\rho \rangle_q \\
\frac{\partial}{\partial t}\langle \mathcal{P}\rho \rangle_q &= -\frac{1}{m}\frac{\partial}{\partial q}\langle \mathcal{P}^2\rho \rangle_q - \frac{\partial V}{\partial q}\langle \rho \rangle_q \\
\frac{\partial}{\partial t}\langle \mathcal{P}^2\rho \rangle_q &= -\frac{1}{m}\frac{\partial}{\partial q}\langle \mathcal{P}^3\rho \rangle_q - 2\frac{\partial V}{\partial q}\langle \mathcal{P}\rho \rangle_q
\end{aligned} \qquad (3.8)$$

The hierarchy can be summarised,

$$\frac{\partial}{\partial t}\langle \mathcal{P}^n \rho \rangle_q = \langle \mathcal{P}^n \{H, \rho_W\}_{qp} \rangle_q + \mathcal{C}_q \qquad (3.9)$$

with classical terms

$$\langle \mathcal{P}^n \{H, \rho_W\}_{qp} \rangle_q = -\frac{1}{m}\frac{\partial}{\partial q}\langle \mathcal{P}^{n+1}\rho \rangle_q - n\frac{\partial V}{\partial q}\langle \mathcal{P}^{n-1}\rho \rangle_q \qquad (3.10)$$

and a quantum part

$$\mathcal{C}_q = -\sum_{k=3,\mathrm{odd}}^{n} \binom{n}{k} \left(\frac{\hbar}{2i}\right)^{k-1} \frac{\partial^k V}{\partial q^k}\langle \mathcal{P}^{n-k}\rho \rangle_q \qquad (3.11)$$

The first term in Eq. (3.10) is the kinetic energy part of the equation of motion. Note that this part couples the nth order moment $\langle \mathcal{P}^n \rho \rangle_q$

34

to the $(n+1)$th moment $\langle \mathcal{P}^{n+1}\rho \rangle_q$. The coupling to higher (and lower) order moments suggests that an infinite hierarchy is generated and this becomes a major drawback and a central theme of the hybrid quantum-classical approach that is pursued in Chapter 4. In the case of a pure state however, the hierarchy can be closed at the first moment. Also, for Gaussian mixed state densities, the hierarchy closes at the second moment. Unfortunately, there is no simple closure relation for general mixed quantum states.

3.3 Pure State and link to Bohmian Mechanics

For pure states described by a wavefunction where $\rho(x, x^{'}) = \psi(x)\psi^*(x)$, the hierarchy of equations of motion for the moments close with the first two equations. Indeed all higher order moments can be expressed in terms of the zeroth and first moments. As an example the second moment can be expressed as [16]

$$\langle \mathcal{P}^2\rho \rangle_q \bigg|_{pure} = \bar{p}_q^2 \langle \rho \rangle_q - \frac{\hbar^2}{4}\langle \rho \rangle_q \frac{\partial^2}{\partial q^2}\ln\langle \rho \rangle_q \qquad (3.12)$$

where $\bar{p}_q$ is defined as the momentum field related to the moments by $\langle \mathcal{P}\rho \rangle_q = \bar{p}_q \langle \rho \rangle_q$. This closure at the second order yields equations of motion for pure state hydrodynamics, or Bohmian mechanics [16]. It is not surprising that only the first two moments are required for a pure state description, as the wavefunction may be fully characterised by the local density $\langle \rho \rangle_q$ and the current density $\langle \mathcal{P}\rho \rangle_q$. From the polar representation of the wavefunction,

$$\psi(x) = R(x)e^{(iS(x)/\hbar)} \qquad (3.13)$$

the local density and current density (momentum field) is given by

$$\langle \rho \rangle_q = R^2(q)$$
$$\langle \mathcal{P} \rho \rangle_q = \bar{p}_q \langle \rho \rangle_q = \frac{\partial S}{\partial q} \langle \rho \rangle_q \tag{3.14}$$

In the hydrodynamic picture, the equations of motion for the first two moments are,

$$\frac{\partial \langle \rho \rangle_q}{\partial t} = -\frac{1}{m} \frac{\partial}{\partial q} \langle \mathcal{P} \rho \rangle_q$$
$$\frac{\partial}{\partial t} \langle \mathcal{P} \rho \rangle_q = -\frac{1}{m} \frac{\partial}{\partial q} \langle \mathcal{P}^2 \rho \rangle_q \Big|_{\text{pure}} - \frac{\partial V}{\partial q} \langle \rho \rangle_q \tag{3.15}$$

The second moment here is that of the pure state limit, so it is decoupled from the rest of the hierarchy.

These equation are in the Eulerian frame of hydrodynamics. In this picture, the evolution of the function (e.g. density) is observed from a fixed point in space. The equations of motion in the Eulerian framework always contain *partial* time derivatives. In trajectory equations of motion, a different framework must be used, the Lagrangian picture. Here, the observer is following the trajectory $x(t)$ at a velocity of,

$$v = \frac{p}{m} = \frac{1}{m} \frac{\partial S}{\partial x} \tag{3.16}$$

For a short time step, the change in the function f, as seen from the observer in the interval $x(t)$ to $x(t + dt)$, is given by

$$df = \frac{\partial f}{\partial t} dt + \frac{\partial f}{\partial x} dx \tag{3.17}$$

On division by dt, the following expression defines the Lagrangian framework from the Eulerian picture.

$$\frac{df}{dt} = \frac{\partial f}{\partial t} + \frac{dx}{dt} \frac{\partial f}{\partial x} = \frac{\partial f}{\partial t} + v \frac{\partial f}{\partial x} \tag{3.18}$$

36

The second term in Eq. (3.18) is the convective term that translates from one picture to the other. To this end the Lagrangian equations of Bohmian mechanics may be written, [24],

$$\begin{aligned}
\frac{d\langle\rho\rangle_q}{dt} &= -\frac{\langle\rho\rangle_q}{m}\frac{\partial\bar{p}}{\partial q} \\
\frac{d\bar{p}(q,t)}{dt} &= -\frac{\partial V}{\partial q} + F_{\mathrm{hyd}}\bigg|_{\mathrm{pure}}
\end{aligned} \tag{3.19}$$

where F_{hyd} is the hydrodynamic force [16, 25, 26],

$$F_{\mathrm{hyd}}\bigg|_{\mathrm{pure}} = -\frac{1}{m}\langle\rho\rangle_q^{-1}\frac{\partial\sigma_q}{\partial q}\bigg|_{\mathrm{pure}} \tag{3.20}$$

The variance, σ_q is a measure of the 'broadness' of the distribution and of fluctuations about the mean value of the momentum,

$$\sigma_q\bigg|_{\mathrm{pure}} = \langle\mathcal{P}^2\rho\rangle_q\bigg|_{\mathrm{pure}} - \bar{p}_q^2\langle\rho\rangle_q \tag{3.21}$$

For the case of pure states, the variance is given by,

$$\sigma_q\bigg|_{\mathrm{pure}} = -\frac{\hbar^2}{4}\langle\rho\rangle_q\frac{\partial^2}{\partial q^2}\ln\langle\rho\rangle_q \tag{3.22}$$

Note that there is no dependence on higher order moments. This hydrodynamic force for pure states is entirely equivalent to the quantum force that appears in Bohmian mechanics,

$$F_{\mathrm{hyd}}\bigg|_{\mathrm{pure}} = -\frac{\partial Q}{\partial q} \tag{3.23}$$

which is the gradient of the Bohmian quantum potential as defined previously [16],

$$Q = -\frac{\hbar^2}{2m}\frac{1}{\langle\rho\rangle_q^{1/2}}\frac{\partial^2\langle\rho\rangle_q^{1/2}}{\partial q^2} \tag{3.24}$$

This term introduces all the quantum effects into the hydrodynamic equations. It can also be regarded as a measure of the shape induced internal stress and hence is closely related to the stress tensor for the

37

probability fluid. Another important property of the quantum potential is that it retains information on the initial conditions of the wavefunction at $t = 0$. Quantum mechanics is known as a *non-local* theory i.e. every part of the quantum system depends on all other parts. In the conventional interpretation of quantum theory, it is not immediately obvious of the root of this non-locality. However, in this hydrodynamic derivation of quantum theory this non-locality is attributable to the quantum potential.

If the quantum potential is neglected then classical equations are yielded that are *local* in nature. This fundamental difference is illustrated further in the results section.

3.4 Hydrodynamic Force for Mixed States and Classical Distributions: Defining a classical limit

The discussion above for pure states can be expanded to include mixes states [28]. The same general form of the equations of motion,

$$\frac{d\langle\rho\rangle_q}{dt} = -\frac{\langle\rho\rangle_q}{m}\frac{\partial\bar{p}}{\partial q}$$

$$\frac{d\bar{p}(q,t)}{dt} = -\frac{\partial V}{\partial q} + F_{\text{hyd}}\Big|_{\text{mixed}} \qquad (3.25)$$

where F_{hyd} is the now mixed state hydrodynamic force,

$$F_{\text{hyd}}\Big|_{\text{mixed}} = -\frac{1}{m}\langle\rho\rangle_q^{-1}\frac{\partial\sigma_q}{\partial q}\Big|_{\text{mixed}} \qquad (3.26)$$

with variance

$$\sigma_q\Big|_{\text{mixed}} = \langle\mathcal{P}^2\rho\rangle_q\Big|_{\text{mixed}} - \bar{p}_q^2\langle\rho\rangle_q \qquad (3.27)$$

Although the equations are general for both mixed and pure states, the notation is added for clarity. However, the moment hierarchy

does not close for a mixed state and Eq. (3.22) does not apply. To accurately capture the form of σ_q, the infinite hierarchy of moments is required.

These same equations derived for mixed and pure quantum states are also valid for the equivalent classical phase space distribution, ρ_{cl}. The same procedure for the classical distribution yields a classical hydrodynamic force defined analogous to Eq. (3.26) as,

$$F_{\text{hyd}}^{\text{cl}} = -\frac{1}{m} \langle \rho_{cl} \rangle_q^{-1} \frac{\partial \sigma_q^{\text{cl}}}{\partial q} \qquad (3.28)$$

A classical limit of the hydrodynamic description will therefore yield the classical hydrodynamic force as defined in Eq. (3.28). Note that this is very different to the classical limit as defined in pure state hydrodynamics (i.e. Bohmian dynamics). In the Bohmian derivation, the quantum force simply vanishes, within limit $\hbar \to 0$.

3.5 Hydrodynamic Phase Space and comparison with Liouville space

Liouville phase space trajectories are very different to trajectories from a hydrodynamic representation. This is because the hydrodynamic momentum is an average of the Liouville phase space momentum, given by,

$$\bar{p}(q) = \frac{\langle \mathcal{P} \rho \rangle_q}{\langle \rho \rangle_q} \qquad (3.29)$$

The hydrodynamic phase space [12, 16, 25] is therefore defined with the momentum variable given as $p = \bar{p}$. Distribution functions within this representation is expressed as

$$\rho_{\text{hyd}}(q, p) = \langle \rho \rangle_q \delta(p - \bar{p}_q) \qquad (3.30)$$
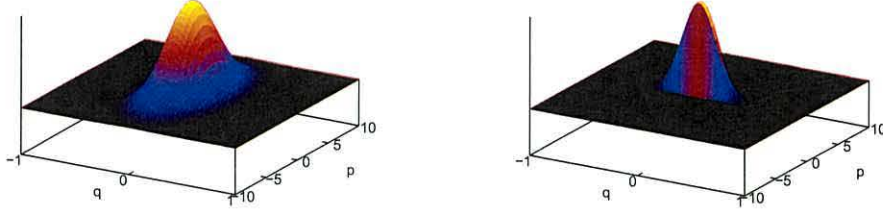
Figure 3.1: Gaussian Wigner function in full phase space along with the hydrodynamic phase space distribution with $p = \bar{p}$.

This is depicted in Fig. (3.1). Note that ρ_{hyd} has a Gaussian form in q but a delta 'spike' in momentum coordinate p. The Lagrangian trajectory equations in hydrodynamic space are given as,

$$\dot{q} = \frac{p}{m}$$
$$\dot{p} = -\frac{\partial}{\partial q}V(q) + F_{\text{hyd}}(q) \qquad (3.31)$$

For the Liouville phase representation however, the momentum p is an actual momentum variable, and hence the distribution function is a full 2D phase space density, also shown in Fig. (3.1). The difference between trajectories as derived from the hydrodynamic and Liouville pictures for a harmonic oscillator is illustrated here. This along with the previous classical limit considerations will form a basis for the combination of the Liouville trajectories with hydrodynamic trajectories in the hybrid approach illustrated in Chapter 4.

Both the Wigner phase space picture and the hydrodynamic picture allow for convenient connection to a classical-like trajectory evolution [27]. The Wigner phase space picture yields Hamilton type Liouville dynamics while the hydrodynamic picture is associated

40

with fluid dynamical, Lagrangian type dynamics. The Lagrangian, hydrodynamic trajectory equations have already been presented in Eq. (3.31), so the trajectory equations for the Liouville/Wigner space are also shown here.

Given the equation of motion for the Wigner function Eq. (2.32) and a phase space continuity equation by analogy to the classical Liouville equation [19] expressed as

$$\frac{\partial}{\partial t}\rho_W = -\nabla_{qp}\mathbf{j_{qp}} \tag{3.32}$$

with the phase space current $\mathbf{j}_{qp} = (\dot{q}\rho_W, \dot{p}\rho_W)$, the trajectory equations are given by [29]

$$\begin{aligned} \frac{dq}{dt} &= \frac{p}{m} \\ \frac{dp}{dt} &= -\frac{\partial V}{\partial q} + \frac{\hbar}{24}\frac{\partial^3 V}{\partial q^3}\frac{1}{\rho_W}\frac{\partial^2 \rho_W}{\partial p^2} + O(\hbar^4) \end{aligned} \tag{3.33}$$

The quantum correction term here is to be interpreted as a different type of quantum force compared to the hydrodynamic force written in Eq. (3.31). An important feature of Eq. (3.33) is that it reduces to classical Hamilton's equations for harmonic potentials since the quantum correction terms involve third order derivatives and higher of the potential. The quantum trajectories from the Wigner function do not fulfil Liouville's theorem. This means that the density is not conserved along a given trajectory. This along with the fact that the quantum correction terms in Eq. (3.33) are difficult to treat computationally, strongly suggest that other quantum trajectory pictures are preferred.

Fig. (3.2) depicts the two different phase space trajectory approaches
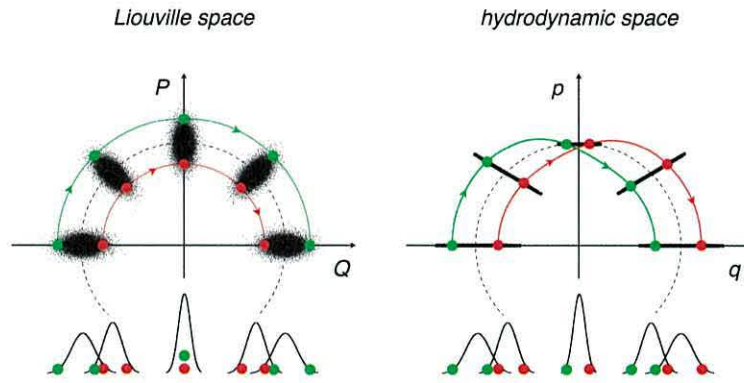
41

Figure 3.2: Time evolution of a Gaussian wavepacket on a harmonic potential. The left hand side shows the Liouville phase space representation while the right hand side panel shows the hydrodynamic space representation. Figure taken from Ref. [27]

for a harmonic oscillator. The hydrodynamic representation contains an additional 'quantum force' even for this harmonic case. Under the phase space plots are the corresponding coordinate space q densities. The initial Gaussian form of the density is retained throughout the propagation. The usual elliptic orbits are observed in Liouville phase space, with maximum momenta at $q = 0$ and a maximum amplitude at $p = 0$; this is characteristic of a harmonic potential. The density in the Wigner picture is shown as an elliptic distribution in phase space. However, the hydrodynamic distribution is represented as a line because of an *average* momentum. The edge of the distribution functions in both the Wigner and hydrodynamic pictures are indicated with green and red points. By following the evolution of these particles (i.e. the trajectory), very different behaviour is observed for the hydrodynamic case as compared to the Wigner representation. For the Wigner picture, the trajectories never cross in phase space as they evolve around the elliptic paths. However, in the coordinate representation, it is evident that the trajectories cross each other at $q = 0$. For a hydrodynamical description, the complete opposite is true. Here the trajectories never cross in positional space owing to the presence of the hydrodynamic force.

The overall conclusion upon comparing the two different representation here, and the classical limits considerations, is that in a mixed quantum-classical scheme, it is preferred that the quantum sector is described hydrodynamically, while the classical sector retains a Hamiltonian/Liouville picture. The classical limit in the hydrodynamical picture yields a classical hydrodynamic force, and so the resulting trajectories are non-Hamiltonian type. The simplicity of

Hamiltonian trajectories is preferred for the classical sector, so a Liouville space representation is used. Furthermore, the Liouville phase space representation is the most natural picture for the classical sector, as it directly relates to conventional molecular dynamics schemes. Of course one may obtain 'quantum' trajectories from a Liouville space representation. Unfortunately, this formulation has its own disadvantages including violating Liouville's theorem. To this end, the mixed quantum-classical approach developed in Chapter 4 is hydrodynamic with respect to the quantum subspace and classical-Liouvillian with respect to the classical subspace.

The following section presents the Wigner function, lowest three hydrodynamic moments and quantum trajectories for the harmonic oscillator, double well potential and Eckart barrier. All the hydrodynamic quantities were derived from the underlying wavefunction for that particular potential. The intention is to illustrate the use of the Wigner function, moments and quantum trajectories as an alternative to propagating wavefunctions for the various systems. Because the hydrodynamic quantities are extracted from the underlying wavefunction, the results presented are for pure quantum states.

3.6 Results

3.6.1 Harmonic Oscillator

The dynamics of a Wigner function, $\rho_W(q, p)$, in a harmonic oscillator potential,

$$V(q) = V_2 q^2 \tag{3.34}$$
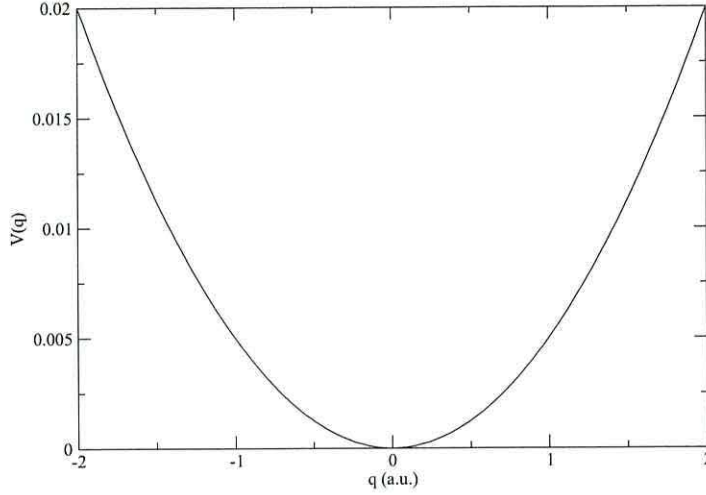
Figure 3.3: Harmonic oscillator potential with $V_2 = 0.005$

with $V_2 = 0.005$ and mass of $10,000$ a.u. is illustrated in Fig. (3.4). The potential is shown in Fig. (3.3). The initial Gaussian form of $\rho_W(q,p)$ is given by,

$$\rho_W(q,p,t_0) = \frac{1}{\pi\hbar}e^{2\beta(q-q_0)^2 - \frac{p^2}{2\beta\hbar^2}} \tag{3.35}$$

with Gaussian width $\beta = 10$ and initial displacement from equilibrium $q_0 = 0.75$. The oscillations within the harmonic potentials occur with a regular period. At $t = 0$, the Wigner function is evenly distributed around the displacement $q_0 = 0.75$ with an overall momentum of $p = 0$. Here it is narrowest in q and widest in p. As the Wigner function moves away from this initial position towards the centre of the well, the distribution spreads in the position q space whilst it narrows and becomes negative in the momentum p space. A maximum negative value in momentum space is reached when the density passes through the centre of the well. At this time, $t = 38.7$ fs, the Wigner function is at its widest in q space and its narrowest in p space. After the density passes through equilibrium position, $q = 0$, the influence of the potential reduces the magnitude of p

45

gradually until the centre of $\rho_W(q, p)$ reaches the turning point of $q = -0.75$. Once the Wigner function reaches the left hand side turning point, the width is once more narrowest in position space and widest in momentum space (net $p = 0$). On the return oscillation, the phase of the momentum is opposite, as seen in the positivity in momentum space at $t = 92$ fs. It is evident that during the propagation that correlations exist between the width of the Wigner function in q and p space: a large uncertainty in position space coincides with little uncertainty in momentum space. The dynamics of the Wigner function is therefore consistent with the Heisenberg uncertainty principle.

The hydrodynamic moments for the harmonic potential described in this section are easily evaluated by a numerical integration of the Wigner function over the momentum space,

$$\langle \mathcal{P}^n \rho \rangle_q = \int dp \, p^n \rho_W \tag{3.36}$$

The moments can be equivalently extracted from the underlying wavefunction, ψ, as follows,

$$
\begin{aligned}
\langle \rho \rangle_q &= \psi^* \psi \\
\langle \mathcal{P} \rho \rangle_q &= m j(q) = \frac{\hbar}{2i} \left(\psi(q, t)^* \frac{\partial \psi(q, t)}{\partial q} - \psi(q, t) \frac{\partial \psi(q, t)^*}{\partial q} \right) \\
\langle \mathcal{P}^2 \rho \rangle_q &= 2mT(q) = \frac{1}{4} \left(\psi^* \frac{\partial^2}{\partial q^2} \psi - 2 \frac{\partial}{\partial q} \psi^* \frac{\partial}{\partial q} \psi + \psi \frac{\partial^2}{\partial q^2} \psi^* \right)
\end{aligned}
\tag{3.37}
$$

The first three hydrodynamic moments are illustrated in Fig. (3.5). Because the 0th moment corresponds to the density, $\rho = \psi^* \psi$, its dynamics is characteristic of a wavefunction in a harmonic potential. The initial density, placed at $q = 0.75$ moved towards the potential

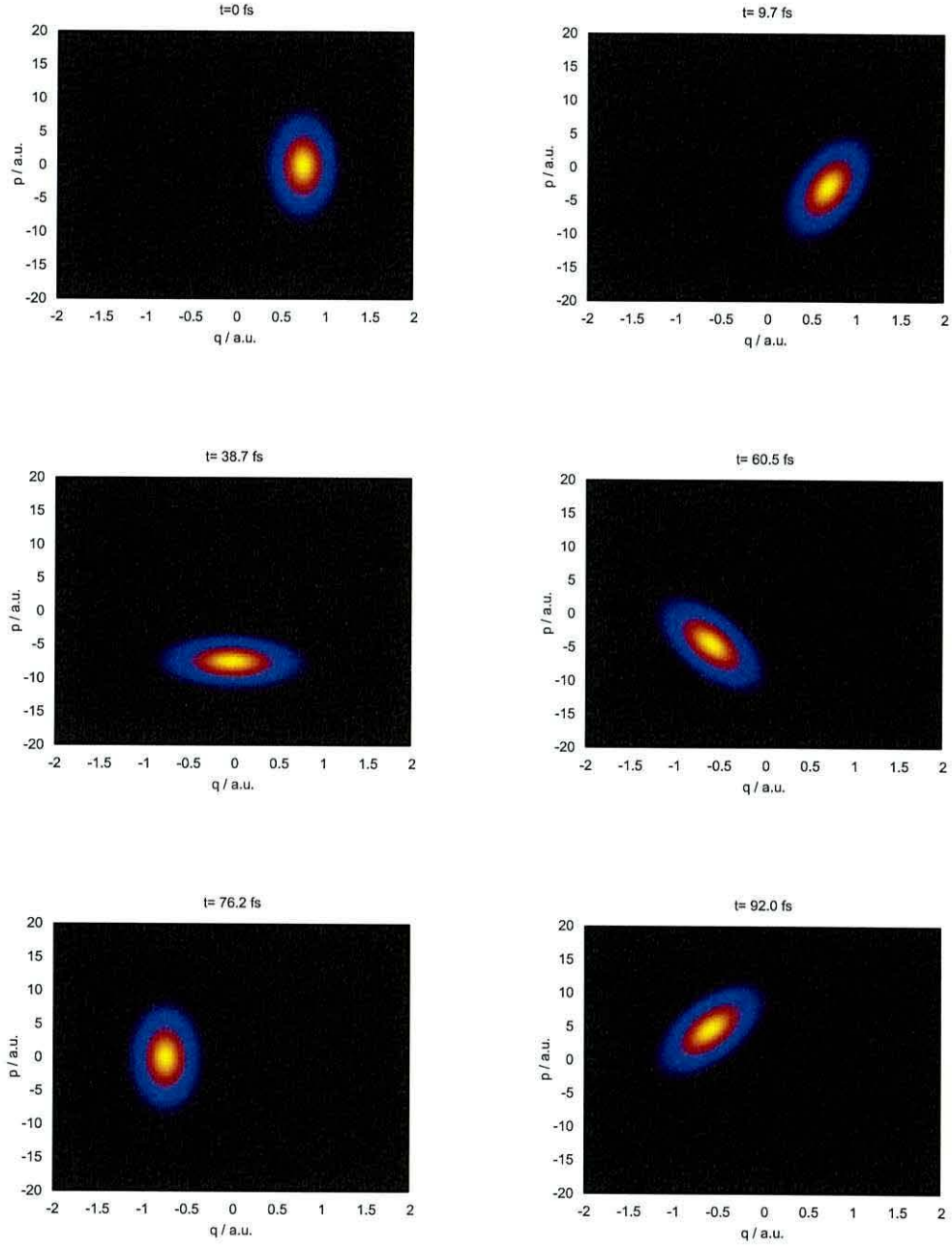46

Figure 3.4: Snapshots of the Wigner function evolving in the harmonic potential. The highest density is denoted by the yellow colour ($\rho = 0.4$), followed by red ($\rho = 0.3$), purple ($\rho = 0.1$) and black ($\rho \leq 0$).

minimum at $q = 0$. This is accompanied by a broadening of the density. As the density passes the equilibrium point and approaches the opposite turning point $q = -0.75$, it narrows to its original width $\beta = 10$. The 0th moment simply broadens and narrows as it oscillates within the well with turning point q_m with frequency defined by the potential.

The 1st moment, initially zero develops a negative Gaussian form that increases in height and width until it peaks at $q = 0$. This suggests that the quantum flux is at maximum when the density is centred at $q = 0$. As the density continues to move towards $q = -0.75$, the Gaussian form of $\langle \mathcal{P} \rho \rangle_q$ reduces in magnitude until it becomes zero at the turning point. The density then returns from $q = -0.75$ towards the equilibrium position. The first moment now acquires an increasing Gaussian profile as before, but in the positive region. This change of polarity is due to the opposite direction in which the density is now moving. This periodic motion of $\langle \mathcal{P} \rho \rangle_q$ between the turning point of the density is seen to continue during the propagation with the frequency of the harmonic oscillator.

Finally, the initial Gaussian form of $\langle \mathcal{P}^2 \rho \rangle_q$ centred at $q = 0.75$ again broadens and increases in height as it moves towards the potential minimum, $q = 0$. This can be rationalised in classical terms, as the second moment corresponds to the kinetic energy density. As the density moves towards the centre of the well, the potential energy decreases to a minimum so for a constant total energy, the kinetic energy must increase. The Gaussian profile of $\langle \mathcal{P}^2 \rho \rangle_q$ then shrinks as the density moves to the opposite turning point $q = -0.75$. This implies the decrease in kinetic energy that occurs is as a result of the potential energy increasing. This oscillatory motion again continues

48

periodically throughout the propagation.

Trajectories are obtained from Eq. (3.31) with hydrodynamic force computed from the moments as defined in Eq. (3.21). In this example, 10 discrete point, equally spaced between $q = 0.6$ and $q = 0.8$ are chosen as initial launch point for subsequent trajectory analysis. This can be considered as discrete sampling of the wavepacket of the system. The evolution of the particles are shown in the trajectories of Fig. (3.6). At $t = 0$, the trajectories are closely spaced, which corresponds to the narrow structure of the initial Wigner function in q space. Both quantum and classical forces (∇Q and ∇V) then act on the particles. The effect of the classical force, ∇V on the particles is linear function in space. This suggests that particles located at q_m feels only a classical force. Particles that are further away from q_m are increasingly influenced by the quantum force, ∇Q. Furthermore, the larger the Gaussian width (corresponds to small β parameter) the less particles far from q_m are influenced by the quantum potential. Hence, the initial closely spaced particles at $t = 0$ are pushed away from the Gaussian maximum, causing a greater spreading of the particles. This increase in width eventually decreases the influence of the quantum potential so that the dominant force acting on the particles is ∇V. This classical force brings the trajectories closer together so the narrow width Wigner density in q space is recovered. This spreading and contracting motion is then repeated with the frequency of the harmonic oscillator.

A further insight is obtained by comparison of the quantum trajectories with their classical counterparts. The classical trajectories
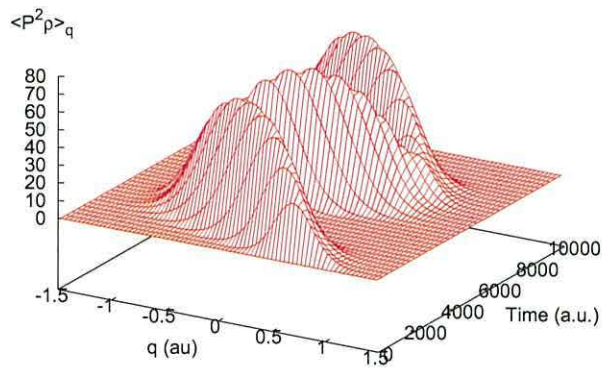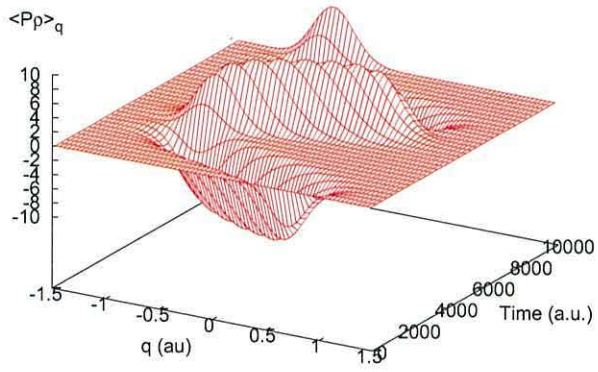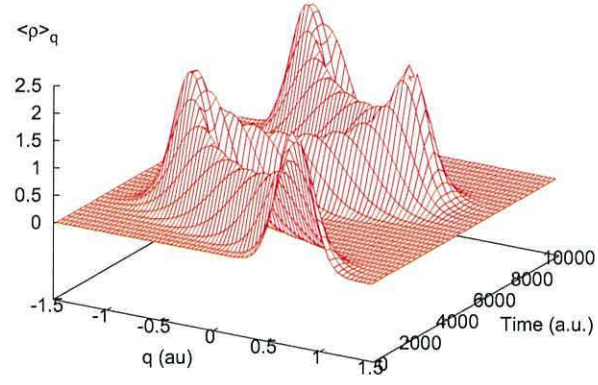
Figure 3.5: The dynamics of the first three hydrodynamic moments of the harmonic oscillator
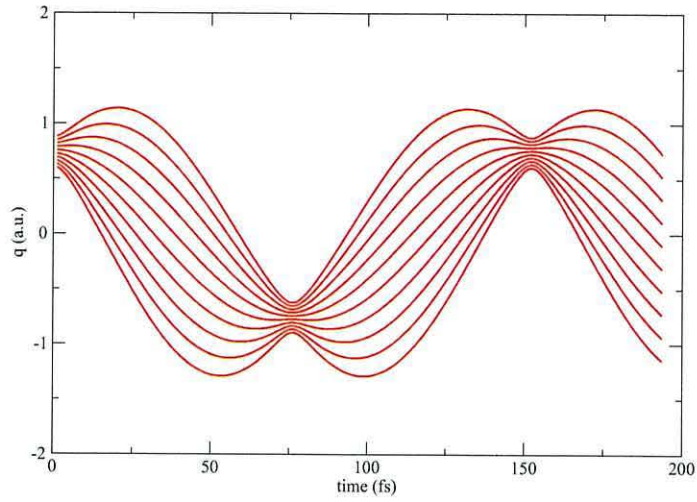
Figure 3.6: Quantum trajectories for the harmonic potential
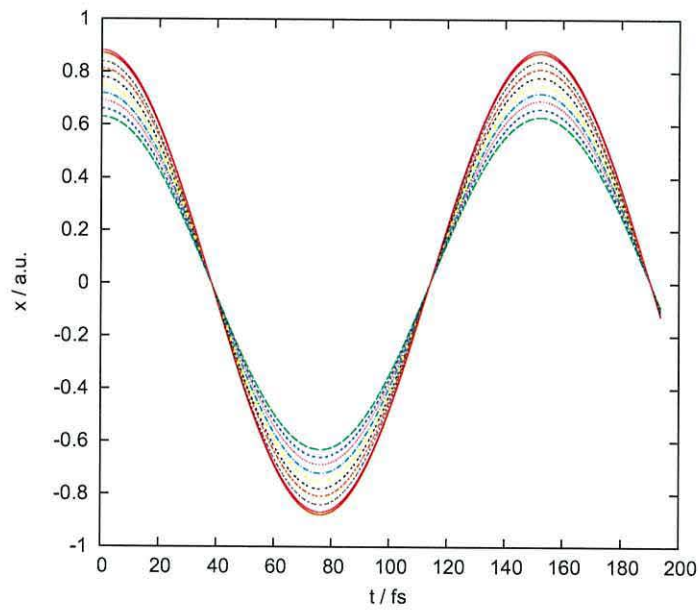
Figure 3.7: Corresponding classical trajectories for the harmonic oscillator.
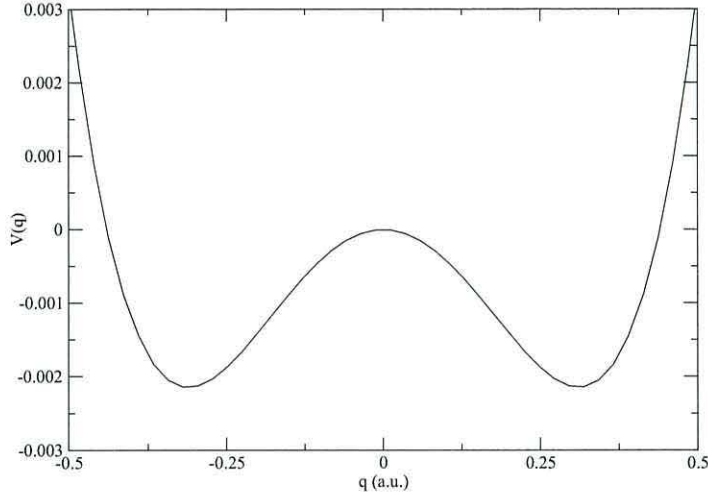
Figure 3.8: Double well potential with $V_2 = -0.044$ and $V_4 = 0.229$.

are obtained by the integration of Newton's equations of motion (or Hamilton's equations). Fig. (3.7) captures the dynamics of the classical trajectories that are launched from exactly the same initial conditions. The most noticeable difference between the two different types of trajectories is that classical trajectories cross in coordinate space (e.g. at $t = 46$ fs). Quantum trajectories, however do not cross. The quantum force prevents the quantum trajectories from crossing each other. This can be traced back to the definition of Q as defined in Eq. (3.24). As the quantum trajectories gets closer, the amplitude R, increases. The quantum potential has the amplitude in the denominator, so Q increases dramatically. This has the effect of pushing the trajectories apart.

3.6.2 Double Well Potential

Phase space analysis can equally be applied to more complex systems such as those governed by double well potentials. The double well
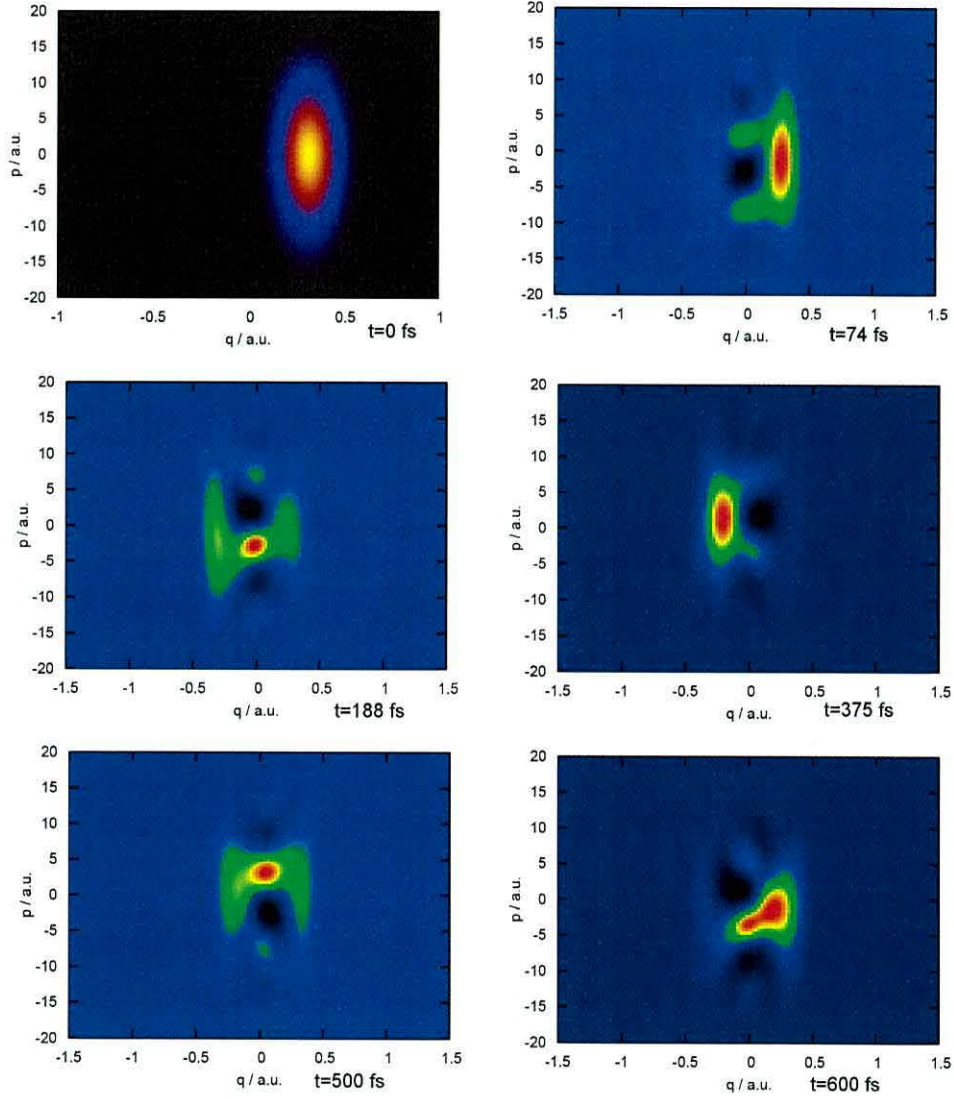
Figure 3.9: Snapshots of the Wigner density evolving in the double well potential. The highest density is denoted by red ($\rho = 0.4$), followed by yellow ($\rho = 0.3$), green ($\rho = 0.2$), purple ($\rho = 0.1$) and black ($\rho < 0$).

53
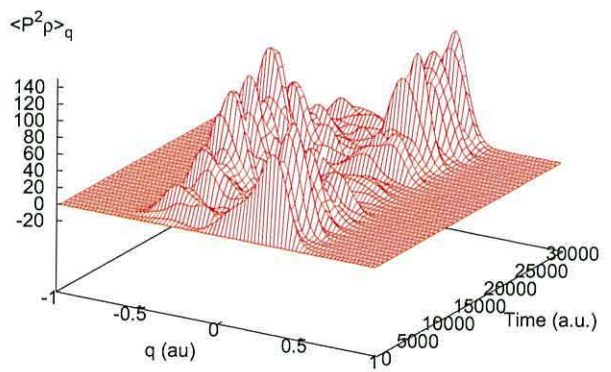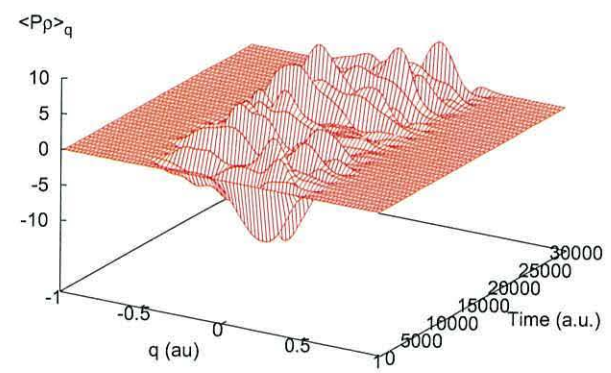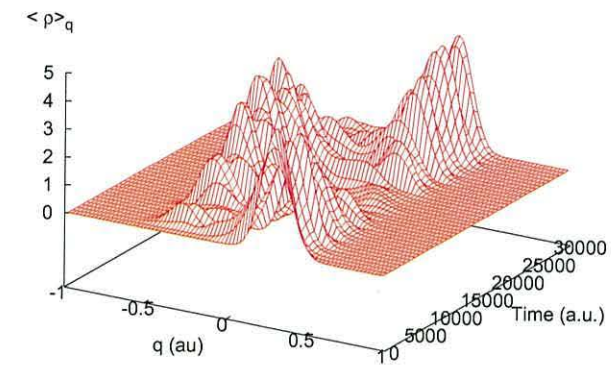
Figure 3.10: First three hydrodynamic moments for the double well potential
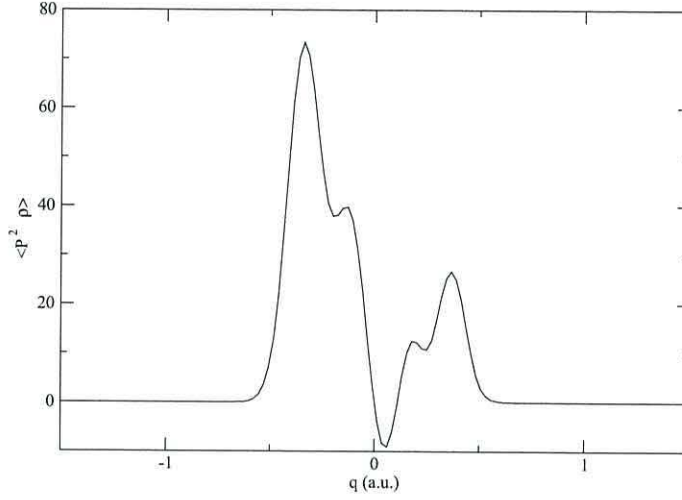
Figure 3.11: The second moment showing negative regions.

used in this example is given by,

$$V(q) = V_2 q^2 + V_4 q^4 \tag{3.38}$$

with parameters $V_2 = -0.044$, $V_4 = 0.229$ and mass of $m = 20341$ a.u, and is illustrated in Fig. (3.8). The initial Gaussian form of $\rho_W(q,p)$ as given in Eq. (3.35) has width $\beta = 32$ and initial displacement from equilibrium $q_0 = 0.313$, shown in Fig. (3.9). As the Wigner function moves from its initial position, it is seen to broaden in q space as it narrows in p space. This initial trend is similar to that observed for the harmonic potential. However, the Wigner density exhibits tiny ripples (starting at $t = 74$ fs). As time progresses, a significant portion of the Wigner density appears in the left hand side well (at $t = 188$ fs). This illustrates the quantum mechanical phenomenon of tunnelling. By $t = 375$ fs, the bulk of the density is in the left hand side well. At $t = 500$ fs, the tunnelling is repeated in the opposite direction, so that the Wigner density transfers back to the initial right hand side well, at $t = 600$ fs.

A particular feature seen in the propagation of the Wigner density that is characteristic for anharmonic potentials such as the double well is the development of 'black' areas, seen particularly at $t = 74$ fs in Fig. (3.9). These represent regions of negative probability density. These negative probability density regions develop as result of the 'quantum' summation that appears in the Wigner Moyal equation. This accentuates the fact that the Wigner function is a pseudo probability density function in that it does not satisfy

$$\rho_Q(q, p, t) \geq 0 \qquad (3.39)$$

As already demonstrated, the negative regions do not appear for Gaussian states in harmonic oscillators since the Wigner Moyal equation Eq. (2.32) is truncated at the $n = 1$ level. In this case, the Wigner Moyal reduces to the classical Liouville equation,

$$\frac{\partial \rho_W}{\partial t} = -\frac{P}{m} \frac{\partial \rho_W}{\partial q} + \frac{\partial V}{\partial q} \frac{\partial \rho_W}{\partial P} \qquad (3.40)$$

The first three hydrodynamic moments for the double well potential were evaluated as defined Eq. (3.36) and are depicted in Fig. (3.10). The 0th moment which represents the density is seen to become delocalised in both minima of the potential at approximately $t = 15000$ a.u. Although the energy of the underlying wavefunction has insufficient energy to surmount the barrier, the transfer of probability density is achieved by quantum tunnelling. Furthermore, by close inspection, it is apparent that at much shorter timescales (e.g. between $1 - 5000$ a.u. and between $25000 - 30000$ a.u. in Fig. (3.10)), $\langle \rho \rangle_q$ exhibits intra-well oscillatory behaviour around the initial displacement $q_0 = 0.313$. Because this initial displacement is very close

56

to the minimum of the double well potential, the intra-well oscillation is extremely small and difficult to observe. A larger displacement from the minimum would ensure more pronounced intra-well dynamics. Note also that the initial Gaussian form of $\langle \rho \rangle_q$ is not retained throughout the propagation, as is the case for the harmonic potential. The complicated profile that develops is characteristic of anharmonic potentials.

The first moment, $\langle \mathcal{P}\rho \rangle_q$, initially zero, acquires a positive profile as the density starts to move within the well. As the density tunnels to the left hand side well at $t = 15000$ a.u., the first moment appears in the well also. The first moment becomes negative as the density, $\langle \rho \rangle_q$, moves in the negative direction within the well. In general, the motion of the first moment captures the quantum flux of the density as it evolves along the double well potential.

The second moment, $\langle \mathcal{P}^2 \rho \rangle_q$, is also illustrated in Fig. (3.10). The dynamics follows closely that of the 0th moment. The initial Gaussian profile quickly spreads into a complex function that spans into the second minimum of the double well potential. Note also that $\langle \mathcal{P}^2 \rho \rangle_q$ contains negative regions during the propagation, as is depicted in Fig. (3.11). The negative region develops due to the negative basins that were seen in the Wigner density for the double well. As described previously, this is due to quantum interference effects.

Quantum trajectories for a double well are shown in Fig. (3.12). The initial equally spaced particles between $q = 0.6$ a.u. to $q = 1.7$ a.u. move away from each other as they evolve within the right hand
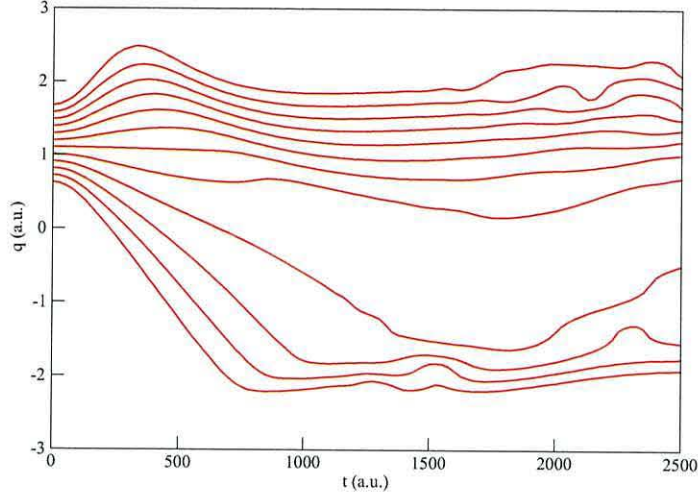
Figure 3.12: Quantum trajectories for the double well potential

side well. Note that at $t = 500$ a.u., 4 of the trajectories tunnel to the left hand side of the well, which corresponds to 30% of the total density. The remaining trajectories remain in the right hand side well, but shows some oscillatory motion within the well. Again, this is a characteristic feature of a non-minimum density evolving in a double well potential. As seen for the quantum trajectories in the harmonic oscillator case, the quantum trajectories keep well apart due to the influence of the quantum potential.

3.6.3 Eckart Barrier

The Eckart barrier used in this example Fig. (3.13) is given by

$$V(q) = V_0 \text{sech}^2[a(q - q_0)] \qquad (3.41)$$

where the barrier of height $V_0 = 0.024$ is placed at $q = 0$ and width parameter $a = 2.5$. The initial Gaussian Wigner function, depicted in Fig. (3.14) is launched towards the barrier with average translational energy $E_{\text{trans}} = 0.018$ au and mass $m = 2000$ au. The Wigner

58
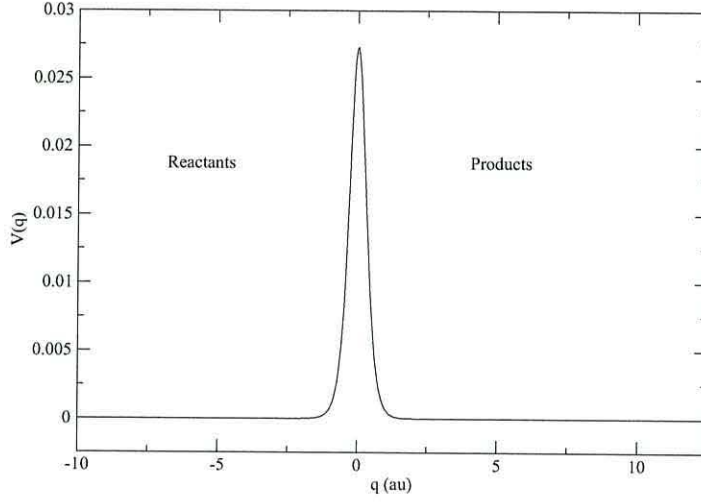
Figure 3.13: Eckart barrier with parameters $V_0 = 0.024$ au and $a = 2.5$

function centred at $q = -2$ is narrower in coordinate q space and wider in momentum p space, as governed by the Heisenberg uncertainty principle. At a later time of $t = 24.2$ fs, the Wigner density can be seen to split after collision with the barrier. The part of the Wigner density that has been reflected now is centred at momentum $p = -7$ a.u. as the direction of motion of the density is reversed. The region that has tunnelled through the barrier is centred at coordinate $q = 3$ retains the initial positive value for momentum as the density still moves in the same direction. Note that the transmitted density is narrower in q space and broader in p space.

The 0th, 1st and 2nd moments as derived from the Wigner function are illustrated in Fig. (3.15). The 0th moment traces exactly the dynamics of the probability density. The initial Gaussian located at $q = -2$ moves towards the barrier. At $t = 12.1$ fs, just as the density collides with the barrier, $\langle \rho \rangle_q$ is seen to split into two parts.

59

Some of the density reflects against the barrier and return towards the initial position of the density. The remainder of the density tunnels through the barrier, and continues to move in the same direction. This is further described by looking at the 1st moment. At time 24.2 fs and later, two distinct regions of $\langle \mathcal{P}\rho \rangle_q$ develop. The reflected region acquires a negative value whilst the transmitted part remains positive. The polarity of $\langle \mathcal{P}\rho \rangle$ is a direct consequence of the direction of motion of the 0th moment. The description is elaborated by considering the dynamics of the 2nd moment. Again, the dynamics is similar to that of the 0th moment, but related to the kinetic energy density.

Trajectories that are obtained from Eq. (3.31) for the Eckart barrier are illustrated in Fig. (3.16). 26 discrete 'particles', equally spaced between $q = -1.35$ and $q = -2.65$ are defined as initial points for the quantum trajectories. As shown for the Wigner density and 0th moment for this Eckart barrier, the density moves towards the right hand side and spreads in q space. This is further illustrated by the trajectories moving away from each other. This displays very similar dynamics to that of a free wavepacket (i.e. $V = 0$). However, at $t = 400$ au, which corresponds to the centre of the density colliding with the barrier, 16 of the trajectories (labelled black) seem to separate from the remaining 10 (labelled red). The black trajectories correspond to the part of the density that is reflected and the red trajectories correspond to the part of the density that tunnel through the barrier. It is again clear that the trajectories do not cross as they are kept apart under the influence of the quantum potential.
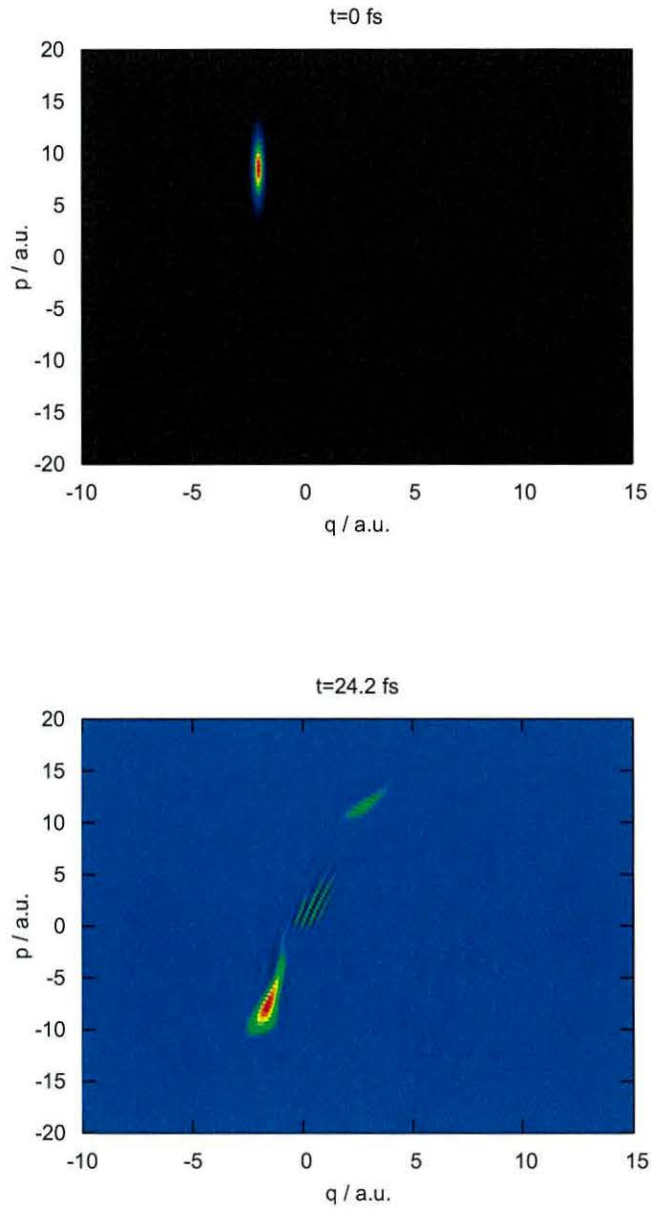
Figure 3.14: Two snapshots of the Wigner density scattering on the Eckart barrier. The highest density is denoted by red ($\rho = 0.4$), followed by yellow ($\rho = 0.3$), green ($\rho = 0.2$), purple ($\rho = 0.1$) and black ($\rho < 0$).
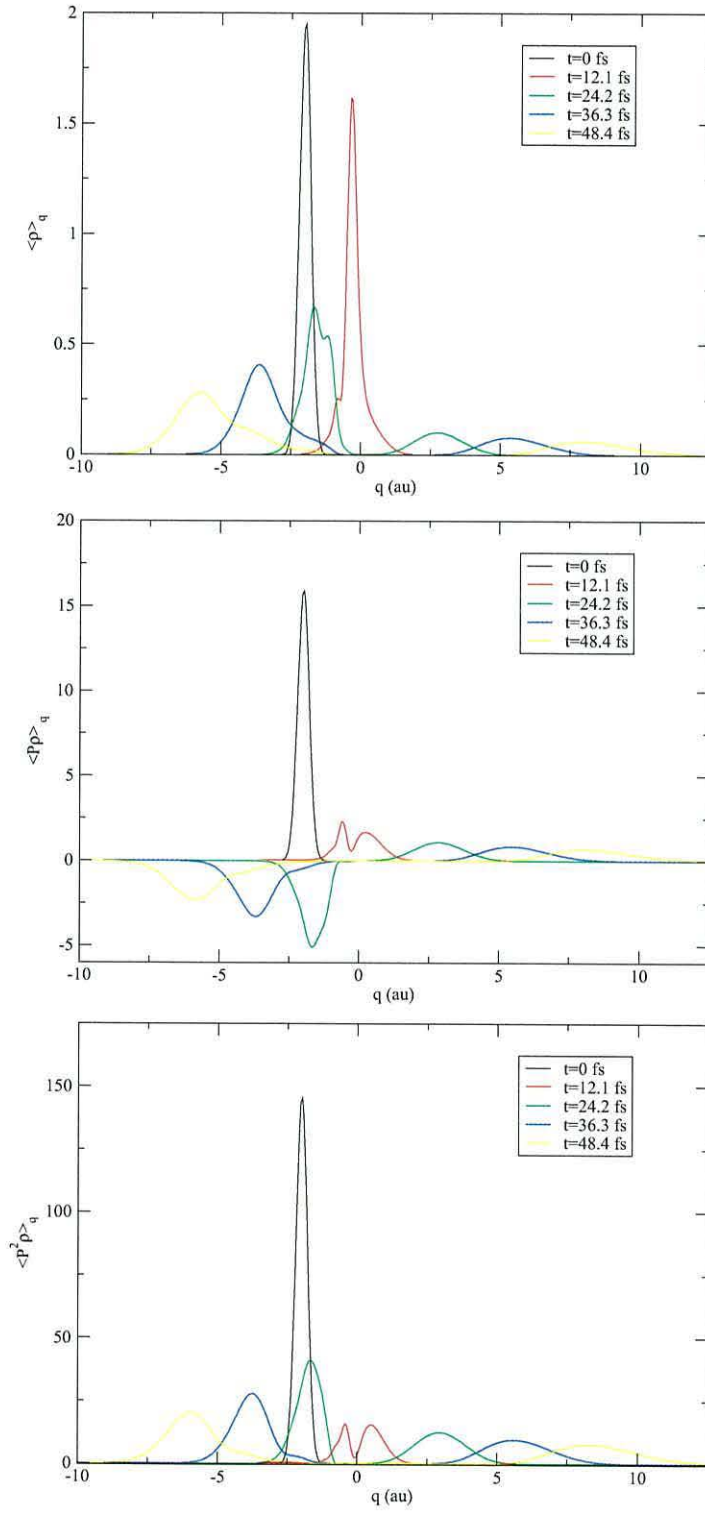
Figure 3.15: 0th, 1st and 2nd hydrodynamic moments for the Eckart barrier.
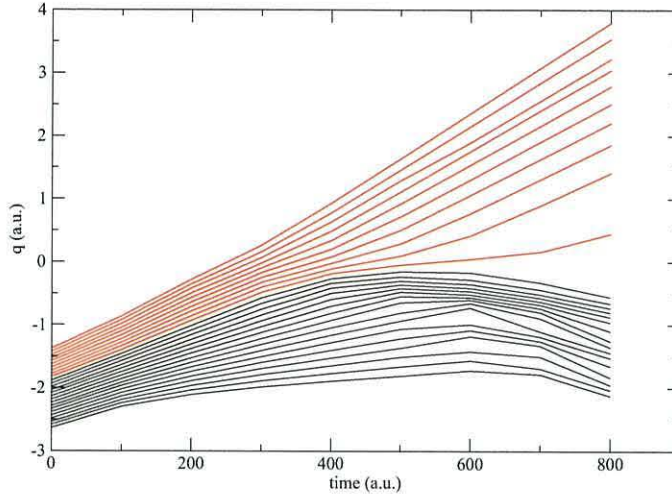
Figure 3.16: Quantum trajectories associated with the Eckart barrier.

3.7 Summaries

This Chapter has shown the derivation of quantum hydrodynamics for mixed quantum states. The derivation can be made from either the density operator or its phase space equivalent, the Wigner function. Moments were derived for mixed states, and it was seen that an infinite hierarchy of hydrodynamic moments were required to fully characterise the quantum density. This was shown to be quite different to the moments of a pure quantum state, where the hierarchy naturally breaks at $n = 1$. The link between the pure state case and Bohmian mechanics was also established.

The mixed state hydrodynamic force was derived from the moments, and was shown to be an integral part of the derived Lagrangian trajectory equations. Classical limit considerations concluded that a classical limit taken in the quantum hydrodynamic picture yields a 'classical' hydrodynamic force. This results in non-Hamiltonian type 'classical' trajectories. A direct comparison was also made of

63

trajectories as obtained for Liouville space and hydrodynamic space. These discussions will ease the justification of combining a hydrodynamic, quantum representation with a classical Liouville picture in the Mixed Quantum-Classical Moment approach of Chapter 4.

The Chapter closed with illustrations of the Wigner function, hydrodynamic moments and quantum trajectories for the harmonic oscillator, double well and Eckart barrier potential functions. This aids in developing an understanding and intuition of the use of hydrodynamics for quantum dynamical problems.

Bibliography

[1] D. J. Tannor, *Introduction to Quantum Mechanics, A Time-Dependent Perspective*, University Science Books, 2007.

[2] E. Madelung, Z. Phys. **40**, 332 (1926).

[3] L. de Broglie, *Introduction a l'etude de la mecanique ondulatoire*, Hermann, Paris, 1930.

[4] D. Bohm, Phys. Rev. **85**, 166 (1952).

[5] L. de Broglie, *Tentative d'interpretation causale et non-lineaire de la mecanique ondulatoire*, Gauthier-Villars, Paris, 1956.

[6] L. de Broglie, Compt. Rend. **183**, 447 (1926).

[7] D. Bohm, Phys. Rev. **85**, 180 (1952).

[8] Z. S. Wang, G. R. Darling and S. Holloway, J. Chem. Phys. **115**, 10373 (2001).

[9] D. Babyuk, R. E. Wyatt and J. H. Frederick, J. Chem. Phys. **119**, 6482 (2003).

[10] A. Sanz, F. Borondo and S. Miret-Artes, J. Chem. Phys. **120**, 8794 (2004).

[11] R. E. Wyatt, *Quantum Dynamics with Trajectories: Introduction to Quantum Hydrodynamics*, Springer, Heidelberg, 2005.

[12] T. Takabayasi, Prog. Theor. Phys. **11**, 341 (1954).

[13] J. E. Moyal, Proc. Cambridge Philos. Soc. **45**, 99 (1949).

[14] J. H. Irving and R. W. Zwanzig, J. Chem. Phys. **19**, 1173 (1951).

[15] H. Fröhlich, Physica **37**, 215 (1967).

[16] I. Burghardt and L. S. Cederbaum, J. Chem. Phys. **115**, 10303 (2001).

[17] E. Wigner, Phys. Rev. **40**, 749 (1932).

[18] M. Hillery, R. F. O'Connell, M. O. Scully, and E. P. Wigner, Phys. Rep. **106**, 121 (1984).

[19] W. P. Schleich, *Quantum Optics in Phase Space*, Wiley-VCH, Berlin, 2001.

[20] M. Ploszajczak and M. J. Rhoades-Brown, Phys. Rev. Lett. **55**, 147 (1985).

[21] W. R. Frensley, Rev. Mod. Phys. **62**, 745 (1990).

[22] J. V. Lill, M. I. Haftel, and G. H. Herling, Phys. Rev. A **39**, 5832 (1989).

[23] L. M. Johansen, Phys. Rev. Lett. **80**, 5461 (1998).

[24] P. R. Holland, *The Quantum Theory of Motion*, Cambridge University Press, New York, 1993.

[25] I. Burghardt and K. B. Møller, J. Chem. Phys. **117**, 7409 (2002).

[26] J. G. Muga, R. Sala, and R. F. Snider, Physica Scripta **47**, 732 (1993).

[27] K. H. Hughes, S. M. Parry, G. Parlant and I. Burghardt, J. Chem. Phys. A **111**, 10269 (2007).

[28] I. Burghardt, K. B. Møller, and K. H. Hughes, Quantum hydrodynamics and a moment approach to quantum-classical theory, in *Quantum Dynamics of Complex Molecular Systems*, edited by D. A. Micha and I. Burghardt, Springer, 2006.

[29] A. Donoso and C. C. Martens, Phys. Rev. Lett. **87**, 223202 (2001).

Chapter 4

Mixed Quantum-Classical Dynamics: The QCM Approach

4.1 Introduction

The main aim of mixed quantum-classical dynamics is to treat the 'light' particles quantum mechanically and use a classical picture (usually a trajectory approach) for the remaining degrees of freedom. As stated in the main Introduction, it is not clear how to combine the quantum and classical subsystems in a single framework [1]. The two approaches are fundamentally different; quantum mechanics is statistical and nonlocal in nature while classical mechanics is local and provided the initial conditions are known, is fully deterministic. Quantum mechanics is only deterministic in that the wavefunction may be calculated for all time given the initial conditions and the Hamiltonian. The major conceptual problem arises at the interface between the two sectors, particularly with regard to how both sectors

influence each other. The motion of the classical particles induces transitions in the quantum part of the system. Hence, the potential energy surface is modified. This in turn changes the force that act on the classical particles. There is a definite dynamical interaction between the two subsystems. This issue of 'self-consistency' is crucial in all hybrid approaches that are developed.

Examples of how the combination of the quantum and classical sectors can be achieved are the Ehrenfest mean-field approach [2], surface hopping methods [3, 4], mixed quantum-classical Liouville approach [6, 7, 8, 9, 10, 11, 12, 13, 14, 5] and the mixed quantum-classical Bohmian (MQCB) method [15, 16].

The earliest attempt at a mixed quantum-classical approach was the mean-field approximation developed by Ehrenfest. When a quantum coordinate q interacts with a classical coordinate Q with momentum P, the total potential energy of the system can be written as a sum of the quantum, classical and interaction contributions,

$$V(q, Q) = V_{qu} + V_{cl} + V_{int} \tag{4.1}$$

This interaction potential, V_{int}, is calculated along a particular classical trajectory which yields a time dependent interaction term, $V_{int}(q, Q(t))$. The dynamics for the quantum part is given by the solution of Schrödinger equation using this time dependent potential, $V_{int}(q, Q(t))$. From the solution, a mean interaction potential $\tilde{V}_{int}(Q; t)$ is evaluated by averaging over the wavefunction,

$$\tilde{V}_{int}(Q; t) = \langle \psi | V_{int}(q, Q(t)) | \psi \rangle \tag{4.2}$$

The dynamics of the classical subsystem is finally obtained by solving Hamilton's equations with this mean potential $\tilde{V}_{int}(Q, t)$. Because the classical part only experiences a mean-field from the quantum part and never truly responds to the instantaneous quantum coordinate, the approach is deemed to be too approximate and is inadequate in particular where nonadiabatic effects play an important role in the dynamics [18, 17]. For the case when these nonadiabatic effects are important, a Surface hopping approach [3, 4] was developed where the probability of hopping from one adiabatic potential to another is incorporated into the classical trajectories.

More recently, better approaches that have been developed include the mixed quantum-classical Bohmian method and the mixed quantum-classical Liouville method. In the MQCB method [15, 16, 19], the dynamics of the whole system is defined in a Langrangian trajectory framework. Central to the Bohmian interpretation of quantum mechanics is the quantum potential [20, 21, 22, 24, 25] $Q = -\hbar^2/(2m)\langle\rho\rangle_q^{-1/2}\partial^2/\partial q^2\langle\rho\rangle_q^{1/2}$. This is a non-local potential that depends on the curvature of the wavefunction and has associated with it all the quantum effects within the system. In the MQCB method, the quantum potential is simply neglected in the classical sector, resulting in Newtonian (totally classical) equations of motion. The quantum subspace, however, has a Bohmian hydrodynamic description where the classical coordinates appear as a parameter.

Finally, in the mixed quantum-classical Liouville approach [6, 7, 8, 9,

10, 11, 12, 13, 14, 5], a partial Wigner transform of the density operator, ρ, is performed on the classical subspace, which maintains the operator form of the quantum part, and the classical part is defined by functions of the classical phase-space variables position, Q and momentum, P. The equations of motion involve a linearized approximation to the exponential time evolution operator in the classical subspace. This keeps terms to lowest order in $\hbar$.

The approach presented and developed in this thesis focuses on the novel quantum-classical moment (QCM) approach [26, 27, 28] introduced by Burghardt and Parlant. Here, the quantum subsystem is treated hydrodynamically and the classical subsystem is kept in a Liouville phase-space setting. The method starts with a Wigner function for the total system, $\rho_W(q, p, Q, P; t)$, where the hybrid quantum-classical equations are defined in terms of particular type of moments which are obtained by integrating over the quantum momentum only, $\langle \mathcal{P}^n \rho \rangle_{qQP} = \int \mathrm{d}p^n \rho_W(q, p; Q, P)$. These key quantities that are central to this approach are referred to as *partial* moments. These are responsible for combining the hydrodynamic representation in the quantum subspace with a Liouvillian phase space picture in the classical subspace. Exact equations of motion can be derived for these partial moments followed by invoking a classical approximation in the classical (QP) subspace. To obtain trajectory equations for this approach, the moment equations must be transformed from a static Eulerian grid to the Lagrangian framework. These trajectory equations involve a quantum force that is dependent on both quantum and classical positions (q, Q) and the classical momentum (P).

This methodology has been applied previously to coupled harmonic oscillators, but the hybrid approach is extended in this Chapter to more complicated systems. The present application focuses on trajectories for a double-well potential coupled to a harmonic coordinate and an Eckart barrier coupled to a harmonic coordinate. Although the illustration here is for pure states, the method naturally extends to mixed states.

4.2 General Formulation

4.2.1 Partial Hydrodynamic Moments

The partial moments are constructed by introducing a hydrodynamic projection for selected degrees of freedom. Starting from the Wigner function for two coordinate degrees of freedom (four-dimensional phase space $\rho_W(q, p, Q, P)$), one integrates over the quantum phase space momentum only [27],

$$\langle \mathcal{P}^n \rho \rangle_{qQP} = \int \mathrm{d}p \ p^n \rho_W(q, p; Q, P) \tag{4.3}$$

These are hydrodynamic moments in quantum coordinate q, parameterised in the classical phase-space variables (QP). The moments can be also obtained from a mixed coordinate space/phase-space representation, given by,

$$\langle \mathcal{P}^n \rho \rangle_{qQP} = \left(\frac{\hbar}{i} \right)^n \frac{\partial^n}{\partial r^n} \rho(q, r; Q, P) \Big|_{r=0} \tag{4.4}$$

The moments can otherwise be considered as the Wigner transform of a set of (q, Q, P) dependent coordinate space partial moments $\langle \mathcal{P}^n \rho \rangle_{qQR}$,

$$\langle \mathcal{P}^n \rho \rangle_{qQP} = \frac{1}{2\pi\hbar} \int \mathrm{d}R \ \exp(-iPR/\hbar) \langle \mathcal{P}^n \rho \rangle_{qQR} \tag{4.5}$$

with

$$\langle \mathcal{P}^n \rho \rangle_{qQR} = \left(\frac{\hbar}{i} \right)^n \frac{\partial^n}{\partial r^n} \rho(q, r; Q, R) \Big|_{r=0} \qquad (4.6)$$

These coordinate space partial moments, $\langle \mathcal{P}^n \rho \rangle_{qQR}$ are in fact coefficients in a Taylor expansion of the mixed coordinate-space-phase-space density, $\rho(q, r; Q, R)$, given by,

$$\rho(q, r; Q, P) = \sum_n \frac{1}{n!} \langle \mathcal{P}^n \rho \rangle_{qQP} \left(\frac{ir}{\hbar} \right)^n \qquad (4.7)$$

Here, the distribution $\rho(q, r; Q, P)$ plays the role of a moment generating function [29].

As is the case for a purely hydrodynamic description developed in Chapter 3, the moments can carry redundant information. If the quantum density is of a pure state, all the dynamical information that is required is embedded within the first two moments and these decouple from the remaining of the hierarchy. Another special case is a Gaussian mixed state density. Here the density is determined by the first three moments [27, 28]. For the general case of a mixed state, an infinite number of moments are required to fully characterise the quantum density. In this case, a numerical truncation scheme is required to approximately terminate the moment hierarchy at a certain order.

4.2.2 Partial Moment Equations

Equations of motion for the partial moments can be derived systematically from the quantum Liouville equation $\partial \rho / \partial t = -i/\hbar [H, \rho]$, in a coordinate-space representation or else from the phase-space Wigner representation [27]. Because of the Taylor series expansion

of Eq. (4.7), it is more convenient to carry out part of the derivation in coordinate space before using a Fourier transform relation to obtain the moments in terms of phase-space variables. For this derivation, which follows Ref. [27], consider the following Hamiltonian,

$$H = \frac{p^2}{2m} + \frac{P^2}{2M} + V(q, Q) \tag{4.8}$$

The (x, x') coordinate space representation of the Liouville-von Neumann equation for this Hamiltonian is given by,

$$
\begin{aligned}
\frac{\partial}{\partial t}\rho(x, x'; X, X') &= \left[\frac{i\hbar}{2m}\left(\frac{\partial^2}{\partial x^2} - \frac{\partial^2}{\partial x'^2} \right) + \frac{i\hbar}{2M}\left(\frac{\partial^2}{\partial X^2} - \frac{\partial^2}{\partial X'^2} \right) \right]\rho(x, x'; X, X') \\
&\quad - \frac{i}{\hbar}[V(x, X) - V(x', X')]\rho(x, x'; X, X')
\end{aligned} \tag{4.9}
$$

A simple transformation to the sum x and difference r coordinates with $q = (x + x')/2$ and $r = x - x'$ yields the following form,

$$\frac{\partial}{\partial t}\rho(q, r; Q, R) = \frac{\partial_k}{\partial t}\rho(q, r; Q, R) + \frac{\partial_v}{\partial t}\rho(q, r; Q, R) \tag{4.10}$$

with both kinetic (k) and potential (v) parts. The kinetic part is given by,

$$\frac{\partial_k}{\partial t}\rho(q, r; Q, R) = i\hbar \left(\frac{1}{m}\frac{\partial^2}{\partial r \partial q} + \frac{1}{M}\frac{\partial^2}{\partial R \partial Q} \right)\rho(q, r; Q, R) \tag{4.11}$$

and the potential part,

$$
\begin{aligned}
\frac{\partial_v}{\partial t}\rho(q, r; Q, R) = \quad &- \frac{i}{\hbar}\Big[V\left(q + \frac{r}{2}, Q + \frac{R}{2} \right) \\
&- V\left(q - \frac{r}{2}, Q - \frac{R}{2} \right) \Big]\rho(q, r; Q, R)
\end{aligned} \tag{4.12}
$$

To ease the derivation, the kinetic and potential energy terms are discussed separately.

Kinetic Part

By taking successive moments of $\rho(q, r; Q, R)$ as defined in Eq. (4.6) and inserting them into Eq. (4.11) , it is evident that the first term on the right hand side is a moment of one order greater than that on the left hand side i.e.

$$
\begin{aligned}
i\hbar \frac{1}{m} \frac{\partial^2}{\partial r \partial q} \rho(q, r; Q, R) &= \frac{i^2}{m} \frac{\hbar}{i} \frac{\partial^2}{\partial r \partial q} \rho(q, r; Q, R) \\
&= -\frac{1}{m} \frac{\partial}{\partial q} \langle \mathcal{P} \rho \rangle_{qQR} \qquad (4.13)
\end{aligned}
$$

giving the general form,

$$
\frac{\partial_k}{\partial t} \langle \mathcal{P}^n \rho \rangle_{qQR} = -\frac{1}{m} \frac{\partial}{\partial q} \langle \mathcal{P}^{n+1} \rho \rangle_{qQR} + \frac{i\hbar}{M} \frac{\partial^2}{\partial R \partial Q} \langle \mathcal{P}^n \rho \rangle_{qQR} \quad (4.14)
$$

On Fourier transform $R \to P$, i.e. $\langle \mathcal{P} \rho \rangle_{qQP} = \int_{-\infty}^{\infty} \langle \mathcal{P}^n \rho \rangle_{qQR} \exp(-iPR/\hbar) \mathrm{d}R$, in a phase-space setting, the kinetic part is written,

$$
\begin{aligned}
\frac{\partial_k}{\partial t} \langle \mathcal{P}^n \rho \rangle_{qQP} = &- \frac{1}{m} \frac{\partial}{\partial q} \langle \mathcal{P}^{n+1} \rho \rangle_{qQP} \\
&+ \frac{i\hbar}{M} \int_{-\infty}^{\infty} \frac{\partial^2}{\partial R \partial Q} \langle \mathcal{P}^n \rho \rangle_{qQR} \exp\left(-\frac{iPR}{\hbar}\right) \mathrm{d}R
\end{aligned}
$$

$$(4.15)$$

Recognising that

$$
\int_{-\infty}^{\infty} \frac{\partial}{\partial R} \langle \mathcal{P}^n \rho \rangle_{qQR} \exp\left(-\frac{iPR}{\hbar}\right) \mathrm{d}R = \frac{i}{\hbar} P \langle \mathcal{P}^n \rho \rangle_{qQP} \qquad (4.16)
$$

the kinetic part reads,

$$
\frac{\partial_k}{\partial t} \langle \mathcal{P}^n \rho \rangle_{qQP} = -\frac{1}{m} \frac{\partial}{\partial q} \langle \mathcal{P}^{n+1} \rho \rangle_{qQP} - \frac{P}{M} \frac{\partial}{\partial Q} \langle \mathcal{P}^n \rho \rangle_{qQP} \qquad (4.17)
$$

The up-coupling to a higher order moment $(n + 1)$ in the kinetic part of the moment equation is the origin of the infinite hierarchy of momentum moments for mixed state densities.

Potential Part

To obtain the potential part of the moment equations, a Taylor expansion of both sides of Eq. (4.12) with respect to r is taken. Because the time derivatives of the coordinate space moments $\langle \mathcal{P}^n \rho \rangle_{qQR}$ are given by,

$$\frac{\partial_v}{\partial t} \rho(q, r; Q, R) = \sum_n \frac{1}{n!} \frac{\partial_v}{\partial t} \langle \mathcal{P}^n \rho \rangle_{qQR} \left(\frac{ir}{\hbar} \right)^n \qquad (4.18)$$

coefficients can be matched to obtain equations of motion for the coordinate moments $\langle \mathcal{P}^n \rho \rangle_{qQR}$. A Wigner transform $R \to P$ then yields the corresponding equations of motion for the $\langle \mathcal{P}^n \rho \rangle_{qQP}$. From Eq. (4.12) and Eq. (4.18) , both V and $\rho(q, r; Q, R)$ are written as a Taylor expansion in r,

$$\begin{aligned}
\sum_n \frac{1}{n!} \frac{\partial_v}{\partial t} \langle \mathcal{P}^n \rho \rangle_{qQR} \left(\frac{ir}{\hbar} \right)^n &= -\frac{i}{\hbar} \sum_l \frac{1}{l!} \Big[V^{(l)} \Big(q, Q + \frac{R}{2} \Big) \\
&\quad -(-1)^l V^{(l)} \Big(q, Q - \frac{R}{2} \Big) \Big] \Big(\frac{r}{2} \Big)^l \\
&\quad \times \sum_\kappa \frac{1}{\kappa!} \langle \mathcal{P}^\kappa \rho \rangle_{qQR} \left(\frac{ir}{\hbar} \right)^\kappa \qquad (4.19)
\end{aligned}$$

where $V^{(l)}(q, Q) = (\partial^l V(q, Q)/\partial q^l)$. By matching coefficients on both sides i.e. $n = l + \kappa$, the potential part of the equation of motion for the partial moments in coordinate-space $\{\langle \mathcal{P}^n \rho \rangle_{qQR}\}$ can be written

$$\begin{aligned}
\frac{\partial_v}{\partial t} \langle \mathcal{P}^n \rho \rangle_{qQR} = &- \sum_{l=0}^{n} \binom{n}{l} \left(\frac{\hbar}{2i} \right)^{l-1} \frac{1}{2} \Big[V^{(l)} \Big(q, Q + \frac{R}{2} \Big) \\
&- (-1)^l V^{(l)} \Big(q, Q - \frac{R}{2} \Big) \Big] \langle \mathcal{P}^{n-1} \rho \rangle_{qQR} \qquad (4.20)
\end{aligned}$$

Upon a transformation $R \to P$, the corresponding Wigner space moments $\{\langle \mathcal{P}^n \rho \rangle_{qQP}\}$ are given by

$$\frac{\partial_v}{\partial t} \langle \mathcal{P}^n \rho \rangle_{qQP} = -\sum_{l=0}^{n} \binom{n}{l} \left(\frac{\hbar}{2i} \right)^{l-1} \int dP' J^{(l)}(q, Q, P')$$

76

$$\times \langle \mathcal{P}^{n-1} \rho \rangle_{qQ(P+P')} \qquad (4.21)$$

where $\langle \mathcal{P}^n \rho \rangle_{qQ(P+P')} = \langle \mathcal{P}^n \rho \rangle(q, Q, P + P')$. The quantity $J^{(l)}$ is the probability of a momentum jump [30] in P, associated with the lth potential derivative in q, $V^{(l)}$

$$\begin{aligned}
J^{(l)}(q, Q, P') &= \frac{1}{4\pi\hbar} \int \mathrm{d}R \left[V^{(l)}\left(q, Q + \frac{R}{2}\right) \right. \\
&\quad \left. - (-1)^l V^{(l)}\left(q, Q - \frac{R}{2}\right) \right] \exp(-iP'R/\hbar) \; (4.22)
\end{aligned}$$

The potential part of the equation of motion for the Wigner space moments can be more conveniently expressed as having separate classical and quantum parts,

$$\begin{aligned}
\frac{\partial_v}{\partial t} \langle \mathcal{P}^n \rho \rangle_{qQP} &= -n \frac{\partial V(q, Q)}{\partial q} \langle \mathcal{P}^{n-1} \rho \rangle_{qQP} \\
&\quad + \frac{\partial}{\partial Q} V(q, Q) \frac{\partial}{\partial P} \langle \mathcal{P}^n \rho \rangle_{qQP} + \mathcal{C}_{\mathrm{qu}} \qquad (4.23)
\end{aligned}$$

The term $\mathcal{C}_{\mathrm{qu}}$ brings in all the quantum effects into the dynamics. The $\hbar$ dependent term may expanded as

$$\begin{aligned}
\mathcal{C}_{\mathrm{qu}} &= -\sum_{l=0}^{n} \binom{n}{l} \left(\frac{\hbar}{2i}\right)^{l-1} \int \mathrm{d}P' \tilde{J}^{(l)}(q, Q, P') \\
&\qquad\qquad\qquad\qquad \times \langle \mathcal{P}^{n-1} \rho \rangle_{qQ(P+P')} \qquad (4.24)
\end{aligned}$$

with $\tilde{J}$ now redefined as,

$$\begin{aligned}
\tilde{J}^{(0)}(q, Q, P') &= \left(\frac{\hbar}{2i}\right) \frac{\partial}{\partial Q} V(q, Q) \frac{\partial}{\partial P'} \delta(P') \\
&\quad + \frac{1}{4\pi\hbar} \int \mathrm{d}R \left[V^{(0)}\left(q, Q + \frac{R}{2}\right) \right. \\
&\quad \left. - (-1)^l V^{(0)}\left(q, Q - \frac{R}{2}\right) \right] \exp(-iP'R/\hbar)
\end{aligned}$$

$$(4.25)$$

and

$$\tilde{J}^{(1)}(q, Q, P') = - \quad V^{(1)}(q, Q)\delta(P')$$

77

$$+\frac{1}{4\pi\hbar}\int \mathrm{d}R\left[V^{(1)}\left(q,Q+\frac{R}{2}\right)\right.$$
$$\left.-(-1)^l V^{(1)}\left(q,Q-\frac{R}{2}\right)\right]\exp(-iP'R/\hbar)$$

$$(4.26)$$

For $l > 1$, $\tilde{J}^{(l)} = J^{(l)}$.

The exact moment equations for the more specific potential $V(q,Q) = V_q(q) + V_{\mathrm{int}}(q,Q) + V_Q(Q)$ can be summarised as

$$\frac{\partial}{\partial t}\langle \mathcal{P}^n \rho\rangle_{qQP} = \langle \mathcal{P}^n\{H,\rho_W\}_{qp}\rangle_{qQP} + \{H,\langle \mathcal{P}^n \rho\rangle_{qQP}\}_{qQP} + \mathcal{C}_{\mathrm{qu}} \quad (4.27)$$

From this moment approach, the structure of the equation has i) a 'classical' hydrodynamic part in the quantum (q,p) subspace

$$\langle \mathcal{P}^n\{H,\rho_W\}_{qp}\rangle_{qQP} = \quad - \quad \frac{1}{m}\frac{\partial}{\partial q}\langle \mathcal{P}^{n+1}\rho\rangle_{qQP}$$
$$- \quad n\frac{\partial[V_q(q)+V_{\mathrm{int}}(q,Q)]}{\partial q}\langle \mathcal{P}^{n-1}\rho\rangle_{qQP}$$

$$(4.28)$$

(ii) a classical Liouvillian part in the (Q,P) subspace,

$$\{H,\langle \mathcal{P}^n \rho\rangle_{qQP}\}_{QP} = \quad - \quad \frac{P}{M}\frac{\partial\langle \mathcal{P}^n \rho\rangle_{qQP}}{\partial Q}$$
$$+ \quad \frac{\partial[V_Q(Q)+V_{\mathrm{int}}(q,Q)]}{\partial Q}\frac{\partial\langle \mathcal{P}^n \rho\rangle_{qQP}}{\partial P}$$

$$(4.29)$$

and (iii) a mixed hydrodynamic-Liouvillian "quantum correction" part that originates from the potential contribution,

$$\mathcal{C}_{\mathrm{qu}} = \sum_{l=0}^{n}\binom{n}{l}\left(\frac{\hbar}{2i}\right)^{l-1}\int \mathrm{d}P'\,\tilde{J}^{(l)}(q,Q,P')\langle \mathcal{P}^{n-1}\rho\rangle_{qQ(P+P')} \quad (4.30)$$

or more explicitly,

$$\mathcal{C}_{\mathrm{qu}} = \sum_{l_1+l_2\geq 3}(-1)^{l_2+1}\frac{1}{l_2!}\binom{n}{l_1}\left(\frac{\hbar}{2i}\right)^{l_1+l_2-1}$$

78

$$\times \left(\frac{\partial^{l_1+l_2}[V_q(q) + V_{\text{int}}(q,Q) + V_Q(Q)]}{\partial q^{l_1} \partial Q^{l_2}} \right) \frac{\partial^{l_2}}{\partial P^{l_2}} \langle \mathcal{P}^{n-l_1} \rho \rangle_{qQP}$$

(4.31)

where the summation runs over odd values of the sum of indices $l_1 + l_2$ and $l_1 \leq n$.

The hydrodynamic part couples the nth order moment $\langle \mathcal{P}^n \rho \rangle$ to orders $\langle \mathcal{P}^{n\pm 1} \rho \rangle_{qQP}$ while the quantum correction part couples the nth order to $\langle \mathcal{P}^{n-l_1} \rho \rangle_{qQP}$. Furthermore, the Liouvillian part acts only on a given order $\langle \mathcal{P}^n \rho \rangle_{qQP}$. The quantum correction part is closely related to the Wigner-Weyl series in that it contains all $\hbar$ terms and involves odd-order derivatives of potential from third order upwards. An important feature to notice is that even the zeroth and first order moment equations carry explicit $\hbar$ terms which is absent in the purely quantum case. This emphasises the hybrid hydrodynamic-Liouvillian nature of the partial moments generated.

4.2.3 Quantum-Classical Approximation

Since the aim of this approach is to combine both classical and quantum dynamics in a hybrid quantum-classical scheme, a classical approximation must be invoked in the (Q, P) subspace. This is achieved by retaining terms in Eq. (4.31) that involve derivatives of order $l_2 = 0, 1,$. This neglects all terms involving multiple order derivatives with respect to the classical coordinate Q within the equations of motion for the partial moments. The quantum-classical equations of motion thus read [27],

$$\frac{\partial}{\partial t} \langle \mathcal{P}^n \rho \rangle^c_{qQP} = \langle \mathcal{P}^n \{H_q + V_{\text{int}}, \rho_W\}_{qp} \rangle^c_{qQP}$$

$$\{H_Q + V_{\text{int}}, \langle \mathcal{P}^n \rho \rangle^c\}_{QP} + \mathcal{C}^c_{\text{qu}}$$

(4.32)

with now an approximate quantum correction part given by

$$
\begin{aligned}
C_{\mathrm{qu}}^c &= -\sum_{\substack{l_1=3\\ \mathrm{odd}}}^{n} \binom{n}{l_1} \left(\frac{\hbar}{2i}\right)^{l_1-1} \frac{\partial^{l_1} V}{\partial q^{l_1}} \langle \mathcal{P}^{n-l_1} \rho \rangle_{qQP}^c \\
&+ \sum_{\substack{l_1=2\\ \mathrm{even}}}^{n} \binom{n}{l_1} \left(\frac{\hbar}{2i}\right)^{l_1} \frac{\partial^{l_1+1} V}{\partial q^{l_1} Q} \frac{\partial}{\partial P} \langle \mathcal{P}^{n-l_1} \rho \rangle_{qQP}^c \quad (4.33)
\end{aligned}
$$

The superscript c here denotes the classical limit and approximate nature of the quantum correction term. This restriction of retaining only $l_2 = 0, 1$ terms corresponds to linearizing Eq. (4.22) so that

$$
\begin{aligned}
&\left[V^{(l)}\left(q, Q+\frac{R}{2}\right) - (-1)^l V^{(l)}\left(q, Q-\frac{R}{2}\right) \right] \\
&\simeq [1 - (-1)^l] V^{(l)}(q, Q) + \frac{1}{2}\left[1 - (-1)^{l+1}\right] \frac{\partial}{\partial Q} V^{(l)} R \quad (4.34)
\end{aligned}
$$

with

$$
\begin{aligned}
J^{(l=\mathrm{odd})}(q, Q, P') &\simeq \frac{1}{4\pi\hbar} 2 V^{(l)}(q, Q) \int \mathrm{d}R \exp(-iP'R/\hbar) \\
&= V^{(l)}(q, Q)\delta(P') \\
J^{(l=\mathrm{even})}(q, Q, P') &\simeq \frac{1}{4\pi\hbar} \frac{\partial}{\partial Q} V^{(l)} \int \mathrm{d}R\, R \exp(-iP'R/\hbar) \\
&= -\left(\frac{\hbar}{2i}\right) \frac{\partial}{\partial Q} V^{(l)} \frac{\partial}{\partial P'} \delta(P') \quad (4.35)
\end{aligned}
$$

Substituting these expressions into Eq. (4.21) gives the results of Eq. (4.33) A key point here is that within this approximation, the quantum correction terms does not appear in the dynamical equations for the zeroth and first moment. This feature has very important consequences for the Lagrangian trajectory dynamics. The first two partial moments are thus written,

$$
\begin{aligned}
\frac{\partial \langle \rho \rangle_{qQP}^c}{\partial t} &= \langle \{ H_q + V_{\mathrm{int}}, \rho_W \}_{qp} \rangle_{qQP}^c + \{ H_Q + V_{\mathrm{int}}, \langle \rho \rangle_{qQP}^c \}_{QP} \\
&= -\frac{1}{m} \frac{\partial \langle \mathcal{P}\rho \rangle_{qQP}^c}{\partial q} + \{ H_Q + V_{\mathrm{int}}, \langle \rho \rangle_{qQP}^c \}_{QP} \quad (4.36)
\end{aligned}
$$
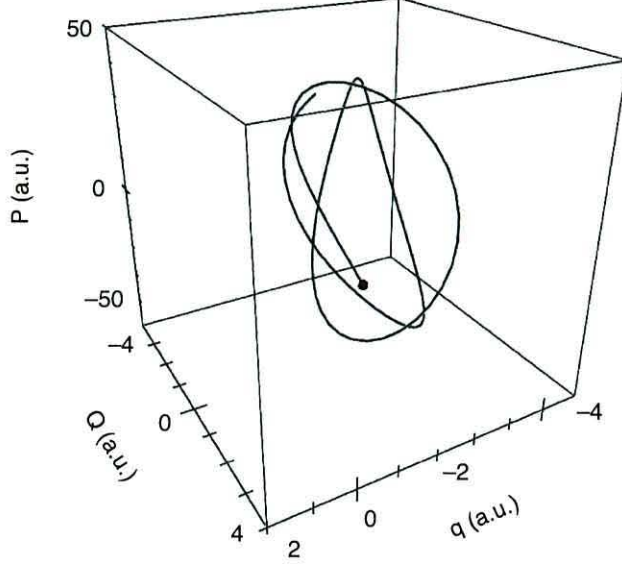
Figure 4.1: Mixed quantum-classical trajectory according to the Lagrangian picture for the three independent variables (qQP). The hydrodynamic fields $\langle \mathcal{P}^n \rho \rangle_{qQP}$ are constructed along the fluid-dynamical path.

and

$$
\begin{aligned}
\frac{\partial \langle \mathcal{P} \rho \rangle^c_{qQP}}{\partial t} &= \langle \mathcal{P} \{ H_q + V_{\text{int}}, \rho_W \}_{qp} \rangle^c_{qQP} + \{ H_Q + V_{\text{int}}, \langle \mathcal{P} \rho \rangle^c \}_{QP} \\
&= -\frac{1}{m} \frac{\partial \langle \mathcal{P}^2 \rho \rangle^c_{qQP}}{\partial q} - \frac{\partial}{\partial q} \Big(V_q(q) + V_{\text{int}}(q, Q) \Big) \langle \rho \rangle^c_{qQP} \\
&\quad + \{ H_Q + V_{\text{int}}, \langle \mathcal{P} \rho \rangle^c_{qQP} \}_{QP}
\end{aligned}
\tag{4.37}
$$

where H_Q is the Hamiltonian for the classical subspace and H_q is the Hamiltonian pertaining to the quantum sector. If the potentials in the classical subspace are harmonic and the coupling between the classical and quantum sectors is at most linear, then the above equations for the partial moments are exact.

81

4.2.4   Lagrangian Trajectory Dynamics

In order to obtain trajectory equations for the mixed quantum-classical scheme, the Eulerian equations of motion for the partial moments must be translated to the Lagrangian framework. To achieve this, the zeroth order moment $\langle \rho \rangle^c_{qQP}$ is interpreted as a hybrid hydrodynamic-Liouvillian continuity equation and the fluid-particle dynamics follows from the definition of the three-component current $\mathbf{j}_{qQP}$

$$
\frac{\partial}{\partial t} \langle \rho \rangle^c_{qQP} = -\frac{1}{m}\frac{\partial}{\partial q} \langle \mathcal{P}\rho \rangle^c_{qQP} + \{ H_Q + V_{\text{int}}, \langle \rho \rangle^c_{qQP} \}_{QP}
$$
$$
\equiv -\nabla_{qQP} \cdot \mathbf{j}_{qQP} \tag{4.38}
$$

with $\nabla_{qQP} = (\partial/\partial q, \partial/\partial Q, \partial/\partial P)$ and the current

$$
\frac{\mathbf{j}_{qQP}}{\langle \rho \rangle^c_{qQP}} = \begin{pmatrix} \dot{q} \\ \dot{Q} \\ \dot{P} \end{pmatrix} = \begin{pmatrix} p_{qQP}/m \\ (\partial H/\partial P) \\ -(\partial H/\partial Q) \end{pmatrix} \tag{4.39}
$$

with the momentum field p_{qQP} defined via,

$$
\langle \mathcal{P}\rho \rangle^c_{qQP} = p_{qQP} \langle \rho \rangle^c_{qQP} \tag{4.40}
$$

This field is the average momentum given by the Wigner function for particular values of (q, Q, P) variables. In the Lagrangian framework, the hydrodynamic fields are calculated along the fluid-particle trajectories as defined by Eq. (4.39). A Lagrangian trajectory evolving in (q, Q, P) space is illustrated in Fig. 4.1. The time evolution in the Lagrangian framework is denoted by the total derivative with respect to time, $d/dt = \partial/\partial t + \mathbf{v}_{qQP} \cdot \nabla_{qQP}$. The translated continuity equation is therefore given by,

$$
\frac{d}{dt} \langle \rho \rangle^c_{qQP} = -\frac{\langle \rho \rangle^c_{qQP}}{m}\frac{\partial}{\partial q} p_{qQP} \tag{4.41}
$$

82

The derivation is completed by combining Eq. (4.39) with the equation for a fluid-particle acceleration dp_{qQP}/dt as obtained from Eq. (4.37) for the first moment $\langle \mathcal{P}\rho \rangle^c_{qQP} = p_{qQP} \langle \rho \rangle^c_{qQP}$. This yields a generalized hydrodynamic force. The resulting trajectory equations [27] correlate the quantum/hydrodynamic variables $(q, p = p_{qQP})$ with the classical variables (Q, P).

$$
\begin{aligned}
\dot{q} &= \frac{p}{m} \\
\dot{p} &= -\frac{\partial}{\partial q}\left(V_q(q) + V_{\text{int}}(q, Q) \right) + F_{\text{hyd}}(q, Q, P) \\
\dot{Q} &= \frac{P}{M} \\
\dot{P} &= -\frac{\partial}{\partial Q}\left(V_Q(Q) + V_{\text{int}}(q, Q) \right)
\end{aligned}
\tag{4.42}
$$

with $p \equiv p_{qQP}$ and the hydrodynamic force

$$
F_{\text{hyd}}(q, Q, P) = -\frac{1}{m \langle \rho \rangle^c_{qQP}} \frac{\partial \sigma_{qQP}}{\partial q}
\tag{4.43}
$$

obtained as the spatial derivative with respect to q of the generalized variance

$$
\sigma_{qQP} = \langle \mathcal{P}^2 \rho \rangle^c_{qQP} - p^2_{qQP} \langle \rho \rangle^c_{qQP}
\tag{4.44}
$$

The term σ_{qQP} describes the width in quantum momentum p for given values of (q, Q, P) of the phase-space distribution function $\rho^c_W(q, p; Q, P)$. Indeed, it is the spatial variation of σ_{qQP} with respect to the quantum coordinate q that defines the hydrodynamic force F_{hyd}. This hybrid hydrodynamic force is equivalent to the hydrodynamic force for the purely quantum case apart from its additional dependence on the classical degrees of freedom (Q, P). Furthermore, if the isolated quantum system is a pure state, then the hydrodynamic force is equivalent to the Bohmian quantum force $F_{\text{hyd}} = -\partial V_{\text{qu}}/\partial q$ [24, 31, 32] with the quantum potential defined as

$$Q = -\hbar^2/(2m)\langle\rho\rangle_q^{-1/2}\partial^2/\partial q^2 \langle\rho\rangle_q^{1/2}.$$

The trajectories of Eq. (4.42) are associated with a phase space distribution function given by,

$$\rho_{\text{hybrid}}(q, p; Q, P) = \langle\rho\rangle_{qQP}^c \delta(p - p_{qQP}) \tag{4.45}$$

This distribution function has characteristics of the underlying Liouville phase space distribution within the classical space. However, it is single valued in quantum momentum p in the quantum space. This is similar to the purely quantum description of Chapter 3, i.e. a delta spike for quantum momentum p.

4.2.5 Pure State Formulation

As shown in Chapter 3 when discussing quantum hydrodynamics, for pure states i.e. $\hat{\rho} = |\psi\rangle\langle\psi|$, certain relations exist between the hydrodynamic moments of $\rho_W^{\text{pure}}(q, p; Q, P)$, that terminates the hierarchy. Particularly, the second order moment $\langle\mathcal{P}^2\rho\rangle_{qQP}$ can be expressed in terms of lower order moment so that these decouple from the rest of the hierarchy [27]. All the required information concerning the state of the system is embedded within the first two moments. The explicit form of the partial moments for a pure state is illustrated here in order to aid the application to the examples presented in this Chapter.

Consider the Wigner function,

$$\rho_W(q, p) = \frac{1}{2\pi\hbar}\int_{-\infty}^{\infty} dr \rho_{\text{pure}}\left(q + \frac{r}{2}, q - \frac{r}{2}\right)\exp\left(-\frac{ipr}{\hbar}\right) \tag{4.46}$$

where

$$\rho_{\text{pure}}\left(q + \frac{r}{2}, q - \frac{r}{2}\right) = \psi\left(q + \frac{r}{2}\right)\psi^*\left(q - \frac{r}{2}\right) \tag{4.47}$$

Taking the partial moments for this distribution by applying a differentiation with respect to the difference coordinate r gives,

$$
\begin{aligned}
\langle \mathcal{P}^n \rho_{\text{pure}} \rangle_{qQP} &= \int \mathrm{d}p\, p^n \rho_W^{\text{pure}}(q, p; Q, P) \\
&= \left(\frac{\hbar}{i} \right)^n \frac{\partial^n}{\partial r^n} \rho_W^{\text{pure}}(q, r; Q, P) \Big|_{r=0} \\
&= \frac{1}{2\pi\hbar} \int_{-\infty}^{\infty} \mathrm{d}R \exp\left(-\frac{iPR}{\hbar} \right) \times \\
\left(\frac{\hbar}{i} \right) \frac{\partial^n}{\partial r^n} &\left[\psi\left(q + \frac{r}{2}, Q + \frac{R}{2} \right) \psi^*\left(q - \frac{r}{2}, Q - \frac{R}{2} \right) \right]_{r=0}
\end{aligned}
\tag{4.48}
$$

Given that the wavefunction is known, the variance $\sigma_{qQP}^{\text{pure}}$ can be constructed from the pure state moments of Eq. (4.48). The hydrodynamic force can then be evaluated,

$$
F_{\text{hyd}}(q, Q, P) = -\frac{1}{m \langle \rho \rangle_{qQP}} \frac{\partial}{\partial q} \sigma_{qQP}^{\text{pure}}
\tag{4.49}
$$

This is the strategy used for the application of the next section.

4.3 Illustrations in Anharmonic Potentials

This section demonstrates the QCM approach for the dynamics of a quantum double well coupled to a classical harmonic coordinate and an Eckart barrier coupled to a harmonic oscillator. Although the QCM approach has been shown to be able to deal with mixed quantum states, this application is for pure states.

The application of the QCM approach to a coupled harmonic oscillator system is shown in detail in Ref. [1]. Although a pair of light (quantum) and heavy (classical) oscillators is considered a relatively 'simple' system to deal with, it poses a significant challenge

for Ehrenfest and surface hopping methods. However, as the calculations involves analytical expressions for the hydrodynamic quantities in the QCM approach, they are not dealt with in this Chapter. The focus of this Chapter is the application of QCM approach to more demanding systems where an analytical solution is not available.

4.3.1 Double Well Coupled to a Harmonic Oscillator

The dynamics of a quantum system subject to a double well potential coupled bilinearly to a classical harmonic oscillator is presented here. The potential function for this system is given by

$$V(q,Q) = V_2 q^2 + V_4 q^4 + V_5 Q^2 + V_6 qQ \qquad (4.50)$$

where the first two terms are the quantum double well, the third term is the classical harmonic mode and the last terms is the bilinear coupling. This potential surface is illustrated in Fig. (4.2) and the parameters are given in Table 1. Because the classical sector is harmonic and the coupling between the sectors is bilinear, the hybrid-hydrodynamic representation of the mixed quantum-classical scheme is exact. Furthermore, the initial pure state of the system is retained throughout the propagation. Because of this, the system is completely defined by the first two moments $\langle \rho \rangle_{qQP}$ and $\langle \mathcal{P}\rho \rangle_{qQP}$.

For the coupled harmonic oscillators, one quantum and one classical [1], an analytical form exists for all the hydrodynamic quantites of the system. However, as the quantum sector in this example is anharmonic, there is no analytical form for the hydrodynamic force. A numeric approach must be adopted here. To this end, the La-
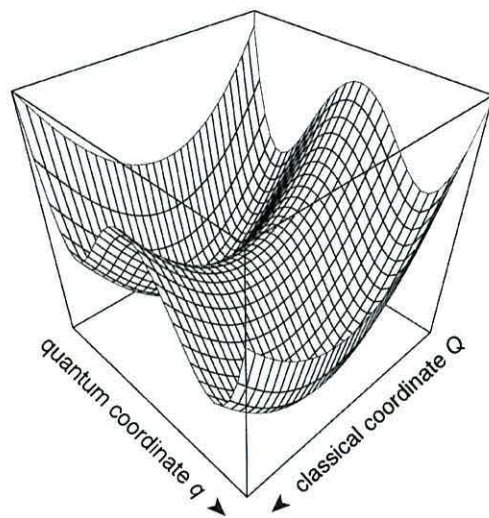
86

Figure 4.2: The double well potential function defined in Eq. (4.50).

grangian trajectory equations of Eq. (4.42) are propagated where the hydrodynamic force F_{hyd} is extracted from the time dependent wavefunction.

In general, numerical approaches to solve dynamical equations in quantum mechanics fall into two main categories; grid based approaches and basis set expansion. In a grid based approach, the Schrödinger equation is solved on discrete points that constitutes an Eulerian grid. Unfortunately, calculating the hydrodynamic force that is required in the trajectory equations would involve interpolating the quantities of interest from the Eulerian grid to a particular point on a Lagrangian grid. This is highly undesirable as is needed at every time step in the propagation scheme. Not only is this computationally expensive, it is a major source of error that is magnified furthermore by derivative calculations required to obtain the hydrodynamic force from the variance σ_{qQP},

$$F(q, Q, P) = -\frac{1}{m\langle\rho\rangle_{qQP}}\frac{\partial}{\partial q}\sigma_{qQP} \qquad (4.51)$$

In a long propagation scheme, the errors are propagated with the trajectories, potentially giving poor results. An alternative method is to utilise a basis set expansion. This is a global method that does not require any interpolation. For non-periodic, bound potentials such as the system studied here, the time-dependent wavefunction $\psi(q, Q, t)$ and therefore the partial moments $\langle\mathcal{P}^n\rho\rangle_{qQP}$ can be expanded in terms of the eigenstates of the system $\phi(q, Q)$ (see Eq. (4.48)),

$$\langle\mathcal{P}^n\rho\rangle_{qQP} =$$
$$\sum_{j,j'} c_j c_{j'} \exp\left(-\frac{i}{\hbar}[E_j - E_{j'}]t\right) \frac{1}{2\pi\hbar} \int \mathrm{d}R \exp\left(-\frac{iPR}{\hbar}\right)$$
$$\times \left(\frac{\hbar}{i}\right)^n \frac{\partial^n}{\partial r^n}\left[\phi_{j'}^*(q - r/2, Q - R/2)\phi_j(q + r/2, Q + R/2)\right]_{r=0}$$

88
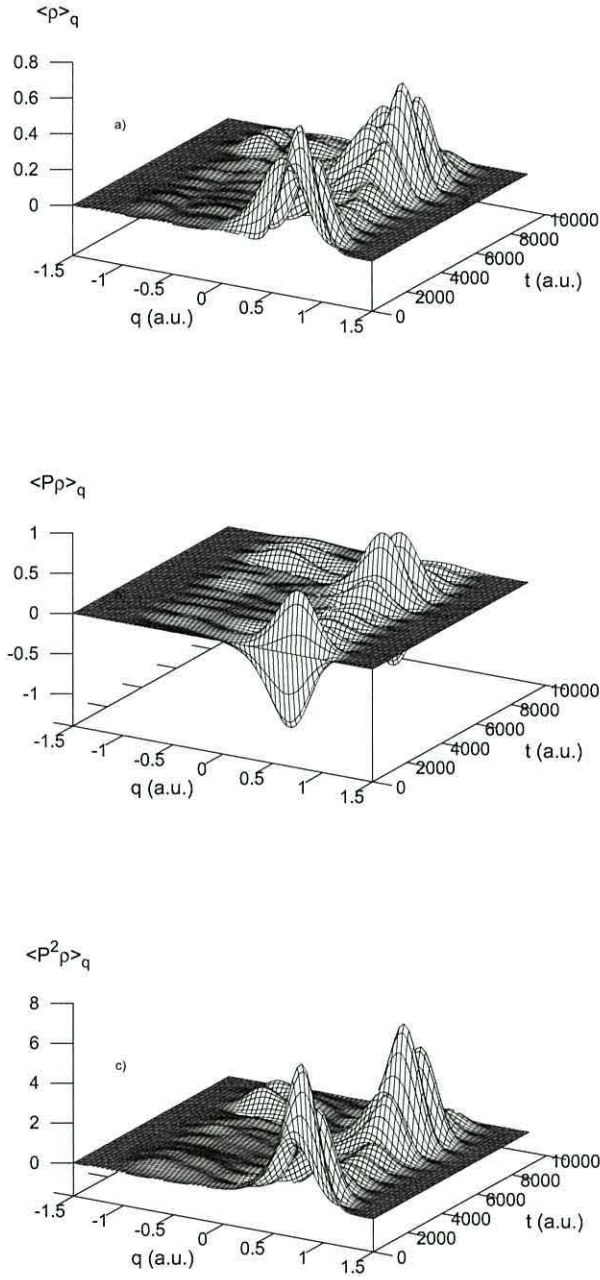
Figure 4.3: The dynamics of the first three moments, calculated in an Eulerian frame for a range of points in the quantum q coordinate and a single point in the classical phase-space $(Q = -0.2, P = 0.0)$, for the double well bilinearly coupled to a classical harmonic oscillator.
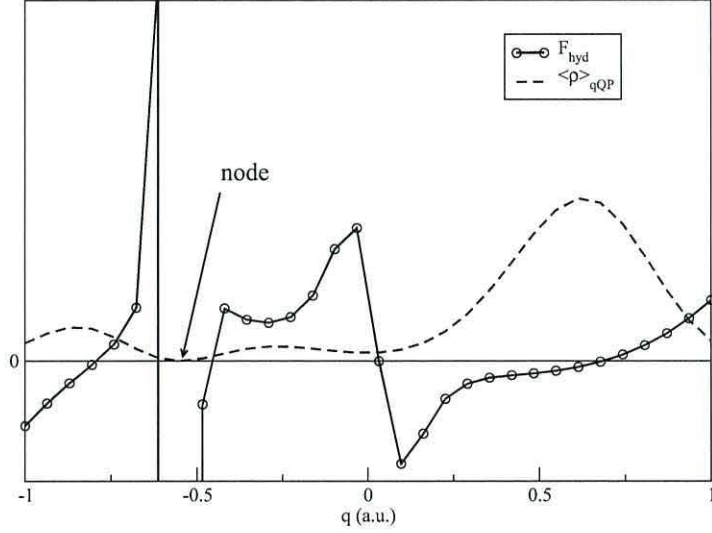
Figure 4.4: Hydrodynamic force F_{hyd} and the 0th moment, $\langle \rho \rangle_{qQP}$, computed at fixed $Q = -0.2, P = 0.0$ and $t = 4410$ a.u. for the double well bilinearly coupled to a classical harmonic oscillator.

$$ \tag{4.52} $$

where E_j are the eigenvalues with coefficients $c_j = \langle \phi_j | \psi \rangle$. The eigenstates themselves are expressed in terms of a product harmonic oscillator basis

$$ \phi_j(q,Q) = \sum_{m,k} a^j_{m,k} \chi_m(q) \xi_k(Q). \tag{4.53} $$

so a general equation can be written for the moments in terms of associated Laguerre polynomials for the classical Q, P phase space and derivatives of the Hermite polynomial in the quantum q coordinate (see Appendix E). Apart from the finite representation of the basis in Eq. (4.52) and Eq. (4.53), the moments and F_{hyd} ,

$$ F_{\text{hyd}} = -\frac{1}{(m\langle \rho \rangle_{qQP})} \frac{\partial}{\partial q} [\langle \mathcal{P}^2 \rho \rangle^c_{qQP} - p^2_{qQP} \langle \rho \rangle^c_{qQP}] \tag{4.54} $$

are evaluated exactly for any point in the entire (qQP) space. This eliminates the need for an interpolation routine. Furthermore, as

90

Figure 4.5: Lagrangian trajectories for 2 points in 3D (qQP) space with initial conditions that differ only in the quantum q coordinate.

the hydrodynamic force is completely defined, there is no need to propagate the continuity equation Eq. (4.41) directly. Instead, the trajectories are propagated by numerically integrating Eq. (4.42) using the explicit Euler solver with time step of $\Delta t = 0.1$ au.

The initial density is taken as a Gaussian in (qQP) given as

$$\langle \rho \rangle_{qQP} = \frac{\sqrt{2\pi\beta_q}}{\pi^2} \exp(-2\beta_q(q - q_e)^2 - 2\beta_Q(Q - Q_e)^2 - \frac{P^2}{2\beta_Q}), (4.55)$$

with parameters given in Table 4.1 and the initial hydrodynamic momentum is set to zero, $p_{qQP}(t_0) = 0$. The dynamics of the first three hydrodynamic moments is illustrated in Fig. (4.3) for fixed values of $QP = Q_0 P_0$. It is evident that the partial moments exhibit complicated dynamics with high-frequency intra-well oscillations occurring on a fast time scale of $t = 2000$ au. On a longer timescale

91

V_2	V_4	V_5	V_6	m
-0.033	0.030	0.010	0.002	2000
β_q	q_e	β_Q	Q_e	M
28	0.8	14	-0.2	20000

Table 4.1: Parameters in atomic units associated with the potential function described in Eq. (4.50), the initial conditions specified in Eq. (4.55) and the masses m and M.

of $t = 7000$ au there is tranfer of density along the quantum coordinate q from the right-hand well to the left-hand well via a tunnelling mechanism. An important feature to note also is the widespread formation of nodes within the partial moments.

The formation of nodes in a wavefunction is a well-known problem in Bohmian mechanics. It almost always leads to severe computational problems in calculating the quantum force. Very similar problems arise in the calculation of the hydrodynamic force F_{hyd} here. The presence of nodes in the lowest order moment $\langle \rho \rangle_{qQP}$ leads to singularities in F_{hyd}. Fig. (4.4) shows F_{hyd} along with $\langle \rho \rangle_{qQP}$. The formation of a node in $\langle \rho \rangle_{qQP}$ at $q = -0.6$ au causes F_{hyd} to become singular.

Fig. (4.3) also shows clear variation in the magnitude/norm of the hydrodynamic moments. The density not only flows in a double well potential along the quantum coordinate q but also in elliptic orbits in the classical subspace (Q, P) . This is characteristic of a harmonic oscillator. As the density flows around this elliptic orbit, the amount of density flowing through $Q_0 P_0$ varies periodically with
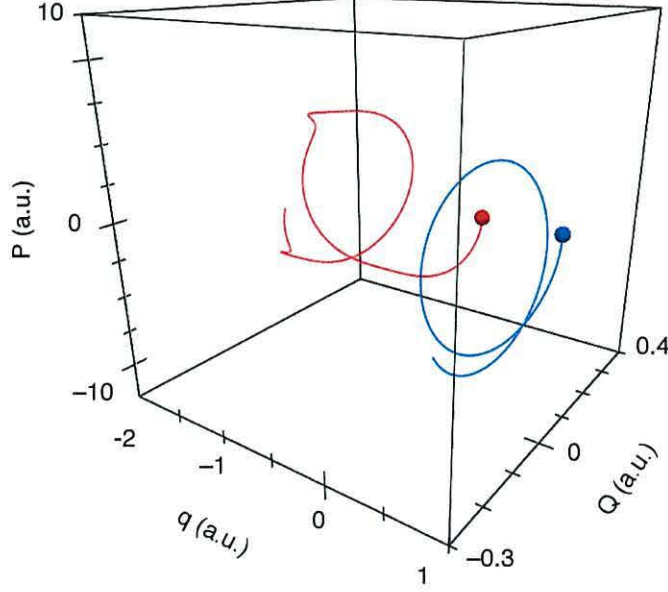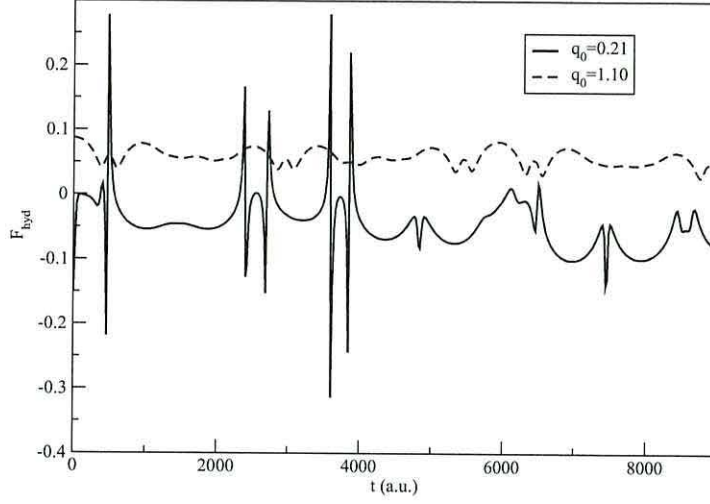
Figure 4.6: F_{hyd} evaluated along Lagrangian trajectories for 2 points in 3D (qQP) space with initial conditions that differ only in the quantum q coordinate.

the frequency of the harmonic oscillator. Between $t = 4000$ au and $t = 6000$ au, the amount of density at $Q_0 P_0$ is at its minimum. The elliptic orbits can be seen in Fig. (4.5) that shows two trajectories in 3D (qQP) space calculated from Eq. (4.42). The trajectories differ in their initial position in quantum coordinate q, the red initially at $q_0 = 0.88$ au and the blue is initially at $q_0 = 0.21$ au. Note that the blue trajectory remains in the right-hand side well of the double minimum potential while the red trajectory tunnels to the adjacent well. The time dependency of the hydrodynamic force that govern the dynamics of the two trajectories is depicted in Fig. (4.6).

The temporal evolution of an array of trajectories is shown in Fig. (4.7). A sample of eight Lagrangian trajectories is illustrated along the quantum coordinate between $0.2 \leq q_0 \leq 1.1$ au for given classical coordinates $Q_0 = -0.2$ au and $P_0 = 0.0$ au. As expected, the tra-

93
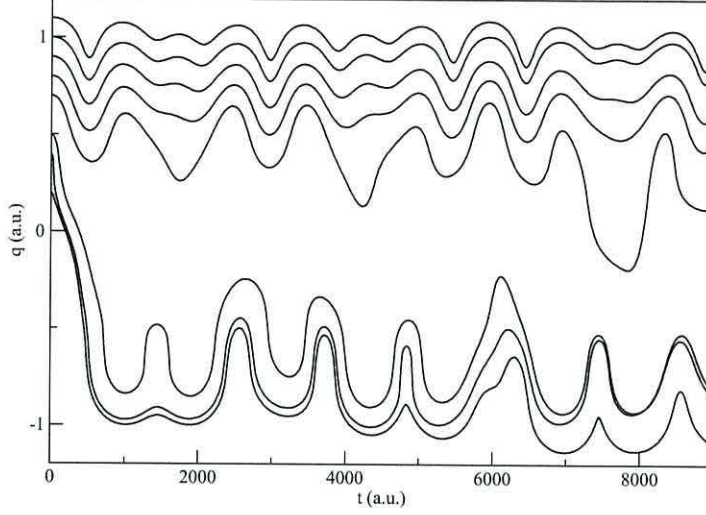
Figure 4.7: Lagrangian trajectories with initial conditions $Q_0 = -0.2, P_0 = 0.0$ au and $0.2 \leq q_0 \leq 1.1$ au for the double well bilinearly coupled to a classical harmonic oscillator.

jectories follow a complicated path along the quantum coordinate q as the trajectories perform high-frequency intra well oscillations. Furthermore, the three trajectories closest to the barrier tunnel to the other potential well with the first high frequency oscillation. The remaining trajectories stay in the initial potential well.

4.3.2 Eckart Barrier Coupled to a Harmonic Oscillator

To conclude, a second example, the dynamics of a system subject to an Eckart barrier coupled to a harmonic oscillator is briefly summarised. The underlying wavefunction for the composite system is obtained by solving the Schrödinger equation on a fixed Eulerian grid. The hydrodynamic quantities are then extracted from the wavefunction and transtaled to the Lagrangian frame in order to ob-

94

V_0	a	V_2	V_3	m
0.03	0.5	0.075	0.005	2000
β_q	q_e	β_Q	Q_e	M
6	-2	7	-0.2	20000

Table 4.2: Parameters in atomic units associated with the potential function described in Eq. (4.56), the initial conditions specified in Eq. (4.57) and the masses m and M.

tain the hydrodynamic force F_{hyd}. The trajectories from Eq. (4.42) can be subsequently computed. Although a scheme based on applying an interpolation at every time step has potential stability issues, it was found that a Lagrangian interpolation routine [23] yielded stable and smooth trajectory dynamics.

The potential of the Eckart barrier coupled to the harmonic oscillator is given by,

$$V(q) = V_0\text{sech}^2 a(q - q_0) + V_2 Q^2 + V_3 qQ \qquad (4.56)$$

where the first term is associated with the 'quantum' Eckart barrier, the second term is the classical harmonic oscillator and the final term represents the bilinear coupling.

The initial 3D Gaussian density was taken similar to Eq. (4.55),

$$\langle \rho \rangle_{qQP} = \frac{\sqrt{2\pi\beta_q}}{\pi^2} \exp(-2\beta_q(q - q_e)^2 - 2\beta_Q(Q - Q_e)^2 - \frac{P^2}{2\beta_Q})(4.57)$$

with a translational energy of $E_{\text{trans}} = 0.01$ au. The parameters of Eq. (4.56) and Eq. (4.57) are given in Table 4.2.
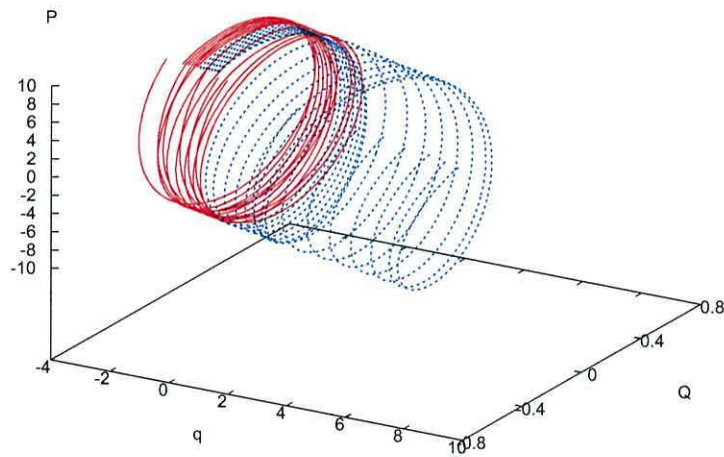
Figure 4.8: Lagrangian trajectories for a range of points in 3D (qQP) space with initial conditions that differ only in the quantum q coordinate. The red coloured trajectories are reflected by the Eckart barrier while the blue trajectories tunnels through the barrier.

The resulting trajectory dynamics as obtained from Eq. (4.42) is presented in Fig. (4.8) and Fig. (4.9). A range of 14 trajectories with differing initial conditions in quantum q coordinate (between -2.5 and -1.5 au) are shown for (qQP) in Fig. (4.8). The flow of density around elliptic orbits is clearly seen in the classical (QP) coordinates. Furthermore, the trajectories coloured blue are seen to tunnel through the barrier while the red trajectories are reflected back towards their initial positions. Fig. (4.9) shows the same Lagrangian trajectories as in Fig. (4.8), but in (q, Q, t). The periodic oscillatory motion characteristic of a harmonic mode is seen in classical Q coordinate. Once more, the trajectories coloured blue tunnel through the barrier towards the right hand side (i.e. positive values of q) while the red trajectories are reflected from the Eckart barrier.
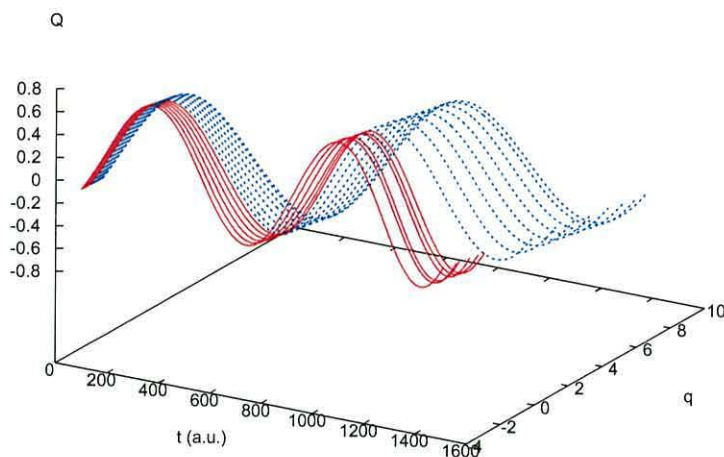
Figure 4.9: Lagrangian trajectories for the same points as in Fig. (4.8) depicted in (q, Q, t) space. The blue trajectories are seen to tunnel through the barrier (in q space) as time progresses while the red trajectories are reflected.

4.4 Conclusions

This Chapter illustrated the application of the QCM approach [27] to anharmonic (double-well and Eckart barrier) oscillator systems coupled to a classical harmonic mode. The dynamical schemes presented for the examples are exact. The key concept of the QCM as a hybrid approach is the combination of the quantum hydrodynamic and classical Hamiltonian trajectory pictures in a mixed Lagrangian scheme. This approach is unique for several reasons,

i) It captures the details of instantaneous phase-space correlations between the quantum and classical parts of the system. This goes far

beyond alternative methods such as mean-field and surface-hopping approach.

ii) The hydrodynamic force within the quantum sector depends on the classical variables (Q, P), but is absent in the classical (Liouvillian) sector.

iii) The equations of motion for the trajectories do not have an explicit dependence on $\hbar$. The equations are in fact formally identical to purely classical mixed hydrodynamic-Liovillian equations.

iv) The coupled trajectory equations Eq. (4.42) are deterministic. This differs from stochastic trajectory dynamics associated with surface hopping type trajectories.

v) The QCM method is exact if the classical sector is harmonic.

Two distinct strategies of propagation were used in the illustrated examples. For the double well potential coupled to a classical harmonic mode, a basis set expansion method was used. For the Eckart potential coupled to a harmonic mode, a grid based approach was used to propagate the quantities. A Lagrangian interpolation routine was then used to interpolate the hydrodynamic quantities from the Eulerian grid to the Lagrangian frame in order to obtain trajectories. Unfortunately, neither of the methods used are fully general. They both rely on information extracted from the underlying wavefunction.

Chapter 5 in this thesis deal with a general propagation scheme that attempts to apply approximate truncation schemes for the moment hierarchy of Eq. (4.32) and Eq. (4.33). This then allows the hydrodynamic quantities to be calculated 'on the fly', in a 'synthetic' trajec-

tory approach similar to the quantum trajectory method (QTM) of Wyatt [25]. Another natural extension to this study is the inclusion of many classical modes constituting a bath to which the quantum subsystem is coupled. This would allow the study of dissipation and decoherence in the hydrodynamic representation.

Bibliography

[1] K. H. Hughes, S. M. Parry, G. Parlant and I. Burghardt, J. Phys. Chem. A **111**, 10269 (2007).

[2] G. D. Billing, Int. Rev. Phys. Chem. **183**, 335 (1994).

[3] J. C. Tully, J. Chem. Phys. **93**, 1061 (1990).

[4] J. C. Tully, Faraday Discuss. Chem. Soc. **110**, 407 (1998).

[5] R. Kapral, Ann. Rev. Phys. Chem. **57**, 129 (2006).

[6] O. V. Prezhdo and V. V. Kisil, Phys. Rev. A **56**, 162 (1997).

[7] I. V. Aleksandrov, Z. Naturforsch. **36**, 902 (1981).

[8] W. Boucher and J. Traschen, Phys. Rev. D **37**, 3522 (1988).

[9] C. C. Martens and J.-Y. Fang, J. Chem. Phys. **106**, 4918 (1996).

[10] E. Roman and C. C. Martens, J. Chem. Phys. **121**, 11572 (2004).

[11] R. Kapral and G. Ciccotti, J. Chem. Phys. **110**, 8919 (1999).

[12] S. Nielsen, R. Kapral, and G. Ciccotti, J. Chem. Phys. **115**, 5805 (2001).

[13] I. Horenko, M. Weiser, B. Schmidt, and C. Schütte, J. Chem. Phys. **120**, 8913 (2004).

[14] D. A. Micha and B. Thorndyke, Adv. Quant. Chem. **47**, 293 (2004).

[15] E. Gindensperger, C. Meier, and J. A. Beswick, J. Chem. Phys. **113**, 9369 (2000).

[16] E. Gindensperger, C. Meier, and J. A. Beswick, J. Chem. Phys. **116**, 8 (2002).

[17] D. Kohen, F. H. Stillinger, and J. C. Tully, J. Chem. Phys. **109**, 4713 (1998).

[18] W. Domcke and G. Stock, Adv. Chem. Phys. **100**, 1 (1997).

[19] C. Meier, Phys. Rev. Lett. **93**, 173003 (2004).

[20] D. Bohm, Phys. Rev. **85**, 166 (1952).

[21] D. Bohm, Phys. Rev. **85**, 180 (1952).

[22] J. S. Bell, *Speakable and Unspeakable in quantum mechanics*, Cambridge University Press, Cambridge, 1989.

[23] C. F. Gerald and P. O. Wheatley, *Applied Numerical Methods*, Addison-Wesley Publishing Company, 1994.

[24] P. R. Holland, *The Quantum Theory of Motion*, Cambridge University Press, New York, 1993.

[25] R. E. Wyatt, *Quantum Dynamics with Trajectories: Introduction to Quantum Hydrodynamics*, Springer, Heidelberg, 2005.

[26] I. Burghardt and G. Parlant, J. Chem. Phys. **120**, 3055 (2004).

[27] I. Burghardt, J. Chem. Phys. **122**, 094103 (2005).

[28] I. Burghardt, K. B. Møller, and K. H. Hughes, Quantum hydrodynamics and a moment approach to quantum-classical theory, in *Quantum Dynamics of Complex Molecular Systems*, edited by D. A. Micha and I. Burghardt, Springer, 2006.

[29] I. Burghardt and K. B. Møller, J. Chem. Phys. **117**, 7409 (2002).

[30] M. Hillery, R. F. O'Connell, M. O. Scully, and E. P. Wigner, Phys. Rep. **106**, 121 (1984).

[31] J. G. Muga, R. Sala and R. F. Snider, Physica Scripta **47**, 732 (1993).

[32] I. Burghardt and L. S. Cederbaum, J. Chem. Phys. **115**, 10303 (2001).

Chapter 5

Closure of Quantum Hydrodynamic Moment Equations

5.1 Introduction

The quantum classical moment approach [1, 2, 3, 4, 5] (QCM) derived in Chapter 4 is fundamentally based on the hydrodynamic picture of mixed quantum states. The hydrodynamic representation has various advantages including reducing the dynamics of a $2N$ dimensional density operator to a series of coupled dynamical equations for the N dimensional hydrodynamic moments. The trajectories are also easily formulated in the Lagrangian framework. Unfortunately, there is also a major drawback in applying the moment method. The hydrodynamic formulation of mixed states is based on generating momentum moments by an integration over the momentum p of the Wigner function, ρ_W. A hierarchy of equations of motion for the moments is obtained that display coupling to both higher and lower

moments. In general, this hierarchy is non-convergent with no simple closure for the hierarchy. However, for two limited cases (pure states [6] and Gaussian moments [7]), analytical closures have been established. For the QCM approach to be of any use in a numerical scheme, a methodology of closing the hierarchy is required. Similar problems arise in classical hydrodynamics as well as in plasma physics with respect to the Vlassov equation [8].

The maximum entropy approach has been applied to quantum and classical hydrodynamics [9, 15]. It has the ability to evaluate higher order moments by finding a phase space distribution function that maximises an entropy functional under the constraint that the lower order moments are known. In its conventional form, the maximum entropy approach has the requirement that the density remains positive. For quantum states, the Wigner density can develop negative regions so the maximum entropy approach is not always the best methodology. An alternative approach that is of interest in this Chapter is based on the maximum entropy ansatz. It involves the linearization of the maximum entropy derived by expanding the quantum state ρ_W in an orthonormal Gauss-Hermite basis. This is similar to the Grad-Hermite approach used in hydrodynamics [10, 11, 12, 13, 14] and differs only in the function that the expansion is based on.

The following section gives a qualitative description of preliminary investigations carried out that employed rather simple truncation strategies for the moment hierarchy.

5.2 Preliminary Work

To investigate the effect of incorporating high order moments on the stability of the propagation of the hydrodynamic fields, $\langle \mathcal{P}^n \rho \rangle_q$ (see Eq.(3.9)), a simple cold cut-off was applied to the hierarchy. A cut-off at many orders, including $n = 3$, $n = 10$, $n = 100$ and $n = 300$ was investigated and this was applied to both harmonic potentials and double well potentials with differing potential parameters. It was found that a cut-off at any order gave very little encouraging results. Indeed, even for very high order truncation of $n = 300$, the propagation is stable for $t << 1$ fs. In this very short timescale, no deviations from the initial ($t = 0$) moments are observed. Not only is it highly undesirable to go beyond $n = 300$ moments, the magnitude of the moments become very large ($\sim 10^{295}$) and solving the moment equation becomes computationally unfeasible.

As a simple introductory investigation, we initially tried a gradual 'dampening' of the moment cut-off. The cold cut-off takes the from of a step function, Fig. (5.1). This cold cut-off itself may cause instabilities. The sigmoidal-type functions that were invoked to gradually decrease the dependence on higher order moments are shown in Fig. (5.1). The dampening associated with the three differing curves was applied to both harmonic and double well potentials, again with differing potential parameters. Very little or no improvement was seen in the timescales of the propagations. Even for the most gradual curve, the dynamics is observed for less than 1 fs.

It is clear that smoothing the cut-off has no influence on the stability of the moment propagation. The hierarchy is non-convergent.
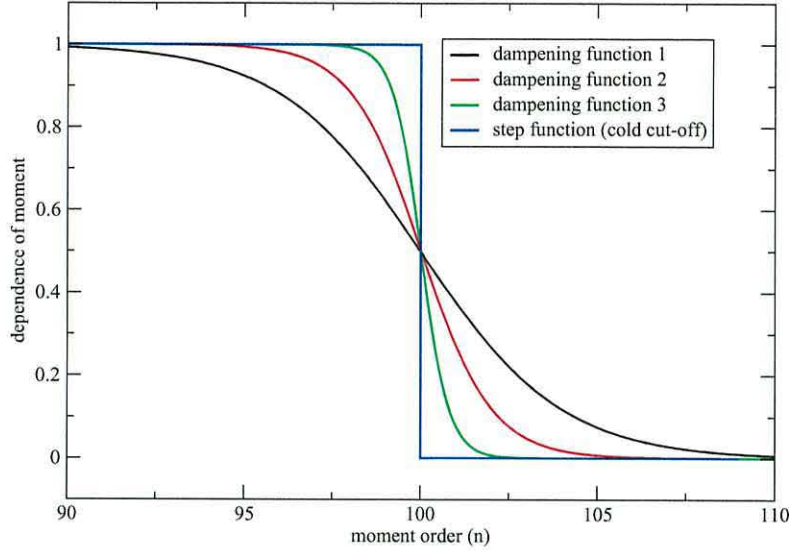
Figure 5.1: Sigmoidal type curves used for dampening the effect of higher order moments. Also depicted is the cold cut-off approach that was investigated.

The dependency of the $(n+1)$th moment cannot be ignored for any value of n, irrespective of how high the hierarchy is taken. For the quantum hydrodynamic equations to be of use in a numerical approach, a moment closure scheme is needed. The remainder of the Chapter presents a moment closure scheme that accurately reconstructs the $(n+1)$th moment based on the information embedded within the known lower order moments.

5.3 Numerical Closure Schemes

In order to close the moment hierarchy, a method of approximating the $(n+1)$th moment is required. Alternatively, the $(n+1)$th moment may be expressed in terms of lower order moments. If the Wigner density, $\rho_W(q, p, t)$ is known then all the hydrodynamic moments are

defined by the following prescription,

$$\langle \mathcal{P}^n \rho \rangle_q = \int dp \; p^n \rho_W(q, p, t) \tag{5.1}$$

However, when the hydrodynamic moments are propagated using the moment equation,

$$\frac{\partial}{\partial t} \langle \mathcal{P}^n \rho \rangle_q = -\frac{1}{m} \frac{\partial}{\partial q} \langle \mathcal{P}^{n+1} \rho \rangle_q - \sum_{\substack{l=1 \\ \text{odd}}}^{n} \binom{n}{k} \left(\frac{\hbar}{2i} \right)^{k-1} \frac{\partial^k V}{\partial q^k} \langle \mathcal{P}^{n-k} \rho \rangle_q$$
$$\tag{5.2}$$

the Wigner density, $\rho_W(q, p, t)$ is generally unknown. Even though the initial density $\rho_W(q, p, t_0)$ is exactly defined, its time dependency cannot be extracted from the finite number of moments used. Some information however can be gleaned about the underlying phase-space distribution from the moments. The first moment gives information about the mean momentum, the second moment provides information about the width of $\rho_W(q, p)$ in momentum space p, while the third moment gives information about the skewness of the distribution. The first few moments are also related to the physical conserved quantities of density $\langle \rho \rangle_q = \rho(q)$, flux density $\langle \mathcal{P} \rho \rangle_q = m j(q)$ and kinetic energy density $\langle \mathcal{P}^2 \rho \rangle_q = 2mT(q)$.

If an infinite number of the moments are known, the Wigner density, $\rho_W(q, p)$ can be reconstructed exactly. Provided a sufficient number of moments are known, it should be possible to construct an *approximate* closure scheme for the hierarchy by finding an explicit expression for $\langle \mathcal{P}^{n+1} \rho \rangle_q$ in terms of known lower order moments. Equivalently, it may be possible to reconstruct the phase-space distribution itself from the known lower order moments. The $(n+1)$th moment is then evaluated using Eq. (5.1).

In the following section, a moment closure scheme based on a Hermite expansion is described. The Hermite expansion method is closely related to the linearisation of the maximum entropy approach [16] that has been widely used in a number of fields [17, 18], classical hydrodynamics in particular [19]. To this end, the maximum entropy approach is first introduced.

5.3.1 Maximum Entropy Approach

In a maximum entropy approach, an entropy functional $S[\rho_W]$ is defined as,

$$S[\rho_W] = -\int (\rho_W \ln \rho_W - \rho_W) dp dq \qquad (5.3)$$

It is convenient to define the entropy relative to some reference distribution, ρ_β, such that,

$$S[\rho_W] = -\int \left(\rho_W \ln \frac{\rho_W}{\rho_\beta} + \rho_\beta - \rho_W \right) dp dq \qquad (5.4)$$

The principle of maximum entropy states that the distribution function that maximises S provides the best unbiased distribution function based on the given information. In this case, the information is the limited number of moments known. The task of finding an approximate phase-space distribution, $\rho_{W_A}(q, p, t)$, that most accurately reproduces the true distribution, $\rho_W(q, p, t)$ then becomes a variational problem of maximising S subject to the constraints that the lower order moments are satisfied. The Lagrangian functional to be maximised is given by

$$\mathcal{J}[\rho_W, \lambda] = S[\rho_W] - \int \sum_n \lambda_n(q, t) \left(\int dp \, p^n \, \rho_W - \langle \mathcal{P}^n \rho \rangle_q \right) dq \quad (5.5)$$

where $\lambda_n(q, t)$ are the position and time dependent Lagrange multipliers. The local extremum of $\mathcal{J}$ is sought by setting its variation

109

with respect to the density ρ_W to zero such that,

$$\delta \mathcal{J} = 0 = -\ln\frac{\rho_W}{\rho_\beta} - \sum_n \lambda_n p^n \qquad (5.6)$$

The resulting distribution function that maximises the entropy is thus,

$$\rho_{W_A}(q,p) = \rho_\beta \exp(-\sum_n \lambda_n p^n) \qquad (5.7)$$

It is clear from Eq. (5.7) that the term ρ_β is the reference distribution that ρ_{W_A} adopts in the absence of any constraints. In classical kinetic theory approaches, it is usual to define ρ_β as the local Maxwellian. In reality, it can be modelled on any physically justifiable distribution function. In this work, ρ_β is defined as a momentum dependent Gaussian function,

$$\rho_\beta = \left(\frac{\beta}{\pi}\right)^{\frac{1}{2}} \exp(-\beta p^2) \qquad (5.8)$$

Here, β is a freely determined width parameter. In Eq. (5.7), the determination of the Lagrange multipliers involves solving a set of n non-linear equations. In order to obtain the dynamics of a system of interest, this must be implemented in a time stepping propagation scheme. The Lagrange multipliers must be solved for all values of t and q sampled in the simulation; this is computationally intensive and therefore highly undesirable. In the case that the determination of ρ_{W_A} requires information only up to quadratic in the moments, the Lagrangian multipliers $\{\lambda\}_n$ may be re-written explicitly in terms of the conserved quantities $\rho(q)$, $j(q)$ and $T(q)$ [15]. For the quantum hydrodynamic equations of motion, Eq. (5.2), a low level closure of $n = 2$ is insufficient at reconstructing ρ_W accurately.

Another major drawback of the maximum entropy approach as defined here is its inability to deal with distribution functions that have

both positive and negative regions. It is clear from Eq. (5.7) that there is a requirement for $\rho_{W_A} \geq 0 \, \forall \, q, p$. As detailed previously, the Wigner function should be interpreted as a quasi probability distribution function as it can develop negative basins in regions where there is quantum interference e.g. during quantum tunnelling. A Wigner distribution function of this kind cannot be reconstructed using the maximum entropy as defined here.

The maximum entropy approach has been adapted to deal with distribution functions that have both negative and positive parts [20, 21]. This approach has been applied to a number of problems in image or data reconstruction within the field of astronomy [22, 23], geophysics [24, 25] and spectroscopy [26, 27]. In this approach, the image or data that constitutes the distribution function is partitioned into two positive distribution functions labelled ρ_W^+ and ρ_W^-. The total distribution function is then defined as the difference between the two functions, $\rho_W = \rho_W^+ - \rho_W^-$. The total entropy to be maximised is then the sum of the individual entropies associated with ρ_W^+ and ρ_W^- i.e., $S = S^+ + S^-$ where $S^+(S^-)$ are defined according to Eq. (5.4) using $\rho_W^+(\rho_W^-)$. This method is ideal for situations where part of the distribution function known, for example in image reconstruction studies. Unfortunately, this approach is less suitable in situations where only indirect information about the distribution function is known, as is the case for the hydrodynamic moment equations. It also has the same disadvantage as previous discussions in that it still requires a solution of a set of non-linear equations for determining the Lagrange multipliers.

There is an alternative method that is fundamentally based on the maximum entropy approach but with no requirement to solve a set of nonlinear equations. This method also has the advantage that it can cope with the presence of negative regions in the density. The approach involves linearization of the expansion of ρ_{W_A}.

5.3.2 Moment Truncation by Hermite Expansion

Starting from the maximum entropy ansatz, a linearization of ρ_{W_A} leads to a polynomial expansion,

$$\rho_{W_A} = (q, p, t) = \rho_\beta(p) e^{-\sum_m \lambda_M(q,t)p^m} \simeq \rho_\beta \left(1 - \sum_m \lambda_m(q,t)p^m\right) \tag{5.9}$$

The expansion as defined here may be reformulated with different types of polynomials. In this Chapter, the expansion is taken as an orthonormal Hermite basis of the form

$$\left(\frac{\beta}{\pi}\right)^{\frac{1}{4}} H_m(\sqrt{\beta}p) N_m = \left(\frac{\beta}{\pi}\right)^{\frac{1}{4}} \frac{H_m(\sqrt{\beta}p)}{\sqrt{m!2^m}}, \tag{5.10}$$

where $H_m(\sqrt{\beta}p)$ is the mth Hermite polynomial. ρ_{W_A} is then given by

$$\rho_{W_A}(q, p, t) = \sum_m a_m(q, t) N_m \left(\frac{\beta}{\pi}\right)^{\frac{1}{4}} H_m(\sqrt{\beta}p) \exp(-\beta p^2/2), \tag{5.11}$$

The moments are then evaluated by direct integration of the reconstructed density, ρ_{W_A},

$$
\begin{aligned}
\langle \mathcal{P}^n \rho \rangle_q &\simeq \sum_m a_m(q, t) N_m \left(\frac{\beta}{\pi}\right)^{\frac{1}{4}} \int dp\, p^n H_m(\sqrt{\beta}p) \exp(-\beta p^2/2) \\
&= \sum_m a_m(q, t) N_m \left(\frac{\beta}{\pi}\right)^{\frac{1}{4}} h_n^m.
\end{aligned} \tag{5.12}
$$

It is evident from Eq. (5.12) that the time dependence only appears in the expansion coefficients $a_m(q, t)$, the integral itself is time independent. In fact the integral has an analytical solution that contains the hypergeometric series (see Appendix F). Unfortunately, the hypergeometric series is divergent in this case. The integral is however trivial to solve using a numerical method. The coefficients $a_m(q, t)$ are obtained by solving a set of *linear* equations,

$$
\begin{bmatrix} h_0^0 & h_0^1 & \dots & h_0^m \\ h_1^0 & h_1^1 & \dots & h_1^m \\ \vdots & \vdots & \ddots & \vdots \\ h_n^0 & h_n^1 & \dots & h_n^m \end{bmatrix} \begin{bmatrix} a_0(q, t) \\ a_1(q, t) \\ \vdots \\ a_m(q, t) \end{bmatrix} = \begin{bmatrix} \langle \rho \rangle_q(t) \\ \langle \mathcal{P} \rho \rangle_q(t) \\ \vdots \\ \langle \mathcal{P}^n \rho \rangle_q(t) \end{bmatrix}. \tag{5.13}
$$

In conventional matrix notation, this is given as,

$$
\mathbf{ha} = \mathbf{p} \tag{5.14}
$$

The matrix $\mathbf{h}$ is time independent and only needs to be inverted once prior to the time propagation of the moments. Subsequent evaluation of the coefficients $\{a(q, t)\}_m$ are obtained by multiplication of $\mathbf{h}^{-1}\mathbf{p}$ where $\mathbf{p}$ is contains the updated moments at time t. The $(n + 1)$th moment can then be reconstructed from the 'known' lower order moments via the calculated coefficients, $\{a(q, t)\}$.

5.3.3 Hermite Closure derived from $\rho(q, r)$

Another route to generate a moment closure scheme can be established from the Taylor expansion of the coordinate space density $\rho(q, r)$ given by,

$$
\rho(q, r) = \sum_m \frac{1}{m!} \langle \mathcal{P}^m \rho \rangle_q \left(\frac{ir}{\hbar} \right)^m. \tag{5.15}
$$

The Wigner function is generated by taking the Fourier transform of Eq. (5.15),

$$
\begin{aligned}
\rho_W(q,p) &= \frac{1}{2\pi\hbar} \int dr \rho(q,r) \exp(ipr/\hbar) \\
&= \frac{1}{2\pi\hbar} \sum_m \frac{1}{m!} \langle \mathcal{P}^m \rho \rangle_q \int dr \left(\frac{ir}{\hbar} \right)^m \exp(ipr/\hbar) \\
&= \frac{1}{2\pi\hbar} \sum_m \frac{1}{m!} \langle \mathcal{P}^m \rho \rangle_q \frac{\partial^m}{\partial p^m} \int dr \exp(ipr/\hbar) \\
&= \frac{1}{\hbar} \sum_m \frac{1}{m!} \langle \mathcal{P}^m \rho \rangle_q \frac{\partial^m}{\partial p^m} \delta(p).
\end{aligned}
\tag{5.16}
$$

Using the Gaussian approximation for the delta function, the Wigner function becomes,

$$
\begin{aligned}
\rho_W(q,p) &= \frac{1}{\hbar} \sum_m \frac{1}{m!} \langle \mathcal{P}^m \rho \rangle_q \sqrt{\frac{\beta}{\pi}} \frac{\partial^m}{\partial p^m} \exp(-\beta p^2) \\
&= \frac{1}{\hbar} \sqrt{\frac{\beta}{\pi}} \sum_m \frac{1}{m!} \langle \mathcal{P}^m \rho \rangle_q (-1)^m \beta^{\frac{m}{2}} H_m(\sqrt{\beta} p) \exp(-\beta p^2).
\end{aligned}
$$

$$\tag{5.17}$$

The orthogonality of the Hermite polynomial then allows a closed form of the highest $(n+1)$th moment to be established

$$
\begin{aligned}
\int dp \rho_W(q,p) H_{n+1}(\sqrt{\beta} p) &= \frac{1}{\hbar} \sqrt{\frac{\beta}{\pi}} \sum_{m=0}^{n} \frac{1}{m!} \langle \mathcal{P}^m \rho \rangle_q (-1)^m \beta^{\frac{m}{2}} \\
&\quad \int dp H_m(\sqrt{\beta} p) H_{n+1}(\sqrt{\beta} p) \exp(-\beta p^2) \\
&= 0 \\
&= H_{n+1}\left(\sqrt{\beta} \langle \mathcal{P} \rho \rangle_q \right),
\end{aligned}
\tag{5.18}
$$

where

$$
H_{n+1}(\sqrt{\beta} \langle \mathcal{P} \rho \rangle_q) = \sum_{k=0}^{n+1} c_k \langle \mathcal{P}^k \rho \rangle_q
\tag{5.19}
$$

implies taking the order of the moments in the Hermite polynomial and *not* raise the moment to the power of the moment e.g.

114

$H_3(\sqrt{\beta}\langle\mathcal{P}\rho\rangle_q) = 8\beta^{\frac{3}{2}}\langle\mathcal{P}^3\rho\rangle_q - 12\beta^{\frac{1}{2}}\langle\mathcal{P}\rho\rangle_q$, and c_k are the Hermite coefficients of the polynomial. The implication of setting the $(n+1)$th Hermite moment in Eq. (5.18) to zero is that a closure for the moment hierarchy may be established where $\langle\mathcal{P}^{n+1}\rho\rangle_q$ is expressed in terms of the lower moments contained in $H_{n+1}(\sqrt{\beta}\langle\mathcal{P}\rho\rangle_q)$

$$\langle\mathcal{P}^{n+1}\rho\rangle_q = \frac{1}{c_{n+1}}\sum_{k=0}^{n-1} c_k\langle\mathcal{P}^k\rho\rangle_q. \tag{5.20}$$

5.3.4 Grad-Hermite Moment Closure

A final approach, used particularly in classical hydrodynamics and is closely related to the previously discussed methodologies is the Grad-Hermite approach [28]. In this instance, the expansion of $\rho_\beta^{-1/2}\rho_W$ is taken in an orthonormal Gauss-Hermite basis and *not* the direct expansion of ρ_{W_A}

$$\rho_\beta^{-1/2}(p)\rho_{W_A}(q,p,t) = \sum_m a_m(q,t)\left(\frac{\beta}{\pi}\right)^{1/4}\exp(-\beta p^2/2)H_m(\sqrt{\beta}p)N_m \tag{5.21}$$

This ensures that the q dependent coefficients $a_m(q,t)$ may be explicitly and conveniently expressed as Hermite functions of the moments,

$$a_m = \int dp\rho_{W_A}H_m(\sqrt{\beta}p) = N_m H_m(\langle\mathcal{P}\rho\rangle_q) \tag{5.22}$$

Generally, in classical hydrodynamics only the three lowest terms of the expansion are needed. These are then equated with hydrodynamic quantities such as the local density, velocity etc. In quantum hydrodynamics however, a significantly larger number of moments is required to establish a closure and hence the evaluation of $\{a_m(q)\}$ becomes cumbersome and computationally inefficient. In such cases the hierarchy is best closed by following the approach of Eq. (5.18) and setting the $(n+1)$th Hermite moments to zero in Eq. (5.21) to

115

recover Eq. (5.20).

The clear advantage of using Eq. (5.20) for the moment closure is the compact and explicit representation of $\langle \mathcal{P}^{n+1} \rho \rangle_q$ required to close the hierarchy. However, for examples illustrated in this Chapter, it was found that the closure scheme of Eq. (5.13) was more stable than Eq. (5.20) in a time propagation scheme. In terms of numerical efficiency, there was very little difference between the two approaches. The results presented in this Chapter is therefore based on the Hermite expansion approach.

The following section demonstrates the accuracy of the Hermite approach of Eq. (5.13) for reproducing the $(n+1)$th moment given that the lower order moments are known. It is demonstrated for both a Gaussian type Wigner function and for a Wigner function with a complicated profile. The method is then applied to the moment equations of motion as defined in Eq. (5.2) in a dynamical scheme. It is applied to non-dissipative harmonic, double-well and periodic potentials. The section finishes with an application to the dissipative dynamics of a harmonic, double-well and periodic potentials. The moments as obtained from the Hermite approach of Eq. (5.9) to Eq. (5.14) are compared with 'exact' moments extracted from a Wigner function generated either from wavepacket or phase space quantum dynamical calculations.
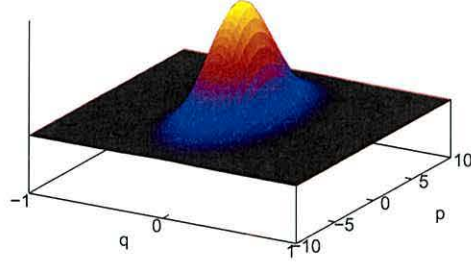
Figure 5.2: A simple 2D Gaussian Wigner Function.

5.4 Moment Reproduction

The accuracy of the reproduction of the $(n+1)$th moment is demonstrated for various values of n. It is assumed in all calculations that the matrix in Eq. (5.13) is a square matrix, hence $n = m$. This is first of all illustrated for a simple Wigner function that has a 2D Gaussian form, as shown in Fig. (5.2). A Gaussian form for the Wigner function is often used as an initial condition for quantum dynamical calculations. As shown previously, in the case of a harmonic potential, this initial Gaussian profile is retained throughout the propagation. This will provide a good starting point in assessing the potential of the Hermite approach in reconstructing an approximate Wigner function from a limited number of known lower order moments. In Fig. (5.3) it is seen that the approximate moment matches the true moment very closely, they are truly superimposable. Note also that this is the case for even a low order truncation at $n = 3$. It seems that for a Gaussian density, a low order truncation is sufficient to reconstruct higher order moments, and hence the Wigner function. This is not surprising since as explained pre-
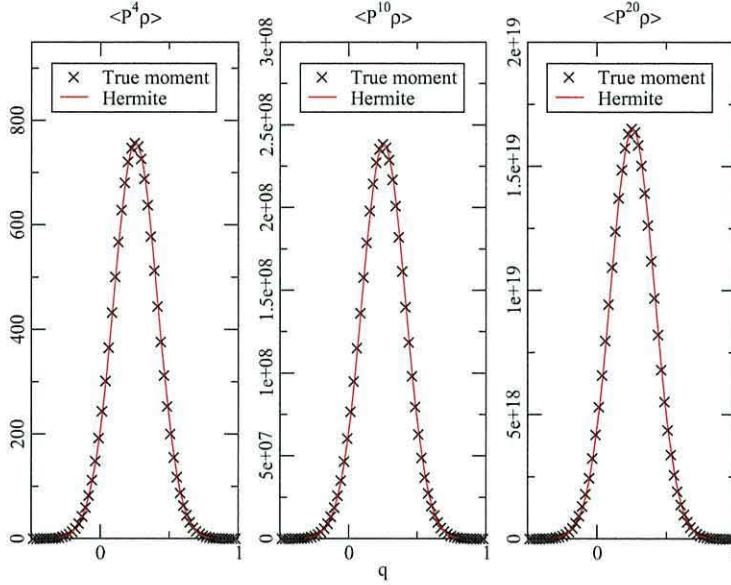
117

Figure 5.3: Moment reconstruction for a Gaussian density. Truncation at various values of n shown.

viously, for Gaussian densities, the third order moment and above may be represented in terms of lower order moments e.g.

$$\langle \mathcal{P}^3 \rho \rangle_q = \bar{p}^3 \langle \rho \rangle_q + 3\bar{p}\sigma \tag{5.23}$$

with $\sigma = \langle \mathcal{P}^2 \rho \rangle_q - \bar{p}^2 \langle \rho \rangle$. In fact, Eq. (5.23) suggest that a trunction at $n = 2$ should be sufficient.

Another more challenging example explored here is a Wigner function with a complicated profile that contains both positive and negative regions. Such a distribution function as shown in Fig.(5.4) is a snapshot obtained from the inversion dynamics of the ammonia molecule. The density is delocalised in both potential wells during quantum tunnelling. The moments are easily obtained up to any order by numerically integrating the density $\rho_W(q, p)$ as defined in Eq. (5.1). For a given n 'known' moments, the Hermite approach
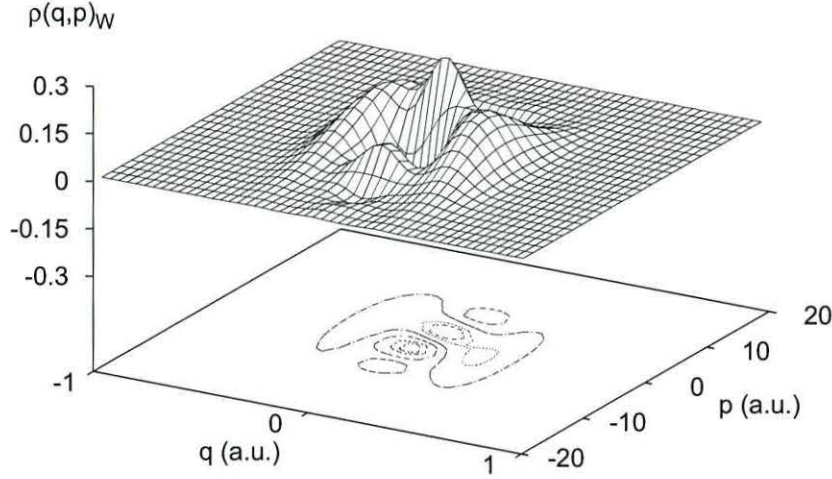
118

Figure 5.4: Wigner phase-space distribution function from the inversion dynamics of ammonia

and Eq. (5.13) is used to determine the $(n+1)$th moment.

The reproduction is depicted for various values of n in Fig. (5.5). It is evident that a very low order termination ($n = 2$), as is often used in classical kinetic theories gives a very poor reproduction. Increasing the number of moments to $n = 10$ improves things somewhat. It reproduces the moment relatively well but differences are still noticeable. Truncating at $n = 19$, the reproduced 20th moment is visually indistinguishable from the true moment. It is possible to further increase the number of moments used to reproduce the $(n + 1)$th moment, but the benefit over using only 19 is negligible. In fact using much more than $n = 29$ is not only unfavourable computationally but gives a poorer moment reconstruction. These
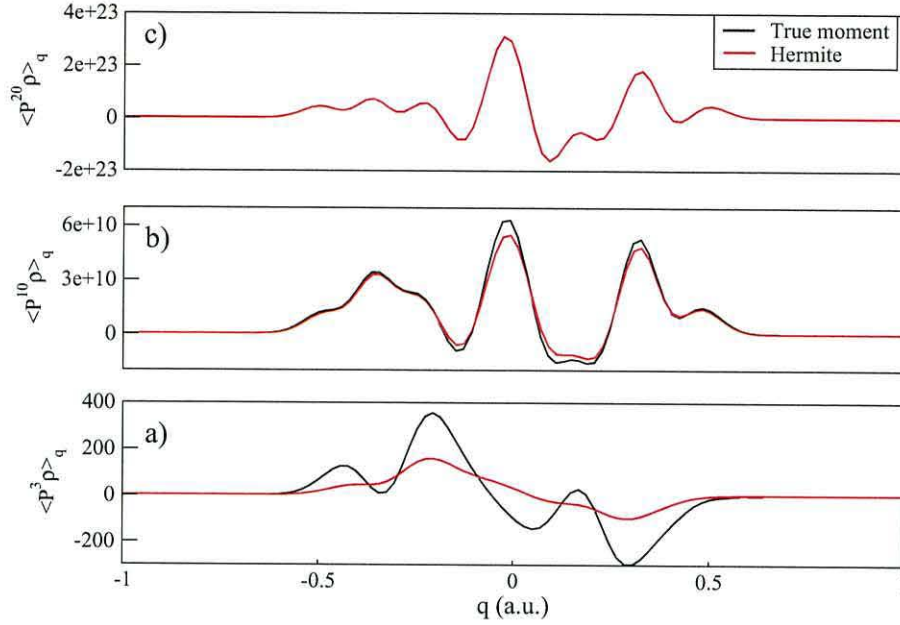
Figure 5.5: Reproduction of moments of the Wigner function depicted in Fig. (5.4) using the Hermite approach.

results illustrate the ability of the Hermite approach to accurately reproduce the $(n+1)$th moment associated with particular examples of static Wigner density $\rho_W(q, p)$. However a true assessment of the effectiveness of the approach can only be demonstrated by its performance in a dynamical time propagation scheme where the closure scheme is applied at every time step.

5.5 Dynamical Calculations

For the dynamical calculations, the moments of an initial Wigner function of the following Gaussian form,

$$\rho_W(q, p, t_0) = \frac{1}{\pi\hbar}\exp(-2\alpha(q - \delta)^2 - p^2/(2\alpha\hbar^2)) \qquad (5.24)$$

are taken as an initial condition. The even order moments therefore have a Gaussian form in q and are zero for the odd order moments,

$\langle \mathcal{P}^{n=\text{odd}}\rho\rangle_q = 0$. For the following nondissipative examples, the reference distribution was defined as the Fourier transform of the initial 0th moment,

$$\rho_\beta = (2\alpha\hbar^2\pi)^{1/2}\exp\left(\frac{-p^2}{(2\alpha\hbar^2)}\right) \tag{5.25}$$

For the dissipative calculations, the reference distribution was taken as the Maxwell-Boltzmann distribution. The time integration of Eq. (5.2) was performed using a fourth order Runge-Kutta propagator with time step $\Delta t = 0.0004$ a.u.

5.5.1 Non-Dissipative Dynamics

Harmonic Oscillator

A harmonic potential of the form $V(q) = V_2 q^2$ with $V_2 = 0.0025$ and a mass of $m = 1$, with parameters $\alpha = 10$ and $\delta = 0.25$ were used in Eq. (5.24). The dynamics of $\langle\rho\rangle_q$ is depicted in Fig. (5.6), $\langle\mathcal{P}\rho\rangle_q$ in Fig. (5.7) and $\langle\mathcal{P}^2\rho\rangle_q$ shown in Fig. (5.8). The moments initially placed at $q = 0.25$ flow from right to left of the well in the negative direction. The direction of the flow is manifested in the dynamics of $\langle\mathcal{P}\rho\rangle_q$ which corresponds to the flux density. The initial flux, $\langle\mathcal{P}\rho\rangle_q = 0$ aquires a dominantly negative value, which reflects the direction of density flow. As $\langle\rho\rangle_q$ returns towards the positive region from left to right, the quantum flux $\langle\mathcal{P}\rho\rangle_q$ becomes positive. In fact the dynamics of $\langle\mathcal{P}\rho\rangle_q$ as the density $\langle\rho\rangle_q$ returns from left to right of the well is a mirror image with respect to the q coordinate axis of the motion of the density from right to left. Finally, the second moment initially placed at $q = 0.25$ moves towards the centre of the well, spreading out over q space. Its dynamics in, this sense, is similar to that of $\langle\rho\rangle$. The above calculations were performed with
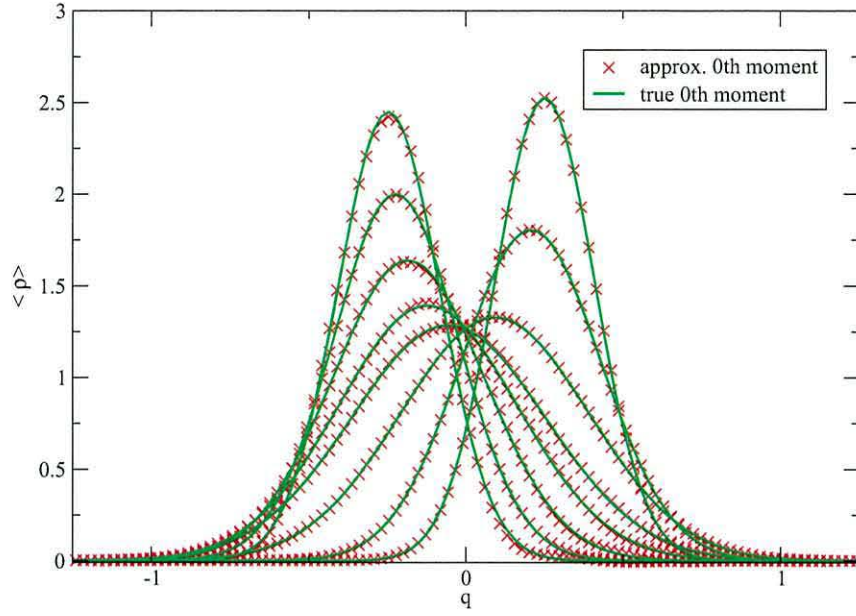
121

Figure 5.6: Dynamics of $\langle \rho \rangle_q$ in a harmonic potential. The moment as obtained from the Hermite approach is plotted against the true moment.
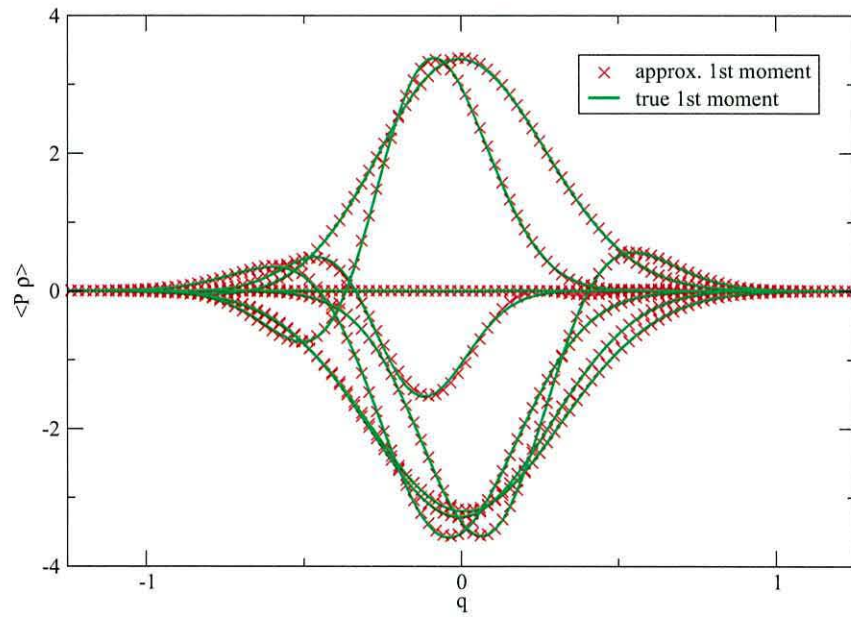

Figure 5.7: Dynamics of $\langle \mathcal{P} \rho \rangle_q$ in a harmonic potential. The moment as obtained from the Hermite approach is plotted against the true moment.
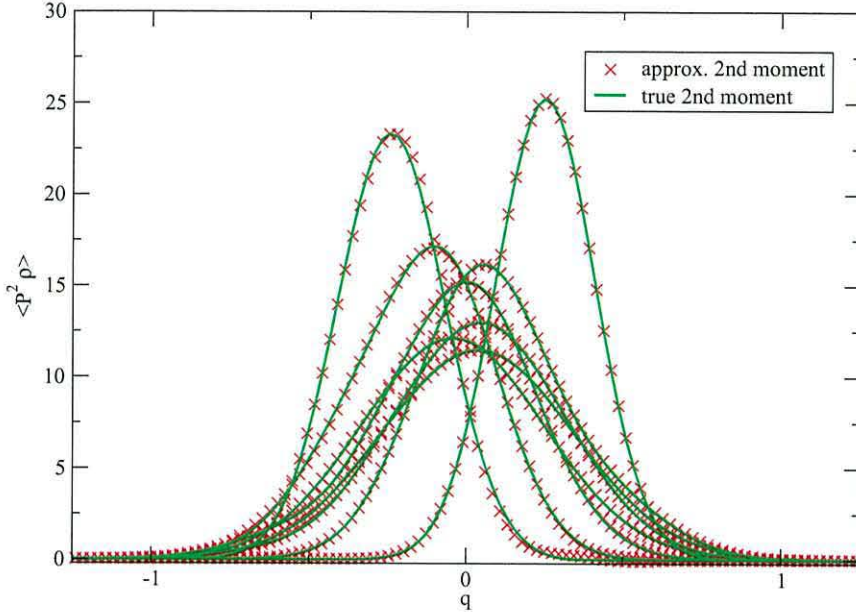
Figure 5.8: Dynamics of $\langle \mathcal{P}^2 \rho \rangle_q$ in a harmonic potential. The moment as obtained from the Hermite approach is plotted against the true moment.

a cut-off at $n = 19$. The three moments are shown with the true moments, as obtained from a propagation of the underlying wavefunction. There is excellent agreement between the two approaches, they are visually indistinguishable.

A comparison of the accuracy of the closure scheme for differing termination values of the moment hierarchy is shown in Fig. (5.9) for $t = 2000$ au. For termination at $n = 3$, the approximated moment has negative regions, which cannot occur for a true density. A termination at $n = 9$ improves the moment reconstruction but there remains deviations from the true moment. A termination at $n = 19$ shows good comparison with the true moment, even at this relatively long time scale. Although the reproduction of Gaussian moments for the static case of Fig. (5.3) shows good results for even
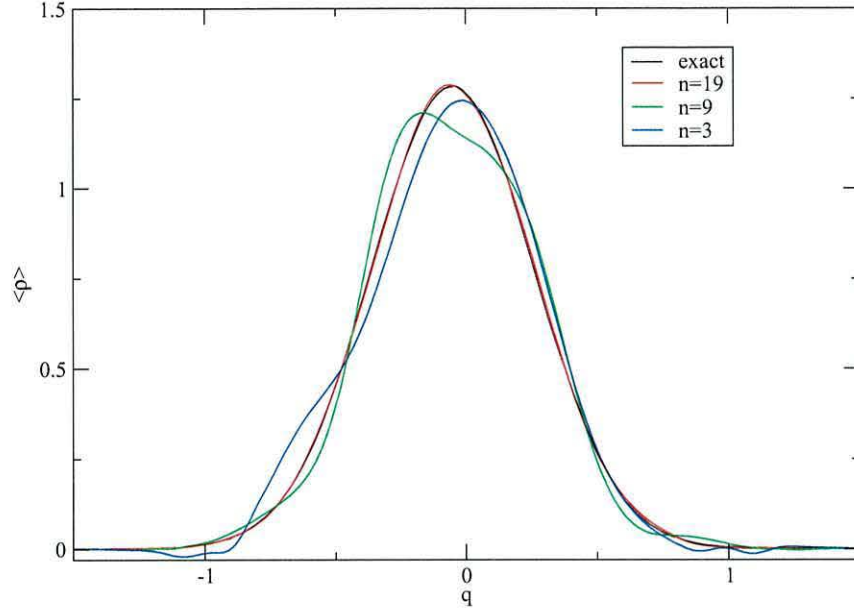
Figure 5.9: $\langle \rho \rangle_q$ depicted at $t = 2000$ au for propagation in a harmonic potential. It is shown for truncation at $n = 3$, $n = 9$ and $n = 19$ levels

low order moments (e.g. $n = 3$), in a dynamical scheme, a higher order truncation is required for longer timescales.

Double Well Potential

A double-well potential of the form,

$$V(q) = V_4 q^4 + V_2 q^2 \tag{5.26}$$

where $V_4 = 0.1$, $V_2 = -0.6$ and mass of $m = 1$ with the parameters $\alpha = 2$ and $\delta = 2$ as defined in Eq. (5.24) were used in this example. The dynamics of the zeroth moment for this potential is summarised in Fig. (5.10). The initial Gaussian profile of the moment rapidly disappears resulting in a moment displaying complicated dynamics. The complicated profile of the moments provides an ideal test case for the robustness of the Hermite approach in reproducing

124
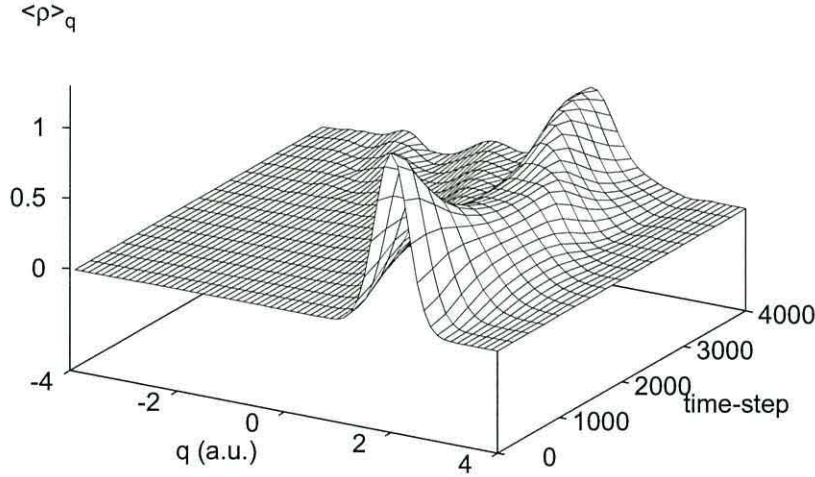
Figure 5.10: Dynamics of $\langle\rho\rangle_q$ in the double-well potential.

the $(n+1)$th moment. A direct comparison of the accuracy of the closure scheme for various termination values of the hierarchy is illustrated in Fig. (5.11) for two different snapshots taken during the propagation. It is clear that a termination at $n = 2$ is unacceptable, there is no similarity whatsoever between the approximated and true density. At a slightly higher value of $n = 9$, the dynamics of the reconstructed moment captures the general form of the true moment but there remains obvious disagreement. In fact, Fig. (5.11) shows the approximate 0th moment (i.e. density) developing negative regions, which is of course impossible. A closure at $n = 19$ is significantly better, with good agreement with the true dynamics even for relatively long time-scales ($1500\Delta t = 0.6$). The moment cut-off was attempted at higher order than $n = 19$ but only very slight improvements were observed. The computational effort was

125
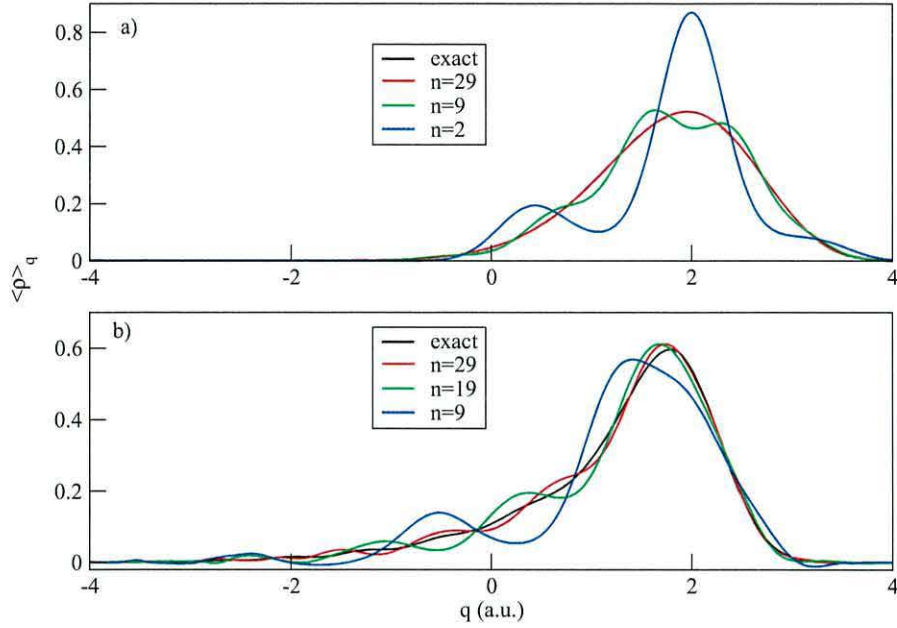
Figure 5.11: For the double-well potential a) and b) depict $\langle\rho\rangle_q$ computed at two different time-steps ($1500\Delta t = 0.6$ a.u. in a) and $2750\Delta t = 1.1$ a.u. in b)) and using different termination values for the hierarchy. In a) the closure applied at $n = 2, 9$ and 29 is depicted. In b) the closure applied at $n = 9, 19$ and 29 is depicted.

also significantly higher for larger values of n hence a maximum of $n = 19$ was chosen as being practicable. Furthermore, over longer time-scales the propagation becomes unstable irrespective of how many moments are used to reconstruct the density.

Although higher order moments are required to capture the small-scale p structure of the Wigner density, the convergence of the expansion of $\rho(q, r)$ is not guaranteed. It is not clear whether the instabilities is due to numerics or to the failure of the truncated moment expansion to reproduce small-scale p structure of the Wigner density.

Periodic Potential

In the illustration of the double well potential in the previous section, the derivatives of the potential terminate at the fourth order level. The summation in Eq.(5.2) thus terminates at $k = 3$. The moment equation contains only two terms involving the potential energy for moments $n \geq 3$.i.e.

$$\frac{\partial}{\partial t}\langle \mathcal{P}^n \rho \rangle = -\frac{1}{m}\frac{\partial}{\partial q}\langle \mathcal{P}^{n+1}\rho \rangle - n\frac{\partial V}{\partial q}\langle \mathcal{P}^{n-1}\rho \rangle_q + \frac{1}{4}\begin{pmatrix} n \\ 3 \end{pmatrix}\frac{\partial^3 V}{\partial q^3}\langle \mathcal{P}^{n-3}\rho \rangle_q$$

(5.27)

For a periodic potential,

$$V(q) = \frac{V_3}{2}(1 - \cos(3q))$$

(5.28)

this is not the case. In the Wigner-Moyal equation, this periodic potential would require the evaluation of high order momentum derivatives of the Wigner function. This can be very difficult in a grid-based numerical scheme and is highly undesirable. In the moment description however, these high order momentum derivatives of the Wigner function are translated to lower order moments $\langle \mathcal{P}^{n-k}\rho \rangle_q$ that involve no derivative evaluation. The moment approach is therefore the preferred scheme here.

The periodic potential defined in Eq. (5.28) contains three energetically equivalent potential wells. Periodic potentials are associated with describing quantum dynamics for phenomena such as bond rotation. A widely investigated example is the internal rotation of a methyl group about a single bond $C - O$ bond in CH_3OH. The three symmetric wells correspond to the three equivalent rotamers for the $360°$ rotation. Using a model system with moment of inertia
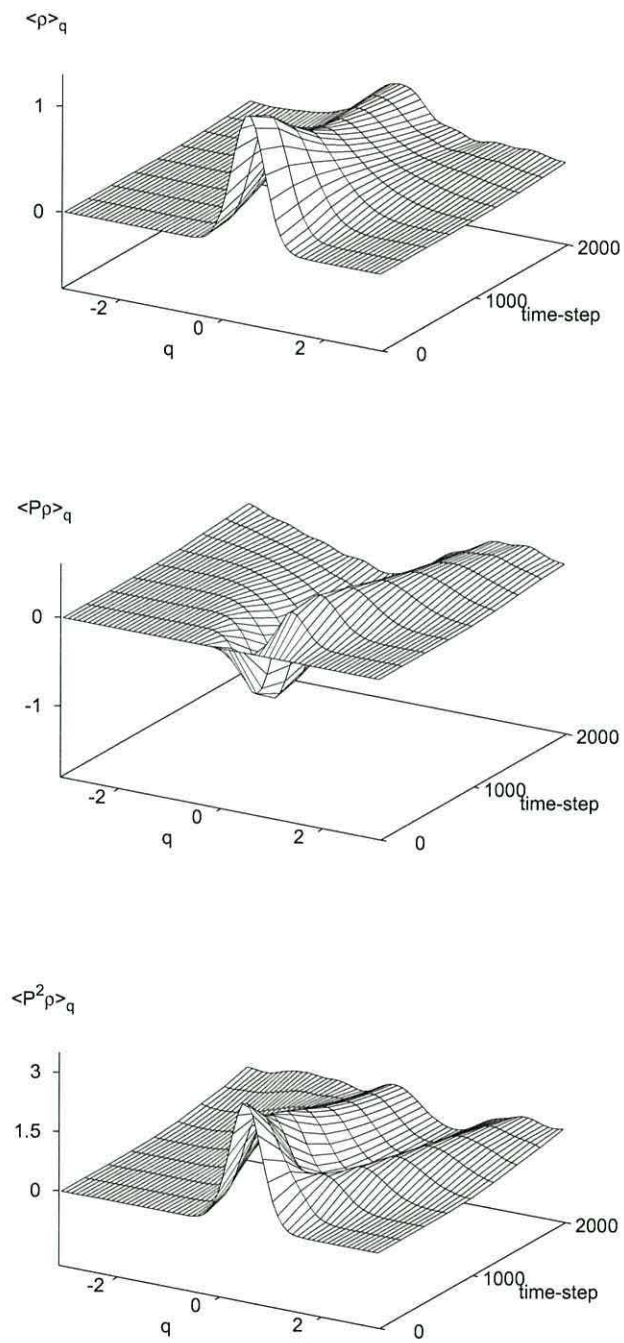
Figure 5.12: The dynamics of the first three moments in the periodic potential.

of $I = 1$, potential parameter $V_3 = 2$ and initial condition parameters of $\alpha = 2.5$ and $\delta = 0.5$, the torsional quantum dynamics of the three lowest order moments are shown in Fig. (5.12). Note that the model potential and inertia parameters used in this calculation (i.e. a relatively small moment of inertia and large potential barrier) dramatically increases the influence of higher order derivatives of the potential on the dynamics. For 'real' cases such as the internal rotation in methanol, the barrier would be much lower and the moment of inertia would be much higher. In this case the truncation of the expansion of the potential derivatives at $k = 3$ would be sufficient for computing accurate quantum dynamics. The model parameters are therefore chosen to magnify the effect of incorporating higher derivatives of potential on the stability of the closure scheme.

The moments in Fig. (5.12) develop oscillations which are typical of interference effects observed in periodic quantum dynamical systems. During the propagation, the moments that are initially displaced to the right move to the left towards the negative region. As time evolves, the density represented by the 0th moments delocalised from the centre well through to the other wells. Because of the flow of the density towards the negative region, the quantum flux, represented by the 1st moment becomes negative. The second moments (kinetic energy density) behaves very similarly to the density, becoming delocalised in all three potential wells.

As a further trial, the influence of incorporating higher terms in the expansion of potential derivatives on the stability of the approach was investigated. In theory, there is an infinite number of spatial
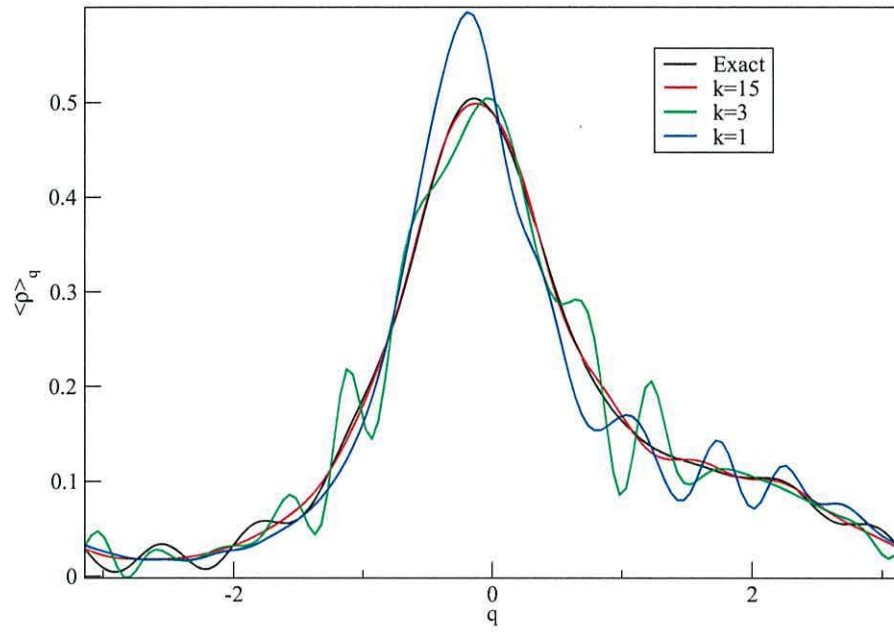
Figure 5.13: $\langle\rho\rangle_q$ depicted at $3500\Delta t = 0.7$ a.u. for propagations in the periodic potential where $n = 19$, using terminations of the expansion of the periodic potential derivatives of Eq. (5.2) at the 1st ($k = 1$), 3rd ($k = 3$), and 15th ($k = 15$) level.

derivatives for periodic potentials,

$$\frac{\partial}{\partial q}\langle \mathcal{P}^n \rho \rangle_q = -\frac{1}{m}\frac{\partial}{\partial q}\langle \mathcal{P}^{n+1} \rho \rangle_q - \sum_{k=1,\text{odd}}^{n} \begin{pmatrix} n \\ k \end{pmatrix} \left(\frac{\hbar}{2i}\right)^{k-1} \frac{\partial^k V}{\partial q^k}\langle \mathcal{P}^{n-k} \rho \rangle_q \quad (5.29)$$

However, in quantum dynamical calculations, the order of derivatives is truncated at a certain value. In Fig. (5.13), a snapshot of moments are shown at $t = 1750$ au for a truncation at the $k = 1$, $k = 3$ and $k = 15$ level. Taking the classical form ($k = 1$), the general form of the 0th moment in captured, but there is clear differences as compared to the numerically exact results. There is particularly poor reproduction at the peak, $q = -0.15$. Increasing to $k = 3$ improves the reconstruction somewhat as compared to the classical case, in particular with respect to the region at $q = -1.5$. Truncation at $k = 15$ improves the reproduction even further, with little deviation from the numerically exact results. It is worth noting that the truncation at $k = 15$ would involve evaluating the 15th derivative of the Wigner density $\rho_W(q, p)$ if the alternative Wigner-Moyal approach was used. It is clear therefore that the moment approach offers the advantage of involving significantly less computational effort for quantum dynamical simulations.

5.5.2 Dissipative Dynamics

As the hydrodynamic equations can be derived from the density matrix or the Wigner function for mixed states as well as pure states, the approach can be extended to be applied to the study of dissipative quantum systems. A study of systems that are coupled to their environment is referred to as theory of open quantum systems. When

the system interacts with its environment, the energy of the system relaxes and quantum coherence is lost. This process is known as decoherence. The dynamics of an open quantum system is described by the *reduced* density operator $\rho_S(t)$, which governs the dynamics of the sub-system only,

$$\rho_S = \mathrm{Tr}_E[\rho(t)] \tag{5.30}$$

where the environment degrees of freedom have been traced out. The equation of motion for the reduced density matrix is called a quantum master equation (QME). Many methods exist for the derivation of QME's and the literature is rich with examples of the various approaches [33]. This section focuses on the Caldeira-Leggett model [29] which describes the Markovian dynamics of a system that is weakly, bilinearly coupled to a bath of harmonic oscillators. The key assumptions underpinning the derivation of the C-L equation are

1. Factorised initial conditions so that the system and environment are uncorrelated at $t = 0$.

2. Markovian approximation i.e. assume the system dynamics is much slower than the environmental fluctuations. The reduced density matrix therefore loses all memory of past.

3. The environment is characterised by a bath of harmonic oscillators.

4. The coupling between the system and environment is weak.

5. High temperature limit, $k_B T \gg \hbar\Omega$, where k_B, T and Ω are

132

the Boltzmann constant, temperature of bath and cut-off frequency of the bath respectively.

The phase space representation of the Caldeira-Leggett equation is given by,

$$\frac{\partial}{\partial t}\rho_W = -\frac{i}{\hbar}\mathcal{L}_W\rho_W + \gamma\frac{\partial}{\partial p}p\rho_W + \gamma M k_B T \frac{\partial^2}{\partial p^2}\rho_W \qquad (5.31)$$

where γ is the friction coefficient and $k_B T$ is the thermal energy. This has the same form as the Wigner-Moyal equation, but has two additional terms. The third term in Eq. (5.31) is the diffusive term that drives the initial density distribution irreversibly to equilibrium. The second term is a friction term which slows down the rate drive to equilibrium. Both these terms are identical to the classical Klein-Kramers equation (i.e. the Fokker-Planck equation). Translated to the hydrodynamic form [7], the Caldeira-Leggett equation is given by,

$$\begin{aligned}
\frac{\partial}{\partial t}\langle \mathcal{P}^n \rho \rangle_q = &- \frac{1}{m}\frac{\partial}{\partial q}\langle \mathcal{P}^{n+1}\rho\rangle_q - \sum_{k=1,odd}^{n}\binom{n}{k}\left(\frac{\hbar}{2i}\right)^{k-1}\frac{\partial^k V}{\partial q^k}\langle \mathcal{P}^{n-k}\rho\rangle_q \\
&- n\gamma\langle \mathcal{P}^n\rho\rangle_q + n(n-1)\gamma M k_B \langle \mathcal{P}^{n-2}\rho\rangle_q \qquad (5.32)
\end{aligned}$$

From the above it is evident that the equation of motion for the 0th moment has no explicit dependence on the dissipative terms. Furthermore, the temperature dependent term only appears from the 2nd moment and above.

Harmonic Oscillator

The irreversible drive of the system to thermodynamic equilibrium is depicted for the average energy $\langle E \rangle$ in Fig. (5.14) a) and b) for a harmonic oscillator of frequency $\omega = 7.1 \times 10^{-4}$. For these calculations

133

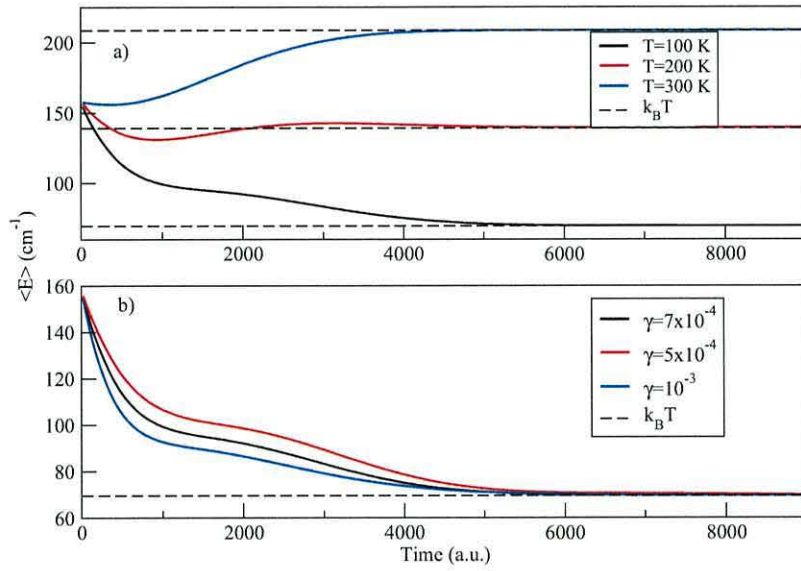Figure 5.14: Average system energy, $\langle E \rangle$, calculated from the Caldeira-Leggett equation using the same initial conditions. In a) $\gamma = 7 \times 10^{-4}$ was used with the bath temperatures $T = 100$ K, 200 K and 300 K. In b) the energy relaxation is depicted for a range of γ values and fixed bath temperature of $T=100$ K. The thermal energy is depicted by the horizontal broken line.

the initial condition $\alpha = 10$ and $\delta = 0.25$ was used in Eq. (5.24). As in previous results, a cut-off of $n = 19$ was used for the moment closure. Fig. (5.14) a) illustrates the approach to $\langle E \rangle = k_B T$ for a range of temperatures but using the same γ and initial conditions. Fig. (5.14) b) illustrates the approach to $\langle E \rangle = k_B T$ for a range of γ but for a fixed temperature and initial conditions. Note how the rate of energy relaxation to thermodynamic equilibrium increases as the friction coefficient γ increases, as is usually the case for a Caldeira Leggett model.

Double- Well Potential

This section illustrates the dissipative dynamics of the double well potential that was defined for the non-dissipative case. To reiterate, the potential parameters were given as $V_4 = 0.1$ and $V_2 = -0.6$ with mass of $m = 1$. The irreversible drive of the system to thermodynamic equilibrium is shown for the average energy $\langle E \rangle$ in Fig. (5.15). Also illustrated is the dynamics of $\langle \rho \rangle_q$. The relaxation of the system is depicted for two differing initial conditions. In the first example the values $\delta = 2$ and $\alpha = 2$ used in Eq. (5.24) centres the initial moments in the right hand side potential well. The other example with parameters $\delta = 0$ and $\alpha = 2$ centres the moments on top of the potential barrier. For both differing initial conditions, the average energy $\langle E \rangle$ relaxes to $k_B T = 0.59$. When taken relative to the potential energy minimum of -0.9 a.u., $k_B = -0.31$, as illustrated in Fig. (5.15). A comparison of the relaxation as calculated from the Caldeira-Leggett equation using the moment approach is made with a phase-space representation of Eq. (5.31). The two different approaches show excellent agreement. The time taken for

135
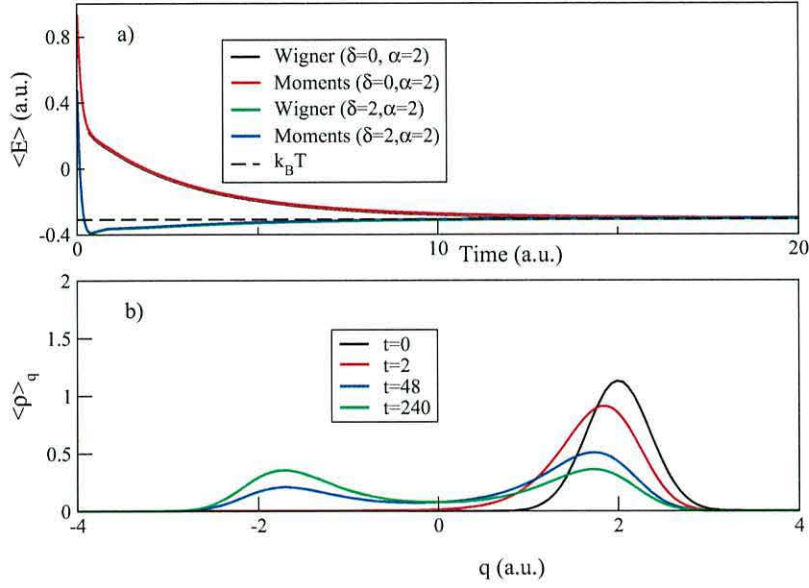
Figure 5.15: Dissipative dynamics of the double-well system using the parameters $\gamma = 5$ and $k_B T = 0.59$ ($k_B T = -0.31$ when taken relative to the potential energy minimum of -0.9 a.u.. a) Average system energy, $\langle E \rangle$, calculated from the Caldeira-Leggett equation using two different initial conditions. The terms in the brackets are the parameters that define initial Gaussian in Eq. (5.24). Also shown in this figure are the corresponding results obtained from the phase-space propagation of Eq. (5.31). b) Snapshots of $\langle \rho \rangle_q$ at various times.
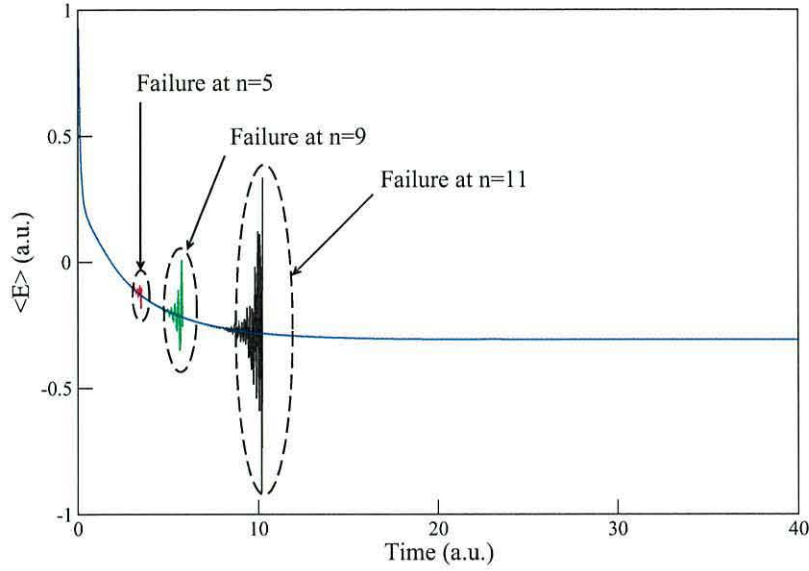
Figure 5.16: System energy relaxation for the double-well system using moment closures at $n = 5, 9$ and 11. The same dissipative parameters of Fig. (5.15) a) were used with initial conditions $\delta = 0$ and $\alpha = 2$.

the energy relaxation to occur is around $t = 15$ a.u.. However, it takes significantly longer for the moments to relax to a stationary distribution where both wells are equally populated. The dynamics of $\langle \rho \rangle_q$ is shown for the case the moments are centred in the right hand side well ($t = 0$). The stationary distribution is shown at $t = 240$ au. For the dissipative examples illustrated above, a moment truncation at $n = 15$ was used. It was found that a lower order truncation would accurately reproduce the dynamics for short time-scales, but would then become catastrophically unstable very rapidly. Fig. (5.16) shows the failure of the moments approach at the lower closure order of $n = 5, 9, 11$.

Periodic Potential

This system discussed here is the periodic potential with the same form as described for the non-dissipative example. The potential parameter $V_3 = 2$ a.u. and mass $m = 1$ is used in the calculations. The relaxation of the average energy of the system is depicted in Fig. (5.17) for a range of friction coefficients, γ. The initial condition of $\delta = 0.5$ and $\alpha = 2.5$ was used for all three examples and in all cases the average energy relaxes to $k_B T = 1.58$ over a time scale of approximately $t = 7$ a.u.. As time evolves, a steady transfer of moment density from the central well to both left and right wells occurs. Fig (5.17) also depicts the stationary distribution that is yielded at $t = 14$ a.u. for $\gamma = 0.75$.

5.6   Conclusions

It is shown in this Chapter that both a simple cut-off and dampening of the effect of higher order moments in the propagation of Eq. (3.9) is met with limited success. The moment hierarchy is non-convergent and a robust strategy is required to approximate the higher order moments. To this end, a variety of numerical methods, based on the maximum entropy approach are introduced. In particular, results are shown for the Hermite closure scheme as defined in Eq. (5.13) to produce accurate and stable dynamics. The approach was illustrated for the nondissipative and dissipative dynamics of a harmonic oscillator, double well and periodic potential. One of the main advantages of the approach is its ability to deal with both positive and negative regions of the Wigner function. This is in contrast to classical approaches to hydrodynamics where the development of a
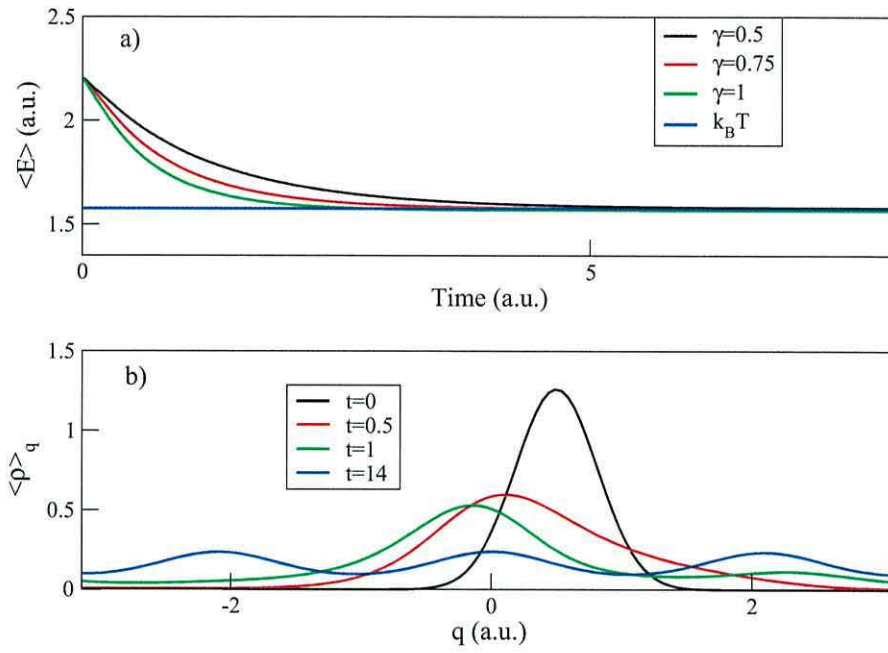
Figure 5.17: Dissipative dynamics of the periodic system with $k_B T = 1.58$. a) Average system energy, $\langle E \rangle$, calculated from the Caldeira-Leggett equation using three different values of γ. b) Snapshots of $\langle \rho \rangle_q$ at various times.

negative region is a disadvantage. Another appealing feature of the approach is its linearity. Furthermore, the evaluation of the linear coefficients involves only a single matrix multiplication at each time step.

The Hermite approach shows a dramatic improvement as compared to a cold truncation or other simple closure schemes. The moment closure issue is a notoriously difficult problem to solve [15, 30] and the stability offered by the Hermite approach is encouraging. However, further improvement of the methodology is required to propagate moments to even longer timescales.

Another drawback of the Hermite approach in its present form is that it requires a relatively large number of moments to close the hierarchy. In this Chapter, the results presented is for a single degree of freedom. If the approach was extended to cope with multidimensional quantum systems, the number of moments required to terminate the hierarchy would be unachievable. For instance, a three dimensional problem would require the evaluation of 1 743 392 200 moments for a truncation at the $n = 19$ level. The purpose of the closure scheme for the present study is its application in the hybrid hydrodynamic-Liouvillian Quantum Classical Moment approach of Burghardt *et al.* [1, 2, 3, 4]. As discussed in detail in previous Chapters, the QCM approach the quantum subsystem is treated hydrodynamically and will usually consist of a single degree of freedom. The classical part on the other hand is treated in a phase-space representation that does not involve any moments whatsoever. This therefore reduces the number of moments for multidimensional sys-

tems, so simplifying the application of the Hermite closure scheme.

In the future, the Hermite closure scheme will be applied to a Lagrangian trajectory representation of the hydrodynamic equations of motion. It is well known that simulating quantum dynamics in the Lagrangian frame is challenging [31, 32, 34], but these can only be investigated once a robust closure scheme for the moment hierarchy has been established. The Hermite approach illustrated in this Chapter shows promise as a closure scheme for the moments equations irrespective of the representation used.

Bibliography

[1] I. Burghardt and G. Parlant, J. Chem. Phys. **120**, 3055 (2004).

[2] I. Burghardt, K. B. Møller, and K. H. Hughes, Quantum hydro-dynamics and a moment approach to quantum-classical theory, in *Quantum Dynamics of Complex Molecular Systems*, edited by D. A. Micha and I. Burghardt, Springer, 2006.

[3] K.H. Hughes, S. M. Parry, G. Parlant and I. Burghardt, J. Phys. Chem. A **111**, 10269 (2007).

[4] I. Burghardt, J. Chem. Phys. **122**, 094103 (2005).

[5] K. H. Hughes, S. M. Parry and I. Burghardt, J. Chem. Phys. **130**, 054115 (2009)

[6] I. Burghardt and L. S. Cederbaum, J. Chem. Phys. **115**, 10303 (2001)

[7] I. Burghardt and K. B. Møller, J. Chem. Phys. **117**, 7409 (2002).

[8] N.A. Krall and A.W. Trivelpiece, *Principles of Plasma Physics*, Mc-Graw Hill, New York, 1973.

[9] M. Trovato and P. Falsaperla, Phys. Rev. B **57**, 4456 (1998).

[10] J. V. Lill, M. I. Haftel, and G. H. Herling, J. Chem. Phys. **90**, 4940 (1989)

[11] M.K. Tippett, J. Plasma Phys. **54**, 77 (1995).

[12] M. Junk, Nonlinearity **14**, 881 (2001).

[13] M. Bisi, G. Spiga and G. Toscani, Phys. Fluids **16**, 4235 (2004).

[14] B. Qiao, X. T. He and S. P. Zhu, Europhys. Lett. **72**, 955 (2005).

[15] P. Degond and C. Ringhofer, J. Stat. Phys. **112**, 587 (2003).

[16] E. T. Jaynes, Phys. Rev. **106**, 620 (2006).

[17] L. M. Martyushev and V. D. Selznev, Phys. Rep. **426**, 1 (2006).

[18] N. Sukumar and R. W. Wright, Int. J. Numer. Methods. Engrg. **70**, 181 (2006).

[19] C. D. Levermore, J. Stat. Phys. **83**, 1021 (1996).

[20] E. D. Laue, M. R. Mayger, J. Skilling and J. Staunton, J. Magn. Reson. **68**, 14 (1986).

[21] P. F. Smith and M. A. Player, J. Phys. D: Appl. Phys. **24**, 1714 (1991).

[22] M. P. Hobson and A. N. Lasenby, Mon. Not. R. Astron. Soc. **298**, 905 (1998).

[23] K. Maisinger, M. P. Hobson and A. N. Lasenby, Mon. Not. R. Astron. Soc. **347**, 339 (2004).

[24] A. Jackson, C. Constable and N. Gillet, Geophys. J. Int. **171**, 995 (2007).

[25] N. Gillet, A. Jackson and C. C. Finlay, Geophys. J. Int. **171**, 1005 (2007).

[26] L. Dobrzynski and E. Zukowski, J. Phys.: Condens. Matter **11**, 8049 (1999).

[27] A. T. N. Kumar, L. Zhu, J. F. Christian, A. A. Demidov and P. M. Champion, J. Phys. Chem. B **105**, 7847 (2001).

[28] H. Grad, Commun. Pure Appl. Math. **2**, 331 (1949).

[29] A. O. Caldeira and A. J. Leggett, Physica A **121**, 587 (1983).

[30] M. Junk, Math. Models Methods Appl. Sci. **10**, 1001 (2000).

[31] R. E. Wyatt, Chem. Phys. Lett. **313**, 189 (1999).

[32] C. J. Trahan, K. H. Hughes and R. E. Wyatt, J. Chem. Phys. **118**, 9911 (2003).

[33] U. Weiss, *Quantum Dissipative Systems*, World Scientific Singapore, 1993.

[34] K. H. Hughes and R. E. Wyatt, Chem. Phys. Lett. **366**, 336 (2002).

Chapter 6

Mixed Quantum-Classical Dynamics: Solvation Phenomena

6.1 Introduction

The properties of a molecule in a vacuum is very different to the properties of the same molecule immersed in a solvent. As chemical reactions often occur in a solvent environment, the study of the effect of the solvent on the solute is crucial and many investigations have been recorded in the literature [1]. Initially, these investigations were concerned with *equilibrium* solvent effects [2]. An example of this is the effect of solvent polarity on the reaction potential surface. It has been observed in more recent work that in fast reactions, solvent dynamics can affect both the rate and outcome of the reaction [3]. There is therefore a need to understand the time dependent response of solvent to a change in the charge distribution of a solute molecule. With developments made in ultrafast time-resolved spectroscopy, it
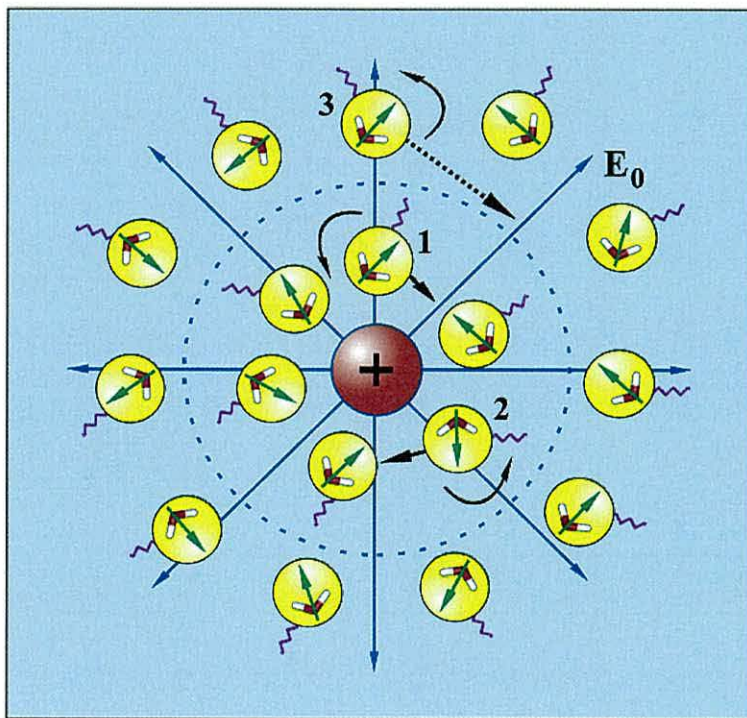
Figure 6.1: A schematic (revised from Ref. [5]) summarising the solvation process. This particular example is for biological water in the role of a solvent. The electric field from solute is denoted by E_0. The solvent molecules (labelled 1, 2 and 3) are shown to rotate or translate in response to the change in the charge distribution of the solute.

is possible to investigate ultrafast events in excited electronic states, and the response of the solvent environment thereafter [3, 4]. This aids in the understanding of the role of solvents in many important chemical and biological processes. Biological macromolecules such as proteins and DNA are physiologically inactive in the absence of water [5]. An understanding of the water as a solvent here is therefore essential to comprehend the basis of many biological phenomena.

In the time dependent picture of solvation, the solute particle is

initially in its ground electronic state in equilibrium with the solvent environment. A sudden change in the solute is made by femtosecond excitation (e.g. by a radiation field), which can lead to the creation (or change) of a dipole. This newly created dipole induces an electric field on the surrounding solvent molecules. The solute, in a sense undergoes a Franck-Condon transition while the solvent retain its previous spatial and orientational configuration. This creates a highly non-equilibrium situation. Subsequently, the solvent molecules move and rearrange themselves to stabilize the new charge distribution. The resultant energy is the solvation energy of the solute, E_{sol}. The motion of the solvent can be either rotational of translational. This process is summarised in Fig. (6.1).

The time dependent response of the solvent (i.e. the progress of solvation) of a newly created charge distribution that often follows an electronic excitation is measured by the 'time dependent fluorescence Stokes shift' (TDFSS) of the emission spectrum of the solute molecules [6, 7, 8, 9]. In these experiments, large dye molecules are used as *solute probes*. These are particularly useful as probes since their dipoles change dramatically in the event of excitation. They also exhibit fluorescence and stay in the excited state for 'longer' periods. This allows the response of the solvent to be investigated. The time dependence of the rearrangement of the solvent environment is reflected in the continuous red shift of the emission and this can be represented by the spectral response function [1],

$$S(t) = \frac{v(t) - v(\infty)}{v(0) - v(\infty)} \qquad (6.1)$$

where $v(t)$ is the emission frequency of the solute. This normalised function, also labelled the solvation time correlation function, decays

147

from unity to zero as time progresses to $t = \infty$. The solvation time correlation is equivalently written in terms of the solvation energy E_{sol}, given by,

$$S(t) = \frac{E_{\text{sol}}(t) - E_{\text{sol}}(\infty)}{E_{\text{sol}}(0) - E_{\text{sol}}(\infty)} \qquad (6.2)$$

An initial theoretical approach to calculate the Stokes shift correlation function of Eq. (6.2) was offered by the continuum model [10, 11]. This is the extension of the equilibrium solvation model invoked by Born [12] and Onsager [13] to the time domain. The general premise of this model is that the dipolar solvent is represented by a homogenous dielectric continuum medium with frequency dependence given by the Debye equation. Furthermore, the polar solute is described as a point dipole at the centre of a spherical molecular cavity. The overall conclusions from application of this approach is that the correlation function should decay exponentially with lifetime τ_L [6]. Because the solvation of a solute is seen to proceed over a range of timescales rather that a single time constant, τ_L, the application of this approach is severely limited. The homogenous continuum models also neglect effects such as solvent-solute interactions, which again limits its applicability.

More recently, *inhomogeneous* dielectric continuum models were developed to address some of the disadvantages of the homogenous approach [14]. In particular, the differences in the response of solvent molecules very close to the solute and those in the 'bulk' were explored. This was primarily achieved by extending the continuum model to include the shape variation of the solute and include

148

space dependence in the frequency dependent dielectric function. The drawback of these models is they are phenomenological, and although they provide a simple and intuitive description of solvation, they neglect any consideration of molecular level effects [1]. Many different theoretical approaches of varying improvement and success over the continuum model have been developed, including, Brownian oscillator models [15], surrogate Hamiltonian approaches [16], instantaneous normal mode descriptions [17] and mode coupling theory [18]. The approach considered in this Chapter is the molecular hydrodynamic approach [19]. This methodology takes into account the microscopic solute-solvent and solvent-solvent interactions. The extended hydrodynamic approach presented in the following sections follows derivation in Ref. [19].

6.2 Extended Hydrodynamic Approach

The extended hydrodynamic molecular theory was developed in the 1970's and has been applied to many liquid state phenomena in chemistry. [19]. The formulation is based fundamentally on the coupled equations for the solvent local density and the momentum density [20, 21, 22, 23, 24]. The equations include a force term written in terms of the functional derivative of the solvent free energy. This includes both the microscopic solvent-solute and solvent-solvent interactions. The extended hydrodynamic approach can be thought of as a classical time-dependent density functional theory (TD-DFT) description [19]. Note that in this hydrodynamic approach, the dynamics of the momentum field is included. This is not usually the case for TD-DFT approaches where the rapid relaxation of the time

dependent momentum is assumed [25]. In TD-DFT, the momentum field is therefore neglected.

6.2.1 Derivation of the dynamical equations

The coupled equations of motion for the hydrodynamic fields are expressed as,

$$
\begin{aligned}
\frac{\partial}{\partial t}\rho(\mathbf{r}, t) &= -\frac{1}{m}\nabla_r \cdot \mathbf{g}(\mathbf{r}, t) \\
\frac{\partial}{\partial t}\mathbf{g}(\mathbf{r}, t) &= -\rho(\mathbf{r}, t)\nabla_r \frac{\delta \mathcal{F}[\rho(t)]}{\delta \rho(\mathbf{r}, t)}
\end{aligned}
\tag{6.3}
$$

where $\rho(\mathbf{r}, t) = \langle f \rangle_q$ is the solvent local density, $\mathbf{g}(\mathbf{r}, t) = \langle \mathcal{P}f \rangle_q$ is the momentum density. These are the same as the hydrodynamic fields detailed in the preceeding chapters. These are functions of the solvent translational coordinate $\mathbf{r}$. The solvent local density is governed by a continuity equation whilst the the equation for $\mathbf{g}(\mathbf{r}, t)$ is a generalized Navier-Stokes equation.

The force term in the equations of motion is given as the functional derivative of the Helmholtz free energy $\delta \mathcal{F}/\delta \rho$. Although the free energy in question is that of the non equilibrium density, $\rho(\mathbf{r}, t)$, the actual form can be taken to be the equilibrium form from statistical mechanics. This approximation is a central theme in the molecular hydrodynamic approach derived in this Chapter.

The Helmholtz free energy is written as a summation of three distinct parts,

$$
\mathcal{F}[\rho(t)] = \mathcal{F}_0[\rho(t)] + \mathcal{F}_{\text{int}}[\rho(t)] + \int d\mathbf{r}\rho(\mathbf{r}, t)U_{\text{ex}}(\mathbf{r})
\tag{6.4}
$$

The first term is the 'ideal' part which comes from a non-interacting Boltzmann gas. This is the entropic contribution to the free energy,

150

given by,

$$\mathcal{F}_0[\rho(t)] = k_B T \int d\mathbf{r} \rho(\mathbf{r}, t)(\ln[\rho(\mathbf{r}, t)\Lambda^3] - 1) \qquad (6.5)$$

where Λ is the thermal wavelength,

$$\Lambda = \left(\frac{h^2}{2\pi m k_B T}\right)^{1/2} \qquad (6.6)$$

The second term is the interaction part written in terms of a binary correlation term,

$$\mathcal{F}_{\text{int}}[\rho(t)] = -\frac{1}{2}k_B T \int d\mathbf{r} \int d\mathbf{r}' \delta\rho(\mathbf{r}, t)C_2(\mathbf{r} - \mathbf{r}')\delta\rho(\mathbf{r}', t) \qquad (6.7)$$

These first two terms in Eq. (6.4) include the Boltzmann constant, k_B and the temperature, T. The term $\delta\rho(\mathbf{r}, t) = \rho(\mathbf{r}, t) - \rho_{\text{eq}}(\mathbf{r})$ is the deviation from the equilibrium density in the presence of a solute. Eq. (6.4) also contains the direct correlation function, $C_2(\mathbf{r} - \mathbf{r}')$, which pertains to the reference equilibrium density, $\rho_{\text{eq}}(\mathbf{r})$. The interaction part, $\mathcal{F}_{\text{int}}[\rho(t)]$ is the first term in a density expansion of the free energy that is expressed in terms of n-particle correlation functions [20, 23]. The direct correlation term, $C_2(\mathbf{r} - \mathbf{r}')$, can include both solvent-solvent *and* solvent-solute interactions if for instance, the solute's internal structure was also of interest. The final term in Eq. (6.4) pertains to an external potential, U_{ex}. This corresponds to solute-solvent interactions.

The functional derivative of the free energy with respect to the density is given as [20, 21, 22, 23, 24],

$$\frac{\partial\mathcal{F}[\rho(t)]}{\partial\rho(\mathbf{r}, t)} = k_B T \left\{\ln\Lambda^3\rho(\mathbf{r}, t) - \int d\mathbf{r}'C_2(\mathbf{r} - \mathbf{r}')\delta\rho(\mathbf{r},' t)\right\} + U_{\text{ex}}(\mathbf{r})$$
$$(6.8)$$

The force term that appears in the equation of motion for the momentum density, $\mathbf{g}(\mathbf{r}, t)$ is the gradient Eq. (6.8).

6.2.2 Hydrodynamic quantities from the phase space density

The equations of motion for the hydrodynamic fields, Eq. (6.3) can be extracted from the equation of motion for the single particle phase space density [26],

$$
\begin{aligned}
\frac{\partial}{\partial t} f(\mathbf{r}, \mathbf{p}, t) &= \left\{ \frac{\mathbf{p}^2}{2m} + V_{\mathrm{eff}}(\mathbf{r}, t) + U_{\mathrm{ex}}(\mathbf{r}), f(\mathbf{r}, \mathbf{p}, t) \right\} \\
&= -\frac{\mathbf{p}}{m} \cdot \nabla_r f(\mathbf{r}, \mathbf{p}, t) + \nabla_r [V_{\mathrm{eff}}(\mathbf{r}, t) + U_{\mathrm{ex}}(\mathbf{r})] \\
&\quad \cdot \nabla_p f(\mathbf{r}, \mathbf{p}, t)
\end{aligned}
\tag{6.9}
$$

In the Enskog-Vlassov approximation, the effective single particle potential V_{eff} is given by [27],

$$
V_{\mathrm{eff}}(\mathbf{r}, t) = -k_B T \int d\mathbf{r}' d\mathbf{p}' C_2(\mathbf{r} - \mathbf{r}') \delta f(\mathbf{r}', \mathbf{p}', t)
\tag{6.10}
$$

where $\delta f = (f - f_{\mathrm{eq}})$ is the deviation from equilibrium. V_{eff} contains the two particle correlation, $C_2(\mathbf{r} - \mathbf{r}')$.

The first two moments of the single particle distribution are given by,

$$
\begin{aligned}
\rho(\mathbf{r}, t) &= \langle f \rangle_q = \int d\mathbf{p}\, f(\mathbf{r}, \mathbf{p}, t) \\
\mathbf{g}(\mathbf{r}, t) &= \langle \mathcal{P} f \rangle_q = \int d\mathbf{p}\, \mathbf{p}\, f(\mathbf{r}, \mathbf{p}, t)
\end{aligned}
\tag{6.11}
$$

where $\rho(\mathbf{r}, t)$ corresponds to the local density and $\mathbf{g}(\mathbf{r}, t)$ is the momentum density. The dynamical equations for the hydrodynamic quantities can be written,

$$
\begin{aligned}
\frac{\partial}{\partial t} \rho(\mathbf{r}, t) &= -\frac{1}{m} \nabla_{\mathrm{r}} \cdot \mathbf{g}(\mathbf{r}, t) \\
\frac{\partial}{\partial t} \mathbf{g}(\mathbf{r}, t) &= -\frac{1}{m} \nabla_{\mathrm{r}} \left[\sigma(\mathbf{r}, t) + \frac{\mathbf{g}(\mathbf{r}, t) \cdot \mathbf{g}(\mathbf{r}, t)}{\rho(\mathbf{r}, t)} \right] \\
&\quad - \rho(\mathbf{r}, t) \nabla_{\mathrm{r}} [V_{\mathrm{eff}}(\mathbf{r}, t) + U_{\mathrm{ex}}(\mathbf{r})]
\end{aligned}
\tag{6.12}
$$

where $\sigma(\mathbf{r}, t)$ is the pressure tensor,

$$\sigma(\mathbf{r}, t) = \int d\mathbf{p} \; \mathbf{p} \cdot \mathbf{p} f(\mathbf{r}, \mathbf{p}, t) - \frac{\mathbf{g}(\mathbf{r}, t) \cdot \mathbf{g}(\mathbf{r}, t)}{\rho(\mathbf{r}, t)} \qquad (6.13)$$

This term $\sigma(\mathbf{r}, t)$, is the equivalent to the variance seen in the hydrodynamic equations from Chapter 3 and 4. It arises from the kinetic part of the Hamiltonian and includes the second momentum moment of the non-equilibrium density. As seen previously, the variance cannot be written as a functional of ρ and $\mathbf{g}$, so Eq. (6.12) do not form an independent closed set [27]. These equations depend on an infinite hierarchy of coupled equation for higher order hydrodynamic fields [29].

The approximation to yield the hydrodynamic equations Eq. (6.3) was taken as replacing the kinetic energy contribution with an ideal non-interacting free energy term [19],

$$-\frac{1}{m}\nabla_{\mathrm{r}}\sigma(\mathbf{r}) \rightarrow -\rho(\mathbf{r})\nabla_{\mathrm{r}}\frac{\delta\mathcal{F}_0[\rho]}{\delta\rho(\mathbf{r})} = -k_B T \rho(\mathbf{r})\nabla_{\mathrm{r}}\ln\Lambda^3\rho(\mathbf{r}) \qquad (6.14)$$

This is the same as truncating the moment hierarchy i.e. a moment closure scheme. The convective term, $\mathbf{g}(\mathbf{r}, t) \cdot \mathbf{g}(\mathbf{r}, t)/\rho(\mathbf{r}, t)$ is also neglected within the approximation. To this end, only the linear terms in $\mathbf{g}(\mathbf{r}, t)$ are retained.

The considerations so far have been limited to hydrodynamic quantities that depend on the solvent translational coordinate (and of course time t) only. This is only valid in some limited cases. In reality, for molecular liquids, this extended hydrodynamic formulation needs to include orientational relaxation effects as well as the translational response [19, 20]. In fact, for polar solvation phenomena, the orientational effects dominate the translational effects.

The orientational component is formally included in the molecular hydrodynamic approach by expressing the relevant hydrodynamic fields as functions of the orientation ω as well as the translation $\mathbf{r}$. To this end, the dynamical equations for the local density and the momentum density (which now has separate orientational and translational parts) are defined [19],

$$
\begin{aligned}
\frac{\partial}{\partial t}\rho(\mathbf{r},\omega,t) &= -\frac{1}{m}\nabla_r \cdot \mathbf{g}_\mathrm{T}(\mathbf{r},\omega,t) - \frac{1}{I}\nabla_\omega \cdot \mathbf{g}_\omega(\mathbf{r},\omega,t) \\
\frac{\partial}{\partial t}\mathbf{g}_\mathrm{T}(\mathbf{r},\omega,t) &= -\rho(\mathbf{r},\omega,t)\nabla_r \frac{\delta\mathcal{F}[\rho(t)]}{\delta\rho(\mathbf{r},\omega,t)} \\
\frac{\partial}{\partial t}\mathbf{g}_\omega(\mathbf{r},\omega,t) &= -\rho(\mathbf{r},\omega,t)\nabla_\omega \frac{\delta\mathcal{F}[\rho(t)]}{\delta\rho(\mathbf{r},\omega,t)}
\end{aligned}
\tag{6.15}
$$

The term I is the moment of inertia and ∇_ω is the angular momentum operator.

Although consideration of both translational and orientational effects is required for many chemical systems, the remainder of the Chapter focuses only on the translational component.

6.2.3 Extended hydrodynamic equations coupled to a quantum system

In this section, the extended hydrodynamic formulation incorporates the coupling to a quantum solute. In particular, the quantum solute is taken as a two level system, although it can also deal with more complex systems such as a quantum subsystem including internal nuclear modes. The derivation follows Ref [19].

The underlying single-particle function for this mixed quantum-classical description is a hybrid quantum-classical density, $\hat{f}(\mathbf{r},\mathbf{p},t)$. This

154

function is therefore a quantum density operator for the two-level system subspace while retaining a classical phase space description of the solvent part [28]. $\hat{f}(\mathbf{r}, \mathbf{p}, t)$ is constructed by taking the classical phase space limit of a partially Wigner transformed density operator. For a two level quantum system, a discretised basis is taken for the quantum part and the mixed density is given by,

$$\hat{f}(\mathbf{r}, \mathbf{p}) = \sum_{nm} f_{nm}(\mathbf{r}, \mathbf{p})|n\rangle\langle m| \tag{6.16}$$

The diagonal elements ($n = m$) correspond to the electronic populations while the off-diagonals ($n \neq m$) are the coherences. In this hybrid approach, these are parameterised by the classical phase space variables $(\mathbf{r}, \mathbf{p})$. The dynamical equation for the quantum-classical single particle density is given by the quantum-classical Liouville equation [28],

$$\frac{\partial}{\partial t}\hat{f} = -\frac{i}{\hbar}[\hat{H}, \hat{f}] + \frac{1}{2}(\{\hat{H}, \hat{f}\} - \{\hat{f}, \hat{H}\}) \tag{6.17}$$

where $[,]$ is the quantum commutator and $\{,\}$ is the classical Poisson bracket. The Hamiltonian operator of this mixed quantum-classical system is written in terms of the same discretised basis of the quantum part [19], such that,

$$\hat{H} = \frac{\mathbf{p}^2}{2m} + \sum_{nm}[V_{nm}^{\text{TLS}} + V_{nm}^{\text{eff}}(\mathbf{r}, t) + U_{nm}^{\text{ex}}(\mathbf{r})|n\rangle\langle m| \tag{6.18}$$

The first term in the summation corresponds to the quantum two level system (TLS) potential while the second term is the effective mean field potential. In this hybrid quantum-classical framework, the effective mean field is state (n, m) specific,

$$V_{nm}^{\text{eff}}(\mathbf{r}, t) = -k_B T \delta_{nm} \int d\mathbf{r}' \int d\mathbf{p}' C_2^{(n)}(\mathbf{r} - \mathbf{r}')\delta f_{nn}(\mathbf{r}', \mathbf{p}', t) \tag{6.19}$$

where the term $\delta f_{nn} = f_{nn} - f_{\text{eq}}^{(n)}$ is the deviation from the reference equilibrium state. The third term in the summation is the external

155

potential it can have both diagonal and off-diagonal components. The hydrodynamic fields of local density and momentum density are derived from the hybrid single particle density in the usual way [29, 30],

$$
\begin{aligned}
\rho_{nm}(\mathbf{r}, t) &= \int d\mathbf{p}\, \hat{f}_{nm}(\mathbf{r}, \mathbf{p}, t) \\
\mathbf{g}_{nm}(\mathbf{r}, t) &= \int d\mathbf{p}\, \mathbf{p}\, \hat{f}_{nm}(\mathbf{r}, \mathbf{p}, t)
\end{aligned}
\tag{6.20}
$$

The dynamical equations for ρ_{nm} (now a 2×2 matrix of scalar quantities) and $\mathbf{g}_{nm}$ (a 2×2 of vectors) are obtained by applying prescription of Eq. (6.20) to the quantum-classical single particle density of Eq. (6.17). The same approximation of Eq. (6.14) is also invoked such that the following matrix equations can be written for the local density,

$$
\frac{\partial}{\partial t}\rho = -\frac{1}{m}\nabla_r \cdot \mathbf{g} - \frac{i}{\hbar}\Big[\Big(V^{\mathrm{TLS}} + \frac{\delta\mathcal{F}}{\delta\rho}\Big)\cdot\rho - \rho\cdot\Big(V^{\mathrm{TLS}} + \frac{\delta\mathcal{F}}{\delta\rho}\Big)\Big] \tag{6.21}
$$

and similarly for the momentum density,

$$
\begin{aligned}
\frac{\partial}{\partial t}\mathbf{g} = &- \frac{1}{2}\Big[\nabla_r\Big(\frac{\delta\mathcal{F}}{\delta\rho}\Big)\cdot\rho + \rho\cdot\nabla_r\Big(\frac{\delta\mathcal{F}}{\delta\rho}\Big)\Big] \\
&- \frac{i}{\hbar}\Big[\Big(V^{\mathrm{TLS}} + \frac{\delta\mathcal{F}}{\delta\rho}\Big)\cdot\mathbf{g} - \mathbf{g}\cdot\Big(V^{\mathrm{TLS}} + \frac{\delta\mathcal{F}}{\delta\rho}\Big)\Big]
\end{aligned}
\tag{6.22}
$$

The associated free energy is a functional of the matrix density ρ,

$$
\mathcal{F}[\rho(t)] = \mathcal{F}_0[\rho(t)] + \mathcal{F}_{\mathrm{int}}[\rho(t)] + \int d\mathbf{r}\rho(\mathbf{r}, t)U_{\mathrm{ex}}(\mathbf{r}) \tag{6.23}
$$

with a non-interacting, entropic term,

$$
\mathcal{F}_0[\rho(t)] = k_B T \sum_{nm}\delta_{nm}\int d\mathbf{r}\rho_{nm}(\mathbf{r}, t)(\ln\Lambda^3\rho_{nm}(\mathbf{r}, t) - 1) \tag{6.24}
$$

The interaction term, $\mathcal{F}_{\mathrm{int}}$, from the state-specific effective potential is given by,

$$
\mathcal{F}_{\mathrm{int}}[\rho(t)] = -\frac{1}{2}k_B T \sum_n \int d\mathbf{r}\int d\mathbf{r}'\,\delta\rho_{nn}(\mathbf{r}, t)C_2^{(n)}(\mathbf{r} - \mathbf{r}')\delta\rho_{nn}(\mathbf{r}', t) \tag{6.25}
$$

156

where $\delta\rho_{nn} = \rho_{nn} - \rho_{\rm eq}^{(n)}$. The final term in Eq. (6.23), the external potential may have both diagonal and off-diagonal terms.

The free energy functional derivative is now of a matrix from, given by,

$$
\left(\frac{\delta\mathcal{F}[\rho(t)]}{\delta\rho(\mathbf{r},t)}\right)_{nm} = \quad k_B T\Big\{\delta_{nm}\ln\Lambda^3\rho_{nm}(\mathbf{r},t)
$$
$$
-\delta_{nm}\int d\mathbf{r}' C_2^{(n)}(\mathbf{r}-\mathbf{r}')\delta_{nm}\rho_{nm}(\mathbf{r}',t)\Big\} + U_{nm}^{\rm ex}(\mathbf{r})
$$

(6.26)

As the classical solvent is now interacting with a two level quantum subsystem, there is coupling between the diagonal ($n = m$) and off-diagonal ($n \neq m$) fields component in addition to the coupling between the hydrodynamic fields. This multiple coupling results in complex dynamical behaviour [29, 30]. The details and effect of the differing coupling can be better understood by looking at individual components of the matrices for the hydrodynamic fields. For example, the density field ground state population, ρ_{11} is given by,

$$
\frac{\partial}{\partial t}\rho_{11} = -\frac{1}{m}\nabla_r\cdot\mathbf{g}_{11} - \frac{i}{\hbar}\Big[V_{12}^{\rm TLS} + \Big(\frac{\delta\mathcal{F}}{\delta\rho}\Big)_{12}\Big](\rho_{21} - \rho_{12}) \quad (6.27)
$$

while the equivalent momentum field,

$$
\frac{\partial}{\partial t}\mathbf{g}_{11} = \quad -\; \rho_{11}\nabla_r\Big(\frac{\delta\mathcal{F}}{\delta\rho}\Big)_{11} - \frac{1}{2}(\rho_{21} + \rho_{12})\nabla_r\Big(\frac{\delta\mathcal{F}}{\delta\rho}\Big)_{12}
$$
$$
-\; \frac{i}{\hbar}\Big[V_{12}^{\rm TLS} + \Big(\frac{\delta\mathcal{F}}{\delta\rho}\Big)_{12}\Big](\mathbf{g}_{21} - \mathbf{g}_{12}) \quad (6.28)
$$

It is clear that the dynamics of the populations of both the local density and momentum density depend on the coherence (off-diagonal) terms. The effect of population transfer mediated by the coherence

157

terms for the local density can be written as a transition flux density given by [30],

$$
\begin{aligned}
\Gamma_{12} &= -\frac{i}{\hbar}\Big[V_{12}^{\mathrm{TLS}} + \Big(\frac{\delta \mathcal{F}}{\delta \rho}\Big)_{12}\Big](\rho_{21} - \rho_{12}) \\
&= \frac{2}{\hbar}\Big[V_{12}^{\mathrm{TLS}} + \Big(\frac{\delta \mathcal{F}}{\delta \rho}\Big)_{12}\Big]\Im\rho_{12}
\end{aligned}
\tag{6.29}
$$

Furthermore, the electronic coherence terms for both the local density and momentum density are seen to be dependent on the population terms. The off-diagonal components can be expressed,

$$
\begin{aligned}
\frac{\partial}{\partial t}\rho_{12} = \ & -\frac{1}{m}\nabla_r \cdot \mathbf{g}_{12} - \frac{i}{\hbar}\mathbf{V}_{\Delta}\rho_{12} \\
& -\frac{i}{\hbar}\Big[V_{12}^{\mathrm{TLS}} + \Big(\frac{\delta \mathcal{F}}{\delta \rho}\Big)_{12}\Big](\rho_{22} - \rho_{11})
\end{aligned}
\tag{6.30}
$$

and

$$
\begin{aligned}
\frac{\partial}{\partial t}\mathbf{g}_{12} = \ & -\frac{1}{2}\rho_{12}\nabla_r \mathbf{V}_{\Sigma} - \frac{i}{\hbar}\mathbf{V}_{\Delta}\mathbf{g}_{12} - \frac{1}{2}(\rho_{11} + \rho_{22})\nabla_r\Big(\frac{\delta \mathcal{F}}{\delta \rho}\Big)_{12} \\
& -\frac{i}{\hbar}\Big[V_{12}^{\mathrm{TLS}} + \Big(\frac{\delta \mathcal{F}}{\delta \rho}\Big)_{12}\Big](\mathbf{g}_{22} - \mathbf{g}_{11})
\end{aligned}
\tag{6.31}
$$

where

$$
\mathbf{V}_{\Sigma/\Delta}(\mathbf{r}) = V_{11}^{\mathrm{TLS}} + \Big(\frac{\delta \mathcal{F}}{\delta \rho}\Big)_{11}\Big(V_{22}^{\mathrm{TLS}} + \Big(\frac{\delta \mathcal{F}}{\delta \rho}\Big)_{22}\Big)
\tag{6.32}
$$

These equations for the populations and coherences explicitly shows the interplay between the diagonal and off-diagonal terms. This complex coupling will be shown in detail in the results section.

6.3   Results

This section present preliminary work done on propagating the hydrodynamic quantities of $\rho(\mathbf{r}, t)$ and $\mathbf{g}(\mathbf{r}, t)$ for a single degree of freedom. The derivation performed in this Chapter focussed on the
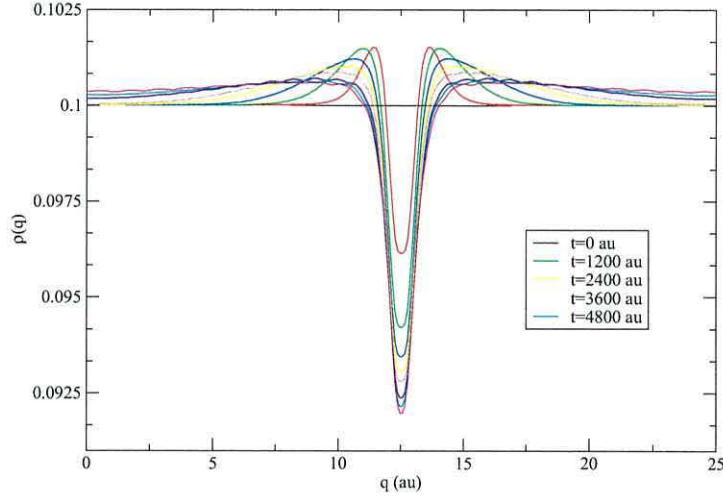
Figure 6.2: Dynamics of the solvent local density $\rho(\mathbf{r}, t)$ as extracted from the phase space single particle density $f(\mathbf{r}, \mathbf{p})$.

translational solvent response $\mathbf{r}$ only, and to this end, only the translational component is shown. Furthermore, calculations were limited to single state dynamics. Since investigations in this field are at a very early stage, it is crucial that the dynamics are well understood at this simple level. In particular, the validity of the hierarchy termination of Eq. (6.14) is investigated.

6.3.1 Hydrodynamic Fields for a single state

To assess the validity of the closure of the hierarchy Eq. (6.14) in the hydrodynamic equations, along with the neglect of the convective term $\mathbf{g}(\mathbf{r}) \cdot \mathbf{g}(\mathbf{r})/\rho(\mathbf{r})$, the dynamics of the hydrodynamic quantities are compared to those obtained directly from the single particle phase space density. In the phase space approach, the local density and momentum field were extracted from time evolution of $f(\mathbf{r}, \mathbf{p}, t)$, by integrating over momentum space. Because these moments are obtained from the evolving phase space density, there is no moment
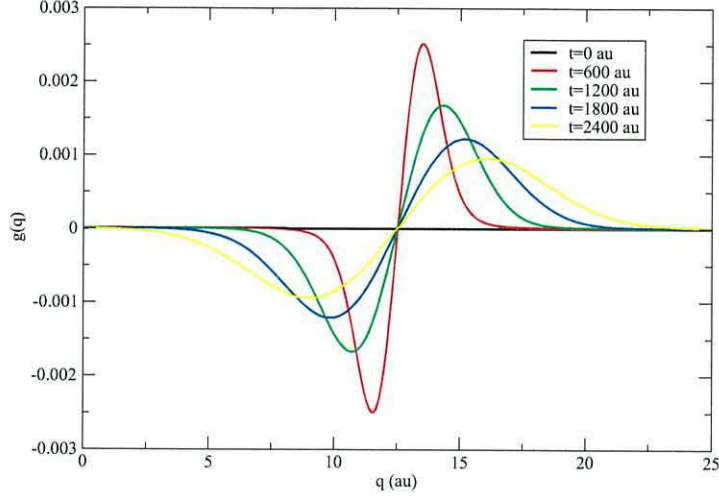
Figure 6.3: The momentum density obtained from the underlying phase space single particle density

hierarchy to consider. Any difference in the resulting dynamics of the two approaches is attributable to the approximation of Eq. (6.14).

The quality of the local equilibrium assumption, i.e. the non-equilibrium free energy corresponding to a particular density taken as the equilibrium free energy, has already been investigated. This was achieved by comparing the approximate TD-DFT approach with the 'known' non-equilibrium dynamics of hard rods [31]. The conclusions from that study is that the assumption is valid for states that are not too far from equilibrium. This is therefore not investigated any further here.

The evolution of $\rho(\mathbf{r}, t)$ and $\mathbf{g}(\mathbf{r}, t)$ as extracted from $f(\mathbf{r}, \mathbf{p})$ is depicted in Fig. (6.2) and Fig. (6.3) respectively. The one dimensional electric field was taken as,

$$E(\mathbf{r}) = \frac{2\mu}{(r - r_{\text{eqm}})^3} \tag{6.33}$$

160

with dipole $\mu = 0.01$ au and $r_{\mathrm{eqm}} = 12.5$ au. This places the solute at $r = 12.5$ au. The two particle correlation function of the reference equilibrium density ($\rho_{\mathrm{eqm}} = 0.1$ au) was modelled as,

$$C_2(r - r') = \cos(r - r')\exp(-(r - r')) \qquad (6.34)$$

which has a form very similar to C_2 obtained from experiments and molecular dynamic (MD) simulations [33]. From the initial uniform density, $\rho(\mathbf{r}, t_0) = 0.1$, Fig. (6.2) shows a solvent 'dip' develops as the electric field generated by the solute placed at $q = 12.5$ au forces the solvent particles away. There is initially an increase in density at the edges of the solvent 'dip', as the solvent molecules rush away from the solute at $t = 1200$ au. As time progresses, this 'build up' of density at the edge of the 'dip' spreads out and decreases in magnitude as the solvent rearranges to stabilise the new charge distribution of the solute.

This is further illustrated by looking at the momentum density in Fig. (6.3). The solvent moving from the solute at $r = 12.5$ au in opposite direction is manifested as an increase in the magnitude of the momentum field. Note that the density moving towards the left is seen to increase the magnitude of the momentum field in the negative direction while the solvent density moving to the right hand side from the solute causes an increase in the positive direction of the momentum density. Fig. (6.4) shows the underlying phase space distribution $f(\mathbf{r}, \mathbf{p})$ for the system. The origin of the 'build up' of density is easier to rationalise here. The phase space density is seen to move away from the solute with opposite momenta.

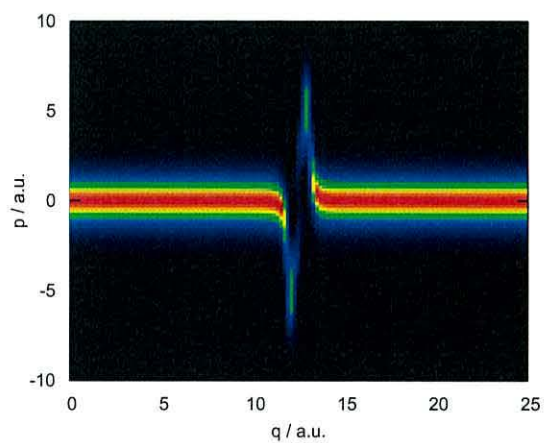The local density and momentum field obtained from the hydro-

Figure 6.4: Snapshot of the phase space single particle density at $t = 2000$ au
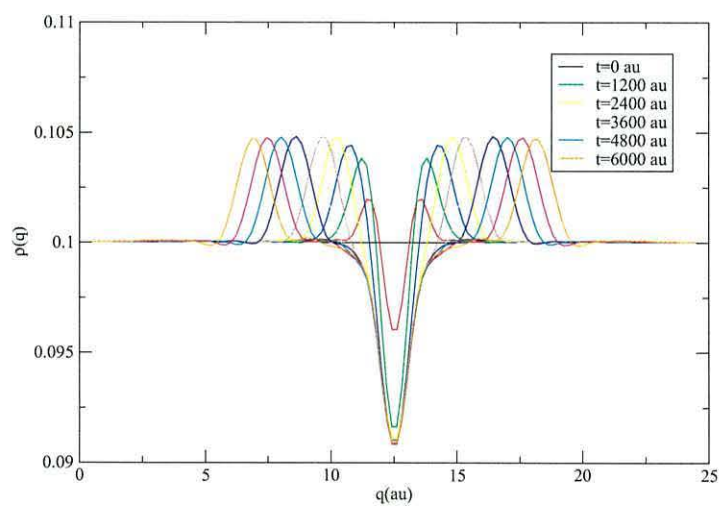

Figure 6.5: Evolution of the solvent local density for a single state solute obtained from the hydrodynamic approach.
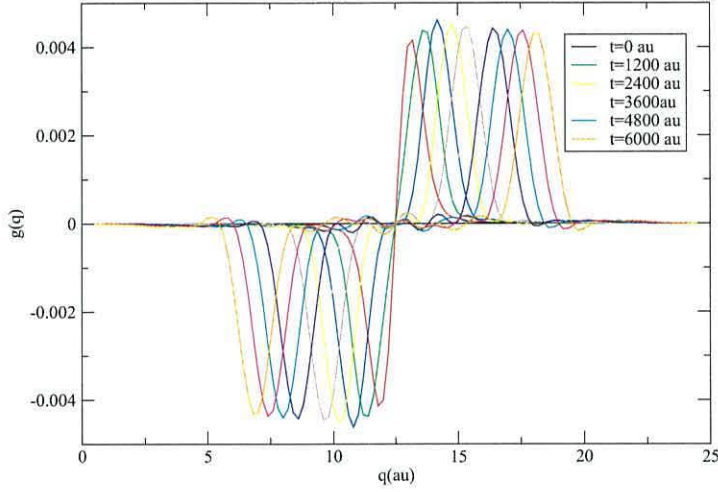
Figure 6.6: Dynamics of the momentum density for a single state solute obtained from the hydrodynamic approach.

dynamic approach of Eq. (6.3) are depicted in Figs. (6.5-6.6) for the same parameters as the phase space calculation. The form of the electric field is shown in Fig. (6.7). Again, a solvent 'dip' forms as the solvent density responds to the electric field. However, a noticeable difference between the dynamics illustrated here as compared to that obtained from the phase space propagation is that the build-up of density around the solvent dip never decreases for the hydrodynamic case. This suggests that the approximations given in Eq. (6.14) is not fully valid for this situation. It appears that the immediate presence of the electric field is more than a perturbation to the homogenous $\rho(\mathbf{r}, t_0) = 0.1$.

To further test the validity of the molecular hydrodynamic approach it would therefore be anticipated that an initial $\rho(\mathbf{r}, t_0)$ chosen not far from ρ_{eqm} (in the presence of the electric field) would reproduce the correct dynamics consistent with the phase space propagation. The
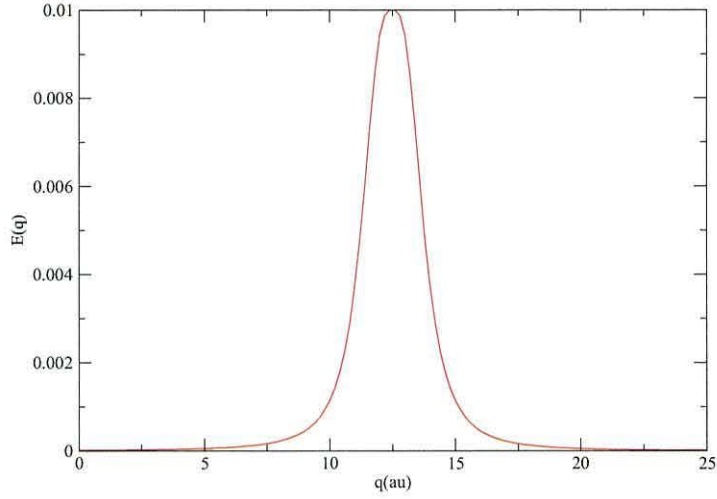
Figure 6.7: The electric field of Eq. (6.33) generated by the solute, with $\mu = 0.01$ au

initial density was therefore chosen as $\rho(\mathbf{r}, t_0) = 0.1 \exp(-0.5 E(\mathbf{r}))$, which has the inverted Gaussian form. The evolution of $\rho(\mathbf{r}, t)$ from both the hydrodynamic approach and the phase space approach is given in Fig. (6.8). Initially, for both the hydrodynamic and phase space approaches, a build up of density is seen at the edges of the dip. Once more, in the case of the hydrodynamic approach, the build-up of solvent density simply moves away from the solute and does not change in width or height. It seems therefore that even for initial conditions close to equilibrium, the results from the two approaches are notably different. This raises some questions over the approximation of Eq. (6.14) and further studies are required to understand and comment on the validity of the hydrodynamic approach in its current form.
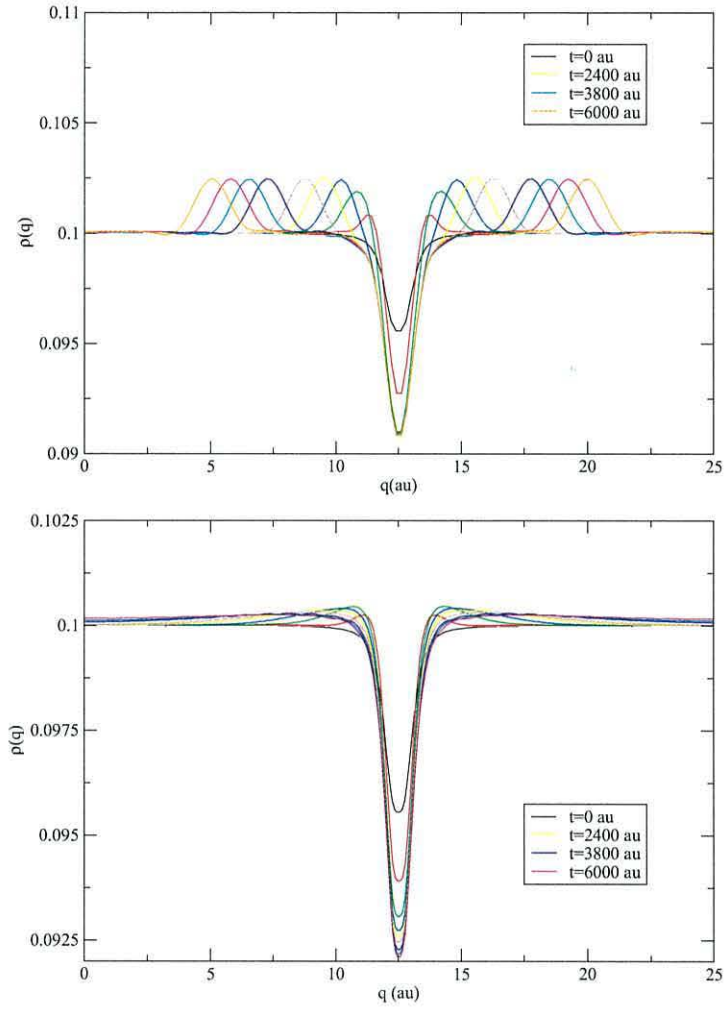
164

Figure 6.8: Dynamics of the local density $\rho(\mathbf{r}, t)$ with an initial field closer to final equilibrium density. The figure on the top is from the hydrodynamic approach of Eq. (6.3) while the figure on the bottom is from a phase space propagation
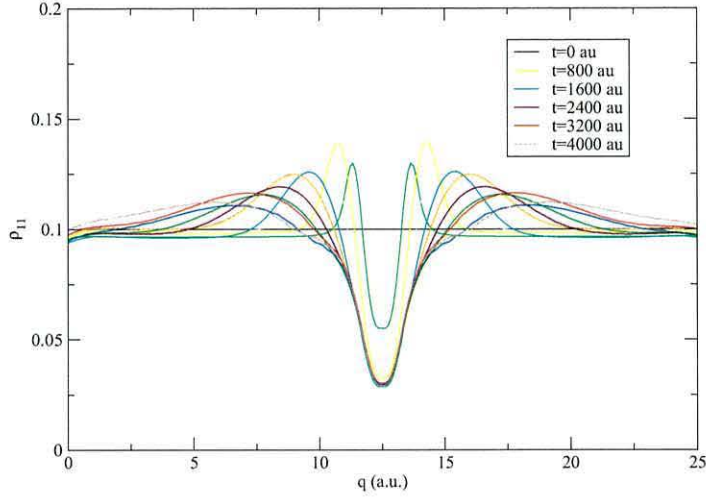
Figure 6.9: Ground state solvent local density ρ_{11} as obtained from the phase space single particle density.

6.3.2 Hydrodynamic fields of a solvent coupled to a 2-state quantum solute

Following on from the conclusions from the single state calculations, it seems there are some issues regarding the closure approximation of Eq. (6.14). These issues need to be resolved before extending the molecular hydrodynamic approach to a 2-state quantum solute. However, to illustrate the coupling between the hydrodynamic moments as well as the interplay between diagonal and off-diagonal elements of the hydrodynamic fields, the dynamics of $\rho(\mathbf{r}, t)_{nm}$ and $\mathbf{g}(\mathbf{r}, t)_{nm}$ are shown here. Figs (6.9-6.12) depicts the hydrodynamic fields (populations only) as obtained from the 2-state mixed quantum-classical single particle phase space density, $\hat{f}(\mathbf{r}, \mathbf{p})$. The same electric field of Eq. (6.33) with a dipole $\mu = 0.1$ au was used for the ground state and $\mu = 0$ au used for the excited electronic state. The same correlation function as in Eq. (6.34) was also employed.
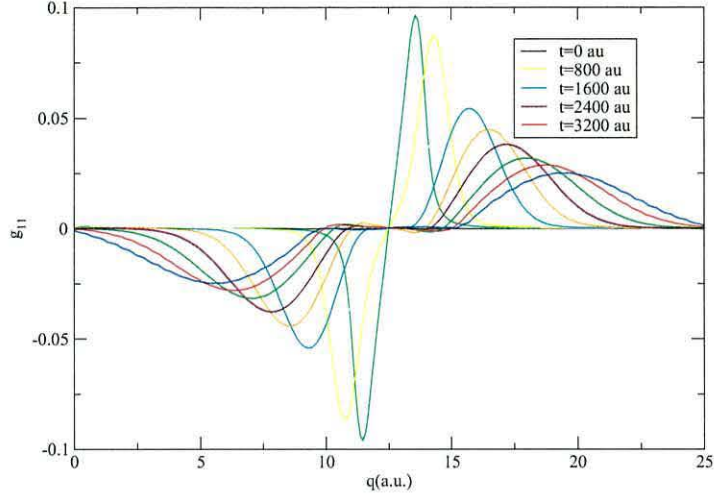
166

Figure 6.10: Ground state momentum density g_{11} as obtained from the phase space single particle density.

The dynamics of $\rho_{11}(\mathbf{r}, t)$ is shown in Fig. (6.9). The evolution is very similar to that obtained for the single state calculation. A 'dip' forms in the solvent density as the solvent moves away from the solute. Again, a build up of density is seen around the edges of the dip. These broaden and decrease in height as the solvent reorientate to stabilise the new charge distribution. A closer inspection of ρ_{11} shows some variation in the conservation of the density. This is attributable to the transfer of density associated with a two state description of the solute. Furthermore, the same behaviour is seen for $\mathbf{g}_{11}$ in Fig. (6.10) as is seen for the single state case. The momentum field increases in positive and negative direction, indicating the movement of solvent particles in opposite directions away from the solute particle.

The dynamics of the hydrodynamics fields associated with the

167
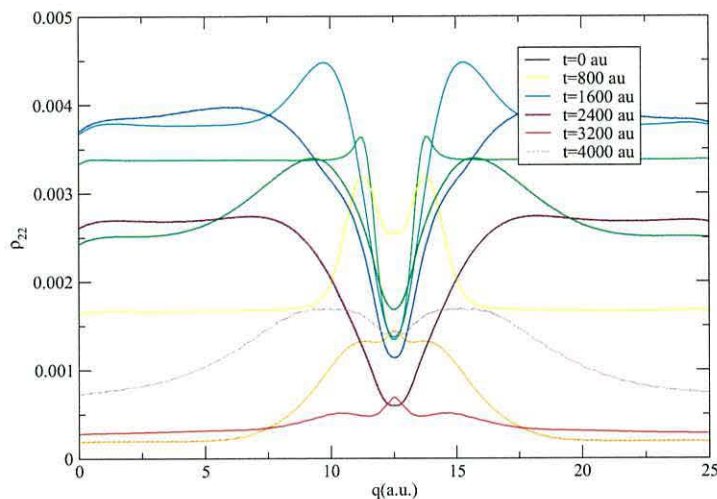
Figure 6.11: The excited state solvent local density ρ_{22} obtained from the single particle phase space density

excited electronic states of the solute are shown in Figs. (6.11-6.12). In particular, for $\rho(\mathbf{r}, t)$, the varying magnitude of density can again be traced back to the population transfer that occurs between the two electronic states of the quantum solute.

6.4 Conclusions and Further Work

In this Chapter, the molecular hydrodynamic approach [19] has been developed to describe the dynamical evolution of a solvent coupled to a quantum solute. The solvent was treated classically whilst the solute was taken as a two level quantum system. In principle, this is therefore a hybrid quantum-classical description [32]. This molecular hydrodynamic approach goes beyond methodologies such as continuum models [10, 11] in that it takes into account molecular level effects (e.g. microscopic solute-solvent interactions).
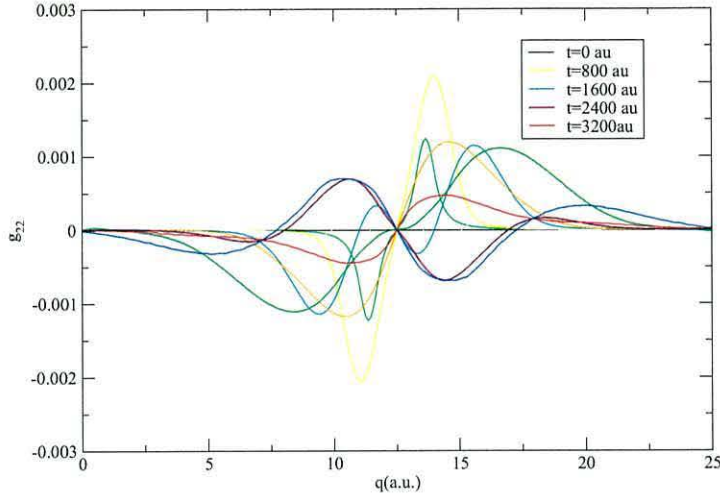
168

Figure 6.12: The excited state momentum field $\mathbf{g}_{22}$ obtained from the single particle phase space density.

The hydrodynamic moments, local density $\rho_{nm}(\mathbf{r})$ and momentum density $\mathbf{g}_{nm}(\mathbf{r})$ are obtained from the hybrid quantum-classical single-particle density [29], $\hat{f}(\mathbf{r}, \mathbf{p}) = \sum_{nm} f_{nm}(\mathbf{r}, \mathbf{p})|m\rangle\langle n|$. The dynamical equations for the hydrodynamic moments exhibit populations/coherence coupling that emerges directly from the two level description of the quantum solute [30]. Furthermore, the equations of motion for $\rho_{nm}(\mathbf{r})$ and $\mathbf{g}_{nm}(\mathbf{r})$ contains the Helmholtz free energy, $\mathcal{F}[\rho]$ acting as the potential term. The solvent-solute interactions and an entropic term is embedded within the Helmholtz free energy. The free energy also identifies the connection of the molecular hydrodynamic approach with dynamical DFT.

Preliminary results are shown for the dynamics of the hydrodynamical quantities. It is seen that differing results obtained from a phase space propagation versus the hydrodynamical approach raises questions on the validity of the hierarchy termination. Certain test cases

169

were explored in this work in an attempt to identify the source of the discrepancies. This needs to be fully resolved before extending the application to more demanding systems.

In future studies, it is anticipated that the incorporation of the angular component (see Eq. (6.15)) to the molecular hydrodynamic approach is investigated. Furthermore, a full three dimensional (x, y, z) component description will need to be investigated. This will naturally extend to a two state quantum solute, as described in this Chapter. As the description of a two level quantum solute accounts for coherences $n \neq m$ as well as populations $n = m$, dissipative effects also can be studied. Further work to develop the molecular hydrodynamic approach will also incorporate electronic structure of the solvent, which now requires a quantum description.

Bibliography

[1] B. Bagchi and R. Biswas, Adv. Chem. Phys. **109**, 207 (1999).

[2] B. Bagchi, Annu. Rev. Phys. Chem. **40**, 115 (1989).

[3] M. Chergui, *Femtochemistry*, World Scientific, Singapore, 1995.

[4] M. M. Martin and J. T. Hynes, *Femtochemistry and Femtobiology-Ultrafast Events in Molecular Science*, Elsevier, Amsterdam, 2004.

[5] S. K. Pal, J. Peon, B. Bagchi and A. H. Zewail, J. Phys. Chem. B. **106**, 12376 (2002)

[6] M. Maroncelli, E. W. Castner, B. Bagchi and G. R. Fleming, Faraday Discuss. Chem. Soc. **85**, 199 (1988).

[7] S. J. Rosenthal, X. Xie, M. Du and G. R. Fleming, J. Chem. Phys. **94**, 4715 (1991).

[8] M. Maroncelli, J. McInnis and G. R. Fleming, Science **243**, 1674 (1989).

[9] G. R. Fleming and M. Cho, Annu. Rev. Phys. Chem. **47**, 109 (1996)

[10] G. van der Zwan and J. T. Hynes, J. Phys. Chem. **89**, 4181 (1985).

[11] B. Bagchi, D. W. Oxtoby and G. R. Fleming, Chem. Phys. **86**, 257 (1984).

[12] M. Born, Z. Phys. **1**, 45 (1920).

[13] L. Onsager, J. Am. Chem. Soc. **58**, 1485 (1935).

[14] B. Bagchi, E. W. Castner and G. R. Fleming, J. Mol. Struc. Theor. Chem. **194**, 171 (1989).

[15] S. Mukamel, *Principles of Nonlinear Optical Spectroscopy*, Oxford University Press Inc, 1999.

[16] B. C. Perng, M. D. Newton, F. O. Raineri and H. L. Friedman, J. Chem. Phys. **104**, 7153 (1996).

[17] R. M. Stratt, Acc. Chem. Res. **28**, 201 (1995).

[18] S. A. Egorov, R. A. Denny and D. R. Reichman, J. Chem. Phys. **116**, 5080 (2002).

[19] I. Burghardt and B. Bagchi, Chem. Phys. **329**, 343 (2006).

[20] B. Bagchi and A. Chandra, Adv. Chem. Phys. **80**, 1 (1991).

[21] T. V. Ramakrishnan and M. Yussouff, Phys. Rev. B **19**, 2775 (1979).

[22] T. R. Kirkpatrick and J. C. Nieuwoudt, Phys. Rev. A **33**, 2651 (1986).

[23] D. F. Calef and P. G. Wolynes, J. Chem. Phys. **78**, 4145 (1983).

[24] A. Chandra and B. Bagchi, J. Chem. Phys. **91**, 1829 (1989).

[25] P. C. Hohenberg and D. I. Halperin, Rev. Mod. Phys. **49**, 435 (1977).

[26] B. Bagchi, J. Chem. Phys. **82**, 5677 (1985).

[27] R. Balescu, *Equilibrium and Nonequilibrium Statistical Mechanics*, Krieger, Malabar, FL, 1991.

[28] I. V. Aleksandrov, Z. Naturforsch. **36**, 902 (1981).

[29] I. Burghardt and L. S. Cederbaum, J. Chem. Phys. **115**, 10312 (2001).

[30] I. Burghardt, K. B. Møller, G. Parlant, L. S. Cederbaum and E. R. Bittner, Int. J. Quant. Chem. **100**, 1153 (2004).

[31] U. M. B. Marconi and P. Tarazona, J. Chem. Phys. **100**, 8032 (1999).

[32] K. H. Hughes, S. M. Parry, G. Parlant and I. Burghardt, J. Chem. Phys. A **111**, 10269 (2007).

[33] N. Phuong, G. Germano and F. Schmid, Comp. Phys. Comm. **147**, 350 (2002).

Appendix A

Separating the real and imaginary parts of the Schrödinger Equation

The Schrödinger equation is given by,

$$i\hbar\frac{\partial\psi}{\partial t} = -\frac{\hbar^2}{2m}\frac{\partial^2}{\partial r^2}\psi + V(r,t)\psi \tag{A.1}$$

where m is the mass and $V(r,t)$ is the potential energy. If the wavefunction, ψ, is represented in the polar form of Madelung,

$$\psi(r,t) = R(r,t)e^{\frac{i}{\hbar}S(r,t)} \tag{A.2}$$

the Schrödinger equation Eq. (A.1) can be rewritten,

$$i\hbar\frac{\partial}{\partial t}Re^{\frac{i}{\hbar}S(r,t)} = -\frac{\hbar}{2m}\frac{\partial^2}{\partial r^2}Re^{\frac{i}{\hbar}S(r,t)} + V(r,t)Re^{\frac{i}{\hbar}S(r,t)} \tag{A.3}$$

Expansion of the derivatives and multiplying by $e^{-\frac{i}{\hbar}S(r,t)}$ yields

$$-R\frac{\partial S}{\partial t} + i\hbar\frac{\partial R}{\partial t} = -\frac{\hbar^2}{2m}\frac{\partial^2 R}{\partial r^2} - i\frac{\hbar}{m}\frac{\partial R}{\partial r}\frac{\partial S}{\partial r}$$
$$- i\frac{\hbar}{2m}R\frac{\partial^2 S}{\partial r^2} + \frac{1}{2m}R\left(\frac{\partial S}{\partial r}\right)^2 + VR \tag{A.4}$$

174

The real and imaginary parts of Eq. (A.4) may be separated. Collecting the real terms and dividing by R gives the *quantum* Hamilton-Jacobi equation,

$$-\frac{\partial S}{\partial t} = \frac{1}{2m}\left(\frac{\partial S}{\partial r}\right)^2 - \frac{\hbar^2}{2mR}\frac{\partial^2 R}{\partial r^2} + V \qquad (A.5)$$

Collecting the imaginary terms and multiplying by $2R\hbar^{-1}$ yields,

$$2R\frac{\partial R}{\partial t} = -\frac{2}{m}R\frac{\partial R}{\partial r}\frac{\partial S}{\partial r} - \frac{R^2}{m}\frac{\partial^2 S}{\partial r^2} \qquad (A.6)$$

Recognising that,

$$2R\frac{\partial R}{\partial t} = \frac{\partial R^2}{\partial t} \qquad (A.7)$$

and

$$\frac{1}{m}\frac{\partial R^2}{\partial r}\frac{\partial S}{\partial r} + \frac{R^2}{m}\frac{\partial^2 S}{\partial r^2} = \frac{1}{m}\frac{\partial}{\partial r}\left(R^2\frac{\partial S}{\partial r}\right) \qquad (A.8)$$

Eq. (A.6) may be written as

$$\frac{\partial R^2}{\partial t} = -\frac{1}{m}\frac{\partial}{\partial r}\left(R^2\frac{\partial S}{\partial r}\right) \qquad (A.9)$$

Appendix B

Taking the gradient of the quantum Hamilton-Jacobi equation

The quantum Hamilton-Jacobi equation is given by,

$$-\frac{\partial S}{\partial t} = \frac{1}{2m}\left(\frac{\partial S}{\partial r}\right)^2 + Q(r,t) + V(r,t) \qquad \text{(B.1)}$$

The gradient of Eq. (B.1) can be written as,

$$-\frac{\partial}{\partial r}\left(\frac{\partial S}{\partial t}\right) = \frac{1}{2m}\frac{\partial}{\partial r}\left(\frac{\partial S}{\partial r}\right)^2 + \frac{\partial Q}{\partial r} + \frac{\partial V}{\partial r} \qquad \text{(B.2)}$$

Since,

$$-\frac{\partial}{\partial r}\left(\frac{\partial S}{\partial t}\right) = -\frac{\partial}{\partial t}\left(\frac{\partial S}{\partial r}\right) \qquad \text{(B.3)}$$

and

$$\frac{\partial}{\partial r}\left(\frac{\partial S}{\partial r}\right)^2 = 2\frac{\partial^2 S}{\partial r^2}\frac{\partial S}{\partial r} \qquad \text{(B.4)}$$

Eq. (B.2) may be re-expressed,

$$-\frac{\partial}{\partial t}\left(\frac{\partial S}{\partial r}\right) = \frac{1}{2m}\frac{\partial^2 S}{\partial r^2}\frac{\partial S}{\partial r} + \frac{\partial Q}{\partial r} + \frac{\partial V}{\partial r} \qquad \text{(B.5)}$$

Since $v = \frac{1}{m}\frac{\partial S}{\partial r}$, therefore $\frac{\partial S}{\partial r} = mv$ and $\frac{\partial^2 S}{\partial r^2} = m\frac{\partial v}{\partial r}$. This means that Eq. (B.5) may be rewritten

$$-m\left(\frac{\partial v}{\partial t}\right) = \frac{\partial v}{\partial r}mv + \frac{\partial Q}{\partial r} + \frac{\partial V}{\partial r} \qquad (B.6)$$

Now,

$$\frac{dv}{dt} = \frac{\partial v}{\partial r}\frac{dr}{dt} + \frac{\partial v}{\partial t}\frac{dt}{dt} \qquad (B.7)$$

Since, $dr/dt = v$, Eq. (B.7) may be written as,

$$\frac{dv}{dt} = v\frac{\partial v}{\partial r} + \frac{\partial v}{\partial t} \qquad (B.8)$$

The total time derivative of Eq. (B.6) is thus given as

$$-m\left(\frac{dv}{dt} - v\frac{\partial v}{\partial r}\right) = \frac{\partial v}{\partial r}mv + \frac{\partial Q}{\partial r} + \frac{\partial V}{\partial r} \qquad (B.9)$$

which reduces to

$$-m\frac{dv}{dt} = \frac{\partial Q}{\partial r} + \frac{\partial V}{\partial r} \qquad (B.10)$$

Appendix C

Derivation of the Wigner-Moyal equation from the quantum Liouville equation

The positional coordinates x and x' are defined as the difference coordinates which are related to the diagonal coordinate q and the off-diagonal part of the coordinate r by $x = q + r/2$ and $x' = q - r/2$. Consequently, $q = 0.5(x + x')$ and $r = x - x'$. With these definitions the Wigner function $\rho_W(q, p)$ is related to the density matrix by

$$
\begin{aligned}
\rho_W(q, p) &= \frac{1}{2\pi\hbar} \int_{-\infty}^{\infty} <x|\rho|x'> e^{-i\frac{rp}{\hbar}} \, dr \\
&= \frac{1}{2\pi\hbar} \int_{-\infty}^{\infty} <q + \frac{r}{2}|\rho|q - \frac{r}{2}> e^{-i\frac{rp}{\hbar}} \, dr \quad \text{(C.1)}
\end{aligned}
$$

and

$$
<x|\rho|x'> = \rho(x, x') = \int_{-\infty}^{\infty} \rho_W(q, p) e^{i\frac{rp}{\hbar}} \, dr. \quad \text{(C.2)}
$$

For a single electronic state system the quantum Liouville equation for the density matrix is given by

$$\frac{\partial}{\partial t}\rho(x,x') = -\frac{i}{\hbar}\left\{ -\frac{\hbar^2}{2m}\left(\frac{\partial^2}{\partial x^2} - \frac{\partial^2}{\partial x'^2}\right) + V(x) - V(x')\right\}\rho(x,x')$$

(C.3)

The equation of motion for $\rho_W(q,p)$ is obtained by taking the Wigner transform of Eq. (C.3). Taking the Wigner transform of the LHS of Eq. (C.3) yields

$$\frac{1}{2\pi\hbar}\int_{-\infty}^{\infty}\frac{\partial}{\partial t}\rho(x,x')e^{-i\frac{rp}{\hbar}}\,dr = \frac{\partial}{\partial t}\frac{1}{2\pi\hbar}\int_{-\infty}^{\infty}\rho(x,x')e^{-i\frac{rp}{\hbar}}\,dr = \frac{\partial}{\partial t}\rho_W(q,p)$$

(C.4)

Wigner transform of the kinetic energy part of the QLE

For the kinetic energy part in the RHS of Eq. (C.3) the following relations between the derivatives are used

$$\frac{\partial}{\partial x} = \frac{dq}{dx}\frac{\partial}{\partial q} + \frac{dr}{dx}\frac{\partial}{\partial r} = \frac{1}{2}\frac{\partial}{\partial q} + \frac{\partial}{\partial r}$$

(C.5)

$$\frac{\partial^2}{\partial x^2} = \frac{\partial}{\partial x}\left(\frac{dq}{dx}\frac{\partial}{\partial q} + \frac{dr}{dx}\frac{\partial}{\partial r}\right)$$

$$= \left(\frac{1}{2}\frac{\partial}{\partial q} + \frac{\partial}{\partial r}\right)\left(\frac{1}{2}\frac{\partial}{\partial q} + \frac{\partial}{\partial r}\right)$$

$$= \frac{1}{4}\frac{\partial^2}{\partial q^2} + \frac{\partial^2}{\partial r\partial q} + \frac{\partial^2}{\partial r^2}$$

(C.6)

$$\frac{\partial}{\partial x'} = \frac{dq}{dx'}\frac{\partial}{\partial q} + \frac{dr}{dx'}\frac{\partial}{\partial r} = \frac{1}{2}\frac{\partial}{\partial q} - \frac{\partial}{\partial r}$$

(C.7)

$$\frac{\partial^2}{\partial x'^2} = \frac{\partial}{\partial x'}\left(\frac{dq}{dx'}\frac{\partial}{\partial q} + \frac{dr}{dx'}\frac{\partial}{\partial r}\right)$$

$$= \left(\frac{1}{2}\frac{\partial}{\partial q} - \frac{\partial}{\partial r}\right)\left(\frac{1}{2}\frac{\partial}{\partial q} - \frac{\partial}{\partial r}\right)$$

$$= \frac{1}{4}\frac{\partial^2}{\partial q^2} - \frac{\partial^2}{\partial r\partial q} + \frac{\partial^2}{\partial r^2}$$

(C.8)

Consequently

$$\frac{\partial^2}{\partial x^2} - \frac{\partial^2}{\partial x'^2} = 2\frac{\partial^2}{\partial r\partial q}.$$

(C.9)

Substituting this expression for the derivatives into the kinetic part of Eq. (C.3) yields

$$\mathrm{i}\frac{\hbar}{m}\frac{\partial^2}{\partial r\partial q}<q+\frac{r}{2}|\rho|q-\frac{r}{2}>. \tag{C.10}$$

Taking the Wigner transform of Eq. (C.10) gives

$$\frac{1}{2\pi\hbar}\int_{-\infty}^{\infty}\mathrm{i}\frac{\hbar}{m}\frac{\partial^2}{\partial r\partial q}\Big(<q+\frac{r}{2}|\rho|q-\frac{r}{2}>\Big)\mathrm{e}^{-\mathrm{i}\frac{rp}{\hbar}}\mathrm{d}r$$
$$=\frac{\mathrm{i}\hbar}{m2\pi\hbar}\frac{\partial}{\partial q}\int_{-\infty}^{\infty}\frac{\partial}{\partial r}<q+\frac{r}{2}|\rho|q-\frac{r}{2}>\mathrm{e}^{-\mathrm{i}\frac{rp}{\hbar}}\mathrm{d}r$$

$$\tag{C.11}$$

Integrating by parts gives

$$\frac{\mathrm{i}\hbar}{m2\pi\hbar}\frac{\partial}{\partial q}\Big[<q+\frac{r}{2}|\rho|q-\frac{r}{2}>\mathrm{e}^{-\mathrm{i}\frac{rp}{\hbar}}\Big]_{-\infty}^{\infty}$$
$$-\frac{\mathrm{i}\hbar}{m2\pi\hbar}\frac{\partial}{\partial q}\int_{-\infty}^{\infty}<q+\frac{r}{2}|\rho|q-\frac{r}{2}>\frac{\partial}{\partial r}\mathrm{e}^{-\mathrm{i}\frac{rp}{\hbar}}\mathrm{d}r$$
$$=\ 0-\frac{\mathrm{i}\hbar}{m2\pi\hbar}\frac{\partial}{\partial q}\int_{-\infty}^{\infty}<q+\frac{r}{2}|\rho|q-\frac{r}{2}>\frac{-\mathrm{i}}{\hbar}p\mathrm{e}^{-\mathrm{i}\frac{rp}{\hbar}}\mathrm{d}r$$
$$=\ -\frac{p}{m}\frac{\partial}{\partial q}\frac{1}{2\pi\hbar}\int_{-\infty}^{\infty}<q+\frac{r}{2}|\rho|q-\frac{r}{2}>\mathrm{e}^{-\mathrm{i}\frac{rp}{\hbar}}\mathrm{d}r$$
$$=\ -\frac{p}{m}\frac{\partial}{\partial q}\rho_W(q,p). \tag{C.12}$$

In the first line of the above expression the term in square brackets is zero because of the boundary conditions that the density matrix tends to zero as $r \to \pm\infty$.

Wigner transform of the potential part of the QLE

For the potential energy part of the QLE it is assumed that V can be expanded in a Taylor series about q,

$$V(x)\ =\ V(q+r/2)\simeq\sum_{n=0}^{\infty}\frac{r^n}{n!2^n}\frac{\partial^n V}{\partial q^n}$$
$$=\ V(q)+\frac{r}{2}\frac{\partial V}{\partial q}+\frac{r^2}{8}\frac{\partial^2 V}{\partial q^2}+\frac{r^3}{48}\frac{\partial^3 V}{\partial q^3}+\ldots \tag{C.13}$$

180

$$V(x') = V(q - r/2) \simeq \sum_{n=0}^{\infty} \frac{-r^n}{n!2^n} \frac{\partial^n V}{\partial q^n}$$

$$= V(q) - \frac{r}{2}\frac{\partial V}{\partial q} + \frac{r^2}{8}\frac{\partial^2 V}{\partial q^2} - \frac{r^3}{48}\frac{\partial^3 V}{\partial q^3} + \dots \quad \text{(C.14)}$$

Taking $V(x) - V(x')$ removes the even powered terms[1]. To 3$^\text{rd}$ order

$$V(x) - V(x') \simeq r\frac{\partial V}{\partial q} + \frac{r^3}{24}\frac{\partial^3 V}{\partial q^3} + \dots \quad \text{(C.15)}$$

Substituting this representation of V into the Liouville equation and taking the Wigner transform gives

$$-\frac{\mathrm{i}}{\hbar}\frac{1}{2\pi\hbar}\int_{-\infty}^{\infty}\left\{V(x) - V(x')\right\}\rho(x,x')\mathrm{e}^{-\mathrm{i}\frac{rp}{\hbar}}\,\mathrm{d}r$$

$$\simeq -\frac{\mathrm{i}}{\hbar}\frac{1}{2\pi\hbar}\int_{-\infty}^{\infty}\left\{r\frac{\partial V}{\partial q} + \frac{r^3}{24}\frac{\partial^3 V}{\partial q^3}\right\}<q+\frac{r}{2}|\rho|q-\frac{r}{2}>\mathrm{e}^{-\mathrm{i}\frac{rp}{\hbar}}\,\mathrm{d}r$$

$$\text{(C.16)}$$

for the potential part. Inserting the relation

$$\left(\frac{-\hbar}{\mathrm{i}}\right)^n\frac{\partial^n}{\partial p^n}\mathrm{e}^{-\mathrm{i}\frac{rp}{\hbar}} = r^n \quad \text{(C.17)}$$

into Eq. (C.16) gives

$$-\frac{\mathrm{i}}{\hbar}\frac{1}{2\pi\hbar}\int_{-\infty}^{\infty}\left\{r\frac{\partial V}{\partial q} + \frac{r^3}{24}\frac{\partial^3 V}{\partial q^3}\right\}<q+\frac{r}{2}|\rho|q-\frac{r}{2}>\mathrm{e}^{-\mathrm{i}\frac{rp}{\hbar}}\,\mathrm{d}r$$

$$= -\frac{\mathrm{i}}{\hbar}\frac{1}{2\pi\hbar}\int_{-\infty}^{\infty}\left\{\frac{\partial V}{\partial q}\frac{-\hbar}{\mathrm{i}}\frac{\partial}{\partial p} + \frac{1}{24}\frac{\partial^3 V}{\partial q^3}\frac{-\hbar^3}{-\mathrm{i}}\frac{\partial^3}{\partial p^3}\right\}<q+\frac{r}{2}|\rho|q-\frac{r}{2}>\mathrm{e}^{-\mathrm{i}\frac{rp}{\hbar}}\,\mathrm{d}r$$

$$= \frac{\partial V}{\partial q}\frac{\partial}{\partial p}\frac{1}{2\pi\hbar}\int_{-\infty}^{\infty}<q+\frac{r}{2}|\rho|q-\frac{r}{2}>\mathrm{e}^{-\mathrm{i}\frac{rp}{\hbar}}\,\mathrm{d}r$$

$$-\frac{\hbar^2}{24}\frac{\partial^3 V}{\partial q^3}\frac{\partial^3}{\partial p^3}\frac{1}{2\pi\hbar}\int_{-\infty}^{\infty}<q+\frac{r}{2}|\rho|q-\frac{r}{2}>\mathrm{e}^{-\mathrm{i}\frac{rp}{\hbar}}\,\mathrm{d}r$$

$$= \frac{\partial V}{\partial q}\frac{\partial}{\partial p}\rho_W(q,p) - \frac{\hbar^2}{24}\frac{\partial^3 V}{\partial q^3}\frac{\partial^3}{\partial p^3}\rho_W(q,p). \quad \text{(C.18)}$$

Finally, the EOM for $\rho_W(q,p)$ for a single state system is given by

$$\frac{\partial \rho_W}{\partial t} = -\frac{p}{m}\frac{\partial \rho_W}{\partial q} + \frac{\partial V}{\partial q}\frac{\partial \rho_W}{\partial p} - \frac{\hbar^2}{24}\frac{\partial^3 V}{\partial q^3}\frac{\partial^3 \rho_W}{\partial p^3} \dots \quad \text{(C.19)}$$

---

[1]For the off-diagonal terms of a multi-state system the even powered terms do not cancel.

Appendix D

Derivation of dynamical equations for hydrodynamic moments

The equations of motion for hydrodynamic moments can be derived either from the quantum Liouville equation for the density operator in the coordinate representation or else from its equivalent Wigner phase space representation. In phase space, the moments are momentum moments of the Wigner function, $\rho_W(q,p)$ and in Liouville space they are momentum superoperators of the difference coordinate, r. The required moment equations are derived from both spaces in this Appendix.

Liouville coordinate space

In coordinate space the Liouville-von-Neumann equation for the density operator $\rho(x, x')$ is given by

$$i\hbar \frac{\partial}{\partial t} \rho(x, x') = [H(t), \rho(x, x')] = \mathcal{L}(t)\rho(x, x')$$

$$= \frac{-\hbar^2}{2m}(\frac{\partial^2}{\partial x^2} - \frac{\partial^2}{\partial x'^2})\rho(x, x') + [V(x) - V(x')]\rho(x, x') \tag{D.1}$$

By defining the following superoperators in the x, x' coordinates,

$$\mathcal{P}_+ = \frac{\hbar}{2i}(\frac{\partial}{\partial x} - \frac{\partial}{\partial x'}) \tag{D.2}$$

$$\mathcal{P}_- = \frac{\hbar}{i}(\frac{\partial}{\partial x} + \frac{\partial}{\partial x'}) \tag{D.3}$$

$$q = \frac{1}{2}(x + x') \tag{D.4}$$

$$r = x - x' \tag{D.5}$$

$$\mathcal{V}_- = V(x) - V(x') \tag{}$$

$$= V(q + r/2) - V(q - r/2), \tag{D.6}$$

Remark 1 $[V(q + r/2) - V(q - r/2)]$ *is an odd function. Consequently,* $\partial_q[V(q + r/2) - V(q - r/2)]$ *is even and* $\partial_q^2[V(q + r/2) - V(q - r/2)]$ *is odd. However,* $\partial_r[V(q + r/2) - V(q - r/2)]$ *is odd.*

Remark 2 *We will often define* $\mathcal{P} = \mathcal{P}_+$.

where q represents the sum coordinate and r the difference coordinates, Eq. (D.1) is given by

$$i\hbar\frac{\partial}{\partial t}\rho(x, x') = \frac{1}{m}\mathcal{P}_-\mathcal{P}_+\rho(x, x') + \mathcal{V}_-\rho(x, x') \tag{D.7}$$

Eqs. (D.2-D.3) can be expressed in terms of q and r. We first express the partial derivatives with respect to x, x' in terms of q, r

$$\frac{\partial}{\partial q} = \frac{dx}{dq}\frac{\partial}{\partial x} + \frac{dx'}{dq}\frac{\partial}{\partial x'} = \frac{\partial}{\partial x} + \frac{\partial}{\partial x'} = \frac{i}{\hbar}\mathcal{P}_- \tag{D.8}$$

$$\frac{\partial}{\partial r} = \frac{dx}{dr}\frac{\partial}{\partial x} + \frac{dx'}{dr}\frac{\partial}{\partial x'} = \frac{1}{2}\frac{\partial}{\partial x} - \frac{1}{2}\frac{\partial}{\partial x'} = \frac{i}{\hbar}\mathcal{P}_+ \tag{D.9}$$

183

The moments of $\mathcal{P}_+$ are defined as

$$< \mathcal{P}_+^n \rho >_q = \int_{-\infty}^{\infty} \delta(r) \mathcal{P}_+^n \rho(q + r/2, q - r/2) \mathrm{d}r \qquad (D.10)$$

where the delta function $\delta(r)$ implies evaluating the operation of $\mathcal{P}_+^n$ on ρ and then letting $r \to 0$ so that the diagonal $x = x' = q$ result is evaluated.

By applying Eq. (D.10) to both sides of the Liouville-von-Neumann equation (D.7) coupled equations of motion for the moments are obtained. For the zeroth moment we make use of Eq. (D.8) to get,

$$\begin{aligned}
\mathrm{i}\hbar \frac{\partial}{\partial t} < \rho >_q &= \mathrm{i}\hbar \frac{\partial}{\partial t} \int_{-\infty}^{\infty} \delta(r) \mathcal{P}_+ \rho(q + r/2, q - r/2) \mathrm{d}r \\
&= \frac{\hbar}{\mathrm{i}m} \frac{\partial}{\partial q} \int_{-\infty}^{\infty} \delta(r) \mathcal{P}_+ \rho(q + r/2, q - r/2) \mathrm{d}r \\
&\quad + \int_{-\infty}^{\infty} \delta(r) \mathcal{V}_- \rho(q + r/2, q - r/2) \mathrm{d}r \\
\frac{\partial}{\partial t} < \rho >_q &= -\frac{1}{m} \frac{\partial}{\partial q} < \mathcal{P}_+ \rho >_q \qquad (D.11)
\end{aligned}$$

In the second integral on line 2 of the above equation $\mathcal{V}_- = V(q + r/2) - V(q - r/2) = 0$ for $\delta(r)$. For the first moment, $< \mathcal{P}_+ \rho >_q$, we have

$$\begin{aligned}
\frac{\partial}{\partial t} < \mathcal{P}_+ \rho >_q &= \frac{\partial}{\partial t} \int_{-\infty}^{\infty} \delta(r) \mathcal{P}_+ \rho(q + r/2, q - r/2) \mathrm{d}r \\
&= -\frac{1}{m} \frac{\partial}{\partial q} \int_{-\infty}^{\infty} \delta(r) \mathcal{P}_+^2 \rho(q + r/2, q - r/2) \mathrm{d}r \\
&\quad -\frac{\mathrm{i}}{\hbar} \int_{-\infty}^{\infty} \delta(r) \mathcal{P}_+ \mathcal{V}_- \rho(q + r/2, q - r/2) \mathrm{d}r \\
&= -\frac{1}{m} \frac{\partial}{\partial q} < \mathcal{P}_+^2 \rho >_q - \int_{-\infty}^{\infty} \delta(r) \frac{\partial}{\partial r} \mathcal{V}_- \rho(q + r/2, q - r/2) \mathrm{d}r
\end{aligned}$$
$$(D.12)$$

Expanding the partial derivative in the integral on the final line,

$$\begin{aligned}
\int_{-\infty}^{\infty} \delta(r) \frac{\partial}{\partial r} \mathcal{V}_- \rho(q + r/2, q - r/2) &= \int_{-\infty}^{\infty} \delta(r) [\rho(q + r/2, q - r/2) \frac{\partial}{\partial r} \mathcal{V}_- \\
&\quad + \mathcal{V}_- \frac{\partial}{\partial r} \rho(q + r/2, q - r/2)] \mathrm{d}r
\end{aligned}$$
$$(D.13)$$

184

As in Eq. (D.11) the second part of the above integral is zero ($\mathcal{V}_- = V(q+r/2) - V(q-r/2) = 0$ for $\delta(r)$). For the first part of the integral we note that

$$\frac{\partial}{\partial r} V(q+r/2) = \frac{\mathrm{d}x}{\mathrm{d}r} \frac{\partial}{\partial x} V(q+r/2) = \frac{1}{2} \frac{\partial}{\partial x} V(q+r/2) \quad \text{(D.14)}$$

$$\frac{\partial}{\partial r} V(q-r/2) = \frac{\mathrm{d}x'}{\mathrm{d}r} \frac{\partial}{\partial x'} V(q-r/2) = -\frac{1}{2} \frac{\partial}{\partial x'} V(q-r/2)$$

(D.15)

giving

$$\frac{\partial}{\partial r} V(q+r/2) - \frac{\partial}{\partial r} V(q-r/2) = \frac{1}{2} \Big[\frac{\partial}{\partial x} V(q+r/2) + \frac{\partial}{\partial x'} V(q-r/2) \Big]$$

$$= \frac{1}{2} \Big[\frac{\partial}{\partial x} V(q) + \frac{\partial}{\partial x'} V(q) \Big] = \frac{\partial V(q)}{\partial q} \qquad r \to 0$$

(D.16)

The equation of motion for $< \mathcal{P}_+ \rho >_q$ is then

$$\frac{\partial}{\partial t} < \mathcal{P}_+ \rho >_q = -\frac{1}{m} \frac{\partial}{\partial q} < \mathcal{P}_+^2 \rho >_q - \frac{\partial V(q)}{\partial q} < \rho >_q \qquad \text{(D.17)}$$

For the second moment, $< \mathcal{P}_+^2 \rho >_q$, we have

$$\frac{\partial}{\partial t} < \mathcal{P}_+^2 \rho >_q = -\frac{1}{m} \frac{\partial}{\partial q} < \mathcal{P}_+^3 \rho >_q$$

$$-\frac{\mathrm{i}}{\hbar} \int_{-\infty}^{\infty} \delta(r) \mathcal{P}_+^2 \mathcal{V}_- \rho(q+r/2, q-r/2) \mathrm{d}r$$

(D.18)

For the potential energy part,

$$-\frac{\mathrm{i}}{\hbar} \int_{-\infty}^{\infty} \quad \delta(r) \mathcal{P}_+^2 \mathcal{V}_- \rho(q+r/2, q-r/2) \mathrm{d}r =$$

$$-\frac{\hbar}{\mathrm{i}} \int_{-\infty}^{\infty} \delta(r) \frac{\partial^2}{\partial r^2} \mathcal{V}_- \rho(q+r/2, q-r/2) \mathrm{d}r$$

$$= -\frac{\hbar}{\mathrm{i}} \int_{-\infty}^{\infty} \delta(r) \Big[\mathcal{V}_- \frac{\partial^2}{\partial r^2} \rho(q+r/2, q-r/2)$$

$$+2 \frac{\partial}{\partial r} \rho(q+r/2, q-r/2) \frac{\partial}{\partial r} \mathcal{V}_-$$

$$+\rho(q+r/2, q-r/2) \frac{\partial^2}{\partial r^2} \mathcal{V}_- \Big] \mathrm{d}r$$

$$= -\frac{\hbar}{\mathrm{i}} \int_{-\infty}^{\infty} \delta(r) [\mathrm{a}) + \mathrm{b}) + \mathrm{c})] \mathrm{d}r \qquad \text{(D.19)}$$

185

As in the equations for the zero and first moments expression a) is zero. Expression b) is evaluated using the same approach for the first moment calculation, giving

$$2\frac{\partial V}{\partial q} < \mathcal{P}_+\rho >_q \qquad \text{(D.20)}$$

Expression c) evaluates to zero as shown in the following. First we express both the partial derivative and $V(q \pm r/2)$ in the x, x' representation

$$
\begin{aligned}
\frac{\partial^2}{\partial r^2}[V(q + r/2) - V(q - r/2)] &= \left(\frac{\partial}{\partial x} - \frac{\partial^2}{\partial x'}\right)\left(\frac{\partial}{\partial x} - \frac{\partial^2}{\partial x'}\right)[V(x) - V(x')] \\
&= \left(\frac{\partial^2}{\partial x^2} - 2\frac{\partial^2}{\partial xx'} + \frac{\partial^2}{\partial x'^2}\right)[V(x) - V(x')]
\end{aligned}
\qquad \text{(D.21)}
$$

Operation of the cross term derivative on either $V(x)$ or $V(x')$ gives zero,

$$
\begin{aligned}
\left(\frac{\partial^2}{\partial x^2} + \frac{\partial^2}{\partial x'^2}\right)[V(x) - V(x')] &= \frac{\partial^2 V(x)}{\partial x^2} - \frac{\partial^2 V(x')}{\partial x'^2} \\
&= \frac{\partial^2 V(q)}{\partial q^2} - \frac{\partial^2 V(q)}{\partial q^2} = 0, \qquad r \to 0
\end{aligned}
\qquad \text{(D.22)}
$$

The equation of motion for $< \mathcal{P}_+^2\rho >_q$ is then

$$\frac{\partial}{\partial t} < \mathcal{P}_+^2\rho >_q = -\frac{1}{m}\frac{\partial}{\partial q} < \mathcal{P}_+^3\rho >_q -2\frac{\partial V(q)}{\partial q} < \mathcal{P}_+\rho >_q \quad \text{(D.23)}$$

Wigner phase space

The momentum moments in the Wigner phase space representation are given by,

$$< \mathcal{P}_+^n\rho >_q = \int_{-\infty}^{\infty} p^n W(q, p, t)\mathrm{d}p = < p^n W > = \bar{p}_n \qquad \text{(D.24)}$$

The equation of motion for the Wigner function is given by

$$\frac{\partial W}{\partial t} = -\frac{p}{m}\frac{\partial W}{\partial q} + \frac{\partial V}{\partial q}\frac{\partial W}{\partial p} - \frac{\hbar^2}{24}\frac{\partial^3 V}{\partial q^3}\frac{\partial^3 W}{\partial p^3} + O(\hbar^4), \text{(D.25)}$$

Equations of motion for the momentum moments are obtained by multiplying each side of the above equation by p^n and integrating over p between $\pm\infty$. Before proceeding it is assumed that the boundary conditions for the Wigner function and its momentum derivatives tend to zero as $p \to \pm\infty$ and so

$$< p^n W >= \int_{-\infty}^{\infty} \frac{\partial^n W}{\partial p^n}\mathrm{d}p = \left[\frac{\partial^{n-1} W}{\partial p^{n-1}}\right]_{-\infty}^{\infty} = 0 \qquad \text{(D.26)}$$

For the zero order moment, i.e. $< W >=< \rho >_q$ the equation of motion is

$$\frac{\partial < W >}{\partial t} = -< \frac{p}{m}\frac{\partial W}{\partial q} >+\frac{\partial V}{\partial q}< \frac{\partial W}{\partial p} > -\frac{\hbar^2}{24}\frac{\partial^3 V}{\partial q^3}< \frac{\partial^3 W}{\partial p^3} >$$

$$= -\frac{1}{m}\frac{\partial}{\partial q}< pW >= -\frac{1}{m}\frac{\partial}{\partial q}< \mathcal{P}_+\rho >_q \qquad \text{(D.27)}$$

In the first part of the right hand side,

$$< \frac{p}{m}\frac{\partial W}{\partial q} >= \frac{1}{m}\int_{-\infty}^{\infty} p\frac{\partial W}{\partial q}\mathrm{d}p = \frac{1}{m}\frac{\partial}{\partial q}\int_{-\infty}^{\infty} pW\mathrm{d}p = \frac{1}{m}\frac{\partial}{\partial q}< pW >$$

$$\text{(D.28)}$$

For the first moment

$$\frac{\partial}{\partial t}< pW > = -\frac{1}{m}\frac{\partial}{\partial q}< p^2 W >+\frac{\partial V}{\partial q}< p\frac{\partial W}{\partial p} > -\frac{\hbar^2}{24}\frac{\partial^3 V}{\partial q^3}< p\frac{\partial^3 W}{\partial p^3} >$$

$$\text{(D.29)}$$

For the second integral on the right, $< p\partial_p W >$ we integrate by parts,

$$\int_{-\infty}^{\infty} p\frac{\partial W}{\partial p}\mathrm{d}p = [pW]_{-\infty}^{\infty} - \int_{-\infty}^{\infty} W\mathrm{d}p = -< W > \qquad \text{(D.30)}$$

For the third integral, $< p\partial_p^3 W >$,

$$\int_{-\infty}^{\infty} p\frac{\partial^3 W}{\partial p^3}\mathrm{d}p = \left[p\frac{\partial^2 W}{\partial p^2}\right]_{-\infty}^{\infty} - \int_{-\infty}^{\infty} \frac{\partial^2 W}{\partial p^2}\mathrm{d}p = 0 \qquad \text{(D.31)}$$

187

The equation of motion for $< pW > = < \mathcal{P}_+\rho >_q$ is then given by,

$$\frac{\partial}{\partial t} < pW > \quad = \quad -\frac{1}{m}\frac{\partial}{\partial q} < p^2 W > -\frac{\partial V}{\partial q} < W > \quad \text{(D.32)}$$

Appendix E

Hydrodynamic Force for the Double Well Potential

The hydrodynamic force is given by

$$
\begin{aligned}
F_{\text{hyd}} &= -\frac{1}{m\langle\rho\rangle_{qQP}}\frac{\partial}{\partial q}\sigma_{qQP} \\
&= -\frac{1}{m\langle\rho\rangle_{qQP}}\left[\frac{\partial}{\partial q}\langle\mathcal{P}^2\rho\rangle_{qQP} - \left(2\langle\rho\rangle_{qQP}\langle\mathcal{P}\rho\rangle_{qQP}\frac{\partial}{\partial q}\langle\mathcal{P}\rho\rangle_{qQP}\right.\right. \\
&\qquad\qquad\qquad \left.\left. -\langle\mathcal{P}\rho\rangle_{qQP}^2\frac{\partial}{\partial q}\langle\rho\rangle_{qQP}\right)\langle\rho\rangle_{qQP}^{-2}\right]
\end{aligned} \tag{E.1}
$$

For bound potentials such as a double well bilinearly coupled to a harmonic oscillator the wavefunction $\psi(q, Q, t)$ and hence the pure state partial moments $\langle\mathcal{P}^n\rho\rangle_{qQP}$ may be expanded in terms of the eigenstates $\phi(q, Q)$ of the system,

$$
\begin{aligned}
\langle\mathcal{P}^n\rho\rangle_{qQP} &= \sum_{j,j'}c_j c_{j'}\exp\left(-\frac{i}{\hbar}[E_j - E_{j'}]t\right)\frac{1}{2\pi\hbar}\int dR\exp\left(-\frac{iPR}{\hbar}\right) \\
&\qquad \times\left(\frac{\hbar}{i}\right)^n\frac{\partial^n}{\partial r^n}\Big[\phi_{j'}^*(q - r/2, Q - R/2) \\
&\qquad\qquad \times\phi_j(q + r/2, Q + R/2)\Big]_{r=0}
\end{aligned} \tag{E.2}
$$

where E_j are the eigenvalues of the composite system and $c_j = \langle\phi_j|\psi\rangle$. The eigenstates can be expressed in terms of a product

189

harmonic oscillator basis

$$
\begin{aligned}
\phi_j(q, Q) &= \sum_{m,k} a^j_{m,k} \chi_m(q) \xi_k(Q) \\
&= \sum_{m,k} a^j_{m,k} N_m \exp\left(-\frac{\gamma q^2}{2}\right) H_m(\sqrt{\gamma} q) \\
&\quad \times N_k \exp\left(-\frac{\delta Q^2}{2}\right) H_k(\sqrt{\delta} Q) \qquad \text{(E.3)}
\end{aligned}
$$

where

$$
N_m = \left[\sqrt{\frac{\gamma}{\pi}} \frac{1}{2^m m!}\right]^{\frac{1}{2}} \qquad N_k = \left[\sqrt{\frac{\delta}{\pi}} \frac{1}{2^k k!}\right]^{\frac{1}{2}} \qquad \text{(E.4)}
$$

and $H_k(v)$ is the kth order Hermite polynomial. (Note that the integer m is to be distinguished from the symbol used for the mass in the preceding sections.) Continuing,

$$
\begin{aligned}
\langle \mathcal{P}^n \rho \rangle_{qQP} &= \frac{1}{2\pi\hbar} \sum_{j,j'} c_j c_{j'} \exp\left(-\frac{i}{\hbar}[E_j - E_{j'}]t\right) \\
&\quad \times \sum_{m,k} a^j_{m,k} a^{j'}_{m',k'} N_k N_{k'} \\
&\quad \times \left(\frac{\hbar}{i}\right)^n \frac{\partial^n}{\partial r^n} \Big[\chi_m(q + r/2) \chi_{m'}(q - r/2)\Big]_{r=0} \\
&\quad \times \int dR \exp(-\frac{\delta}{2}(Q + R/2)^2) H_k(\sqrt{\delta}[Q + R/2]) \\
&\quad \times \exp(-\frac{\delta}{2}(Q - R/2)^2) H_{k'}(\sqrt{\delta}[Q - R/2]) \exp(-\frac{iPR}{\hbar}) \\
&\qquad\qquad\qquad\qquad\qquad\qquad\qquad\qquad\qquad\qquad \text{(E.5)}
\end{aligned}
$$

Setting

$$
u = \frac{\sqrt{\delta}}{2} R + \frac{iP}{\sqrt{\delta}\hbar} \qquad \text{(E.6)}
$$

and using the relation $H_k(-v) = -1^k H_k(v)$ gives

$$
\begin{aligned}
\langle \mathcal{P}^n \rho \rangle_{qQP} &= \frac{1}{2\pi\hbar} \sum_{j,j'} c_j c_{j'} \exp(-\frac{i}{\hbar}[E_j - E_{j'}]t) \sum_{m,k} \sum_{m',k'} a^j_{m,k} a^{j'}_{m',k'} N_k N_{k'} \\
&\quad \times \left(\frac{\hbar}{i}\right)^n \frac{\partial^n}{\partial r^n} \Big[\chi_m(q + r/2) \chi_{m'}(q - r/2)\Big]_{r=0} \exp(-\delta Q^2 - \frac{P^2}{\hbar^2 \delta})(-1)^{k'} \frac{2}{\sqrt{\delta}} \\
&\quad \times \int du \exp(-u^2) H_k(u + z) H_{k'}(u + y) \qquad\qquad\qquad\qquad\qquad \text{(E.7)}
\end{aligned}
$$

190

where

$$y = -\sqrt{\delta}Q - \frac{iP}{\sqrt{\delta}\hbar} \qquad z = \sqrt{\delta}Q - \frac{iP}{\sqrt{\delta}\hbar}$$

The integral in Eq. (E.7) has the solution

$$\int du \exp(-u^2) H_k(u+z) H_{k'}(u+y) = \sqrt{\pi} 2^k k'! z^{k-k'} L_k^{k-k'}(-2yz) \quad k' \le k$$

(E.8)

where $L_k^{k-k'}(-2yz)$ is the associated Laguerre polynomial. For ease of notation the terms with no q dependency are collected into Ω in the following

$$
\begin{aligned}
\langle \mathcal{P}^n \rho \rangle_{qQP} &= \frac{1}{\pi\hbar} \sum_{j,j'} c_j c_{j'} \exp(-\frac{i}{\hbar}[E_j - E_{j'}]t) \sum_{m,k} \sum_{m',k'} a_{m,k}^j a_{m',k'}^{j'} N_k N_{k'} \\
&\quad \times \sqrt{\frac{\pi}{\delta}} \exp(-\delta Q^2 - \frac{P^2}{\delta\hbar^2}) 2^k (-1)^{k'} k'! z^{k-k'} L_k^{k-k'}(-2yz) \\
&\quad \times \left(\frac{\hbar}{i}\right)^n \frac{\partial^n}{\partial r^n} \left[\chi_m(q+r/2) \chi_{m'}(q-r/2) \right]_{r=0} \\
&= \Omega \left(\frac{\hbar}{i}\right)^n \frac{\partial^n}{\partial r^n} \left[\chi_m(q+r/2) \chi_{m'}(q-r/2) \right]_{r=0}
\end{aligned}
$$
(E.9)

For the first two moment we have

$$
\begin{aligned}
\langle \rho \rangle_{qQP} &= \Omega N_m N_{m'} \exp(-\gamma q^2) H_m(\sqrt{\gamma}q) H_{m'}(\sqrt{\gamma}q) \quad \text{(E.10)} \\
\langle \mathcal{P} \rho \rangle_{qQP} &= \frac{\hbar}{2i} \Omega \left[\chi_{m'}(q) \frac{\partial}{\partial q} \chi_m(q) - \chi_m(q) \frac{\partial}{\partial q} \chi_{m'}(q) \right] \\
&= \frac{\hbar}{2i} \Omega N_m N_{m'} \sqrt{\gamma} \exp(-\gamma q^2) \{ H_{m'}[2m H_{m-1} - \sqrt{\gamma}q H_m] \\
&\quad - H_m[2m' H_{m'-1} - \sqrt{\gamma}q H_{m'}] \}
\end{aligned}
$$
(E.11)

For the moment derivatives

$$
\begin{aligned}
\frac{\partial}{\partial q} \langle \rho \rangle_{qQP} &= \Omega N_m N_{m'} \sqrt{\gamma} \exp(-\gamma q^2) \{ H_{m'}(2m H_{m-1} - \sqrt{\gamma}q H_m) \\
&\quad + H_m(2m' H_{m'-1} - \sqrt{\gamma}q H_{m'}) \}
\end{aligned}
$$
(E.12)

191

$$\frac{\partial}{\partial q}\langle\mathcal{P}\rho\rangle_{qQP} = \frac{2\hbar}{i}\Omega N_m N_{m'}\gamma\exp(-\gamma q^2)\{m(m-1)H_{m-2}H_{m'} - \sqrt{\gamma}qmH_{m-1}H_{m'}$$
$$-m'(m'-1)H_{m'-2}H_m + \sqrt{\gamma}qm'H_{m'-1}H_m\} \qquad (E.13)$$

$$\frac{\partial}{\partial q}\langle\mathcal{P}^2\rho\rangle_{qQP} = -\hbar^2\Omega N_m N_{m'}\gamma^{3/2}\exp(-\gamma q^2)\{2m(m-1)(m-2)H_{m-3}H_{m'}$$
$$-2\sqrt{\gamma}qm(m-1)H_{m-2}H'_m$$
$$-mH_{m-1}H_{m'} - m'H_mH_{m'-1} + \sqrt{\gamma}qH_mH_{m'}$$
$$-2mm'(m'-1)H_{m-1}H_{m'-2} - 2mm'(m-1)H_{m-2}H_{m'-1}$$
$$+4\sqrt{\gamma}mm'qH_{m-1}H_{m'-1} + 2m'(m'-1)(m'-2)H_mH_{m'-3}$$
$$-2\sqrt{\gamma}qm'(m'-1)H_mH_{m'-2}\} \qquad (E.14)$$

Appendix F

Evaluation of h_n^m

h_n^m has the solution

$$
\begin{aligned}
h_n^m &= \int dp \; p^n H_m(\sqrt{\beta}p) \exp(-\beta p^2/2) \\
&= \frac{(-1)^{m/2}}{\beta^{n-1/2}} 2^{(m-1/2-n/2)} \frac{\Gamma\left(\frac{n+1}{2}\right)\Gamma\left(\frac{m+1}{2}\right)}{\sqrt{\pi}(1/4)^{0.5(n+1)}} \\
&\quad F\left(-\frac{m}{2},\frac{n+1}{2},\frac{1}{2},2\right) n \text{ and } m \text{ even} \\
&= \frac{(-1)^{m-1/2}}{\beta^{n-1/2}} 2^{(m-n/2)} \frac{\Gamma\left(\frac{n}{2}+1\right)\Gamma\left(\frac{m}{2}+1\right)}{\sqrt{\pi}(1/4)^{0.5(n+1)}} \\
&\quad F\left(-\frac{m-1}{2},\frac{n}{2}+1,\frac{3}{2},2\right) n \text{ and } m \text{ odd} = 0 \text{ otherwise}
\end{aligned}
$$

(F.1)

where Γ is the gamma function and $F(a,b,c,z)$ is a hypergeometric series. Unfortunately the series is divergent for $z = 2$. However, the integral is easily solved numerically.

Appendix G

Published Papers

K. H. Hughes, S. M. Parry, G. Parlant and I. Burghardt, J. Phys. Chem. A **111**, 10269 (2007).

K. H. Hughes, S. M. Parry and I. Burghardt, J. Chem. Phys. **130**, 054115 (2009).